



LIBRARY Michigan State University

This is to certify that the dissertation entitled

MOLECULARLY REINFORCED POLYMERS AND SELF ASSEMBLED NANOCOMPOSITES FOR SECONDARY LITHIUM BATTERIES

presented by

Fadi H Asfour

has been accepted towards fulfillment of the requirements for the

<u>Ph.D.</u>	degree in _	CHEMISTRY
	, ,	?
	In It	ala
	/Major Prof	essor's Signature
	22 De	ecember 2003

MSU is an Affirmative Action/Equal Opportunity Institution

Date

PLACE IN RETURN BOX to remove this checkout from your record. TO AVOID FINES return on or before date due. MAY BE RECALLED with earlier due date if requested.

DATE DUE	DATE DUE	DATE DUE

6/01 c:/CIRC/DateDue.p65-p.15

MOLECULARLY REINFORCED POLYMERS AND SELF ASSEMBLED NANOCOMPOSITES FOR SECONDARY LITHIUM BATTERIES

Ву

Fadi H. Asfour

AN ABSTRACT OF A DISSERTATION

Submitted to
Michigan State University
in partial fulfillment of the requirements
for the degree of

DOCTOR OF PHILOSOPHY

Department of Chemistry

2004

Dr. Gregory L. Baker

ABSTRACT

MOLECULARLY REINFORCED POLYMERS AND SELF ASSEMBLED NANOCOMPOSITES FOR SECONDARY LITHIUM BATTERIES

By

Fadi H. Asfour

A series of soluble poly(p-phenylene)s (PPP) substituted with short poly(ethylene oxide) (PEO) side chains were synthesized. Characterization data for these polymers indicate that they take on hairy rod-like structures. As the side chain increases in length, the characteristics of these materials evolve from those of PPP to resembling those of PEO at long side chains. When the weight fraction of the tethered chains exceeds 80%, the thermal transitions of the polymers and the resulting ionic conductivities nearly match those of polyethylene oxide. Solid polymer electrolytes based on oligo(ethylene oxide)-substituted PPP and lithium perchlorate exhibit conductivities ranging from 10⁻⁶ to 5 × 10⁻⁴ S/cm at 30 °C, with the conductivity dependent on the length of the ethylene oxide chain attached to each ring. When the ethylene oxide chain is short, the solubility of Li-ClO₄ is low, leading to undissolved salt and low conductivities. Lengthening the ethylene oxide chains increases the solubility of LiClO₄ and chain mobility, causing a more than two order of magnitude increase in the room temperature conductivity.

The properties of composites based on modified silica nanoparticles in poly(ethylene oxide) (PEO) is also reported. Silica bound lithium sulfonimide salts were prepared through

the synthesis of triethoxysilane, N-pentane trifluoromethane sulfonimide, subsequent attachment to the surface and formation of the lithium salt. The experimental results of PEO/modified silica composites revealed that an optimum conductivity was attained at a weight loading of 30 wt%. These composites exhibit ionic conductivities that are weakly dependent on temperature and are on the order of 10^{-6} S/cm at 30 °C. The lithium ion transport numbers were determined to be 0.86 ± 0.03 .

To Mom and Dad, Ramzi and my loving wife Lucia

ACKNOWLEDGMENTS

I wish to acknowledge my parents, Juliana C. Ramos and Dr. Hani Shafiq Asfur, my brother Ramzi, my wife Lucia and my friends, Pantelis Trikalitis, Theodore Mertzimekis and Christopher Radano. To these people I owe many thanks and debts of gratitude for their constant support and encouragement.

To my advisor Prof. Gregory L. Baker who has led me through this process by allowing me to err and learn from my mistakes with patience, along with his friendship, to him my deepest gratitude. To the research group past and present, I owe my thanks to for their words of wisdom and encouragement. I also thank my committee members, Prof. Babak Borhan, Prof. Aaron Odom and Prof. Mitch Smith for their guidance off and on the basketball court. Finally I wish to thank Prof. Jim Dye, Prof. Greg Swain and our collaborators at North Carolina State University, Prof. Saad Khan, Prof. Peter Fedkiw, Dr. Xiangwu Zhang and Dr. Jeff Yerian.

Table of Contents

List	of Figu	res	x
List	of Sche	mes	xiv
List	of Tabl	es	xv
List	of Abbi	reviations	xvi
1	Intro	oduction	1
	1.1	Introduction	1
	1.2	General	1
	1.3	Ionic Conductivity	8
	1.4	Ionic Conductivity Measurements – Impedance Spectroscopy	9
	1.5	Electrolytes for Lithium Batteries	14
		1.5.1 Small molecule electrolytes	16
	1.6	Polymer Electrolytes	19
		1.6.1 Poly(ethylene oxide)	22
	1.7	Advances in PEO Based SPE	25

		1.7.1	Gel polymer electrolytes	28
		1.7.2	Filler based electrolytes	30
	1.8	Propo	sed Solid Polymer Electrolyte Systems	32
		1.8.1	Molecularly reinforced electrolytes	32
		1.8.2	Syntheses of rigid polymer systems	35
		1.8.3	Single ion solid polymer electrolytes	36
2	Synth Chain		Substituted Poly(p-phenylene)s with Oligo(ethylene oxide) Sid	le 42
	2.1	Introd	luction	42
	2.2	Result	ts and Discussion	44
		2.2.1	Monomer synthesis	44
		2.2.2	Polymerization	45
		2.2.3	Polymer characterization	46
		2.2.4	Differential scanning calorimetery (DSC)	54
		2.2.5	Thermogravimetric analysis (TGA)	56
		2.2.6	X-ray diffraction (XRD)	58
		2.2.7	Polarized light optical microscopy	62
		228	Conclusions	64

	2.3	Experimental	64
3		um Ion Conductivity of Substituted Rigid Rod Solid Polymer rolytes	73
	3.1	Introduction	73
	3.2	Results and Discussion	75
		3.2.1 Thermal properties	75
		3.2.2 X-ray diffraction	79
		3.2.3 AC impedance spectrscopy	80
	3.3	Conclusions	84
	3.4	Experimental	85
4	Self-	assembled Silica Nano-composite Polymer Electrolytes	87
	4.1	Introduction	87
	4.2	Results and Discussion	89
		4.2.1 Synthesis	89
		4.2.2 Infrared spectroscopy	90
		4.2.3 Thermogravimetric analysis	93
		4.2.4 AC impedance spectroscopy	95
		4.2.5 Transference number measurement	98

		4.2.6 Differential scanning calorimetry	99
	4.3	Conclusion	101
	4.4	Future work	102
	4.5	Experimental	104
5	App	endix A	109
6	Appo	endix B	113
7	Appe	endix C	127
8	Bibli	iography	139

List of Figures

Figure 1.	Zn/Cu electrochemical cell
Figure 2.	Ideal versus actual discharge curves for electrochemical cells
Figure 3.	Comparison of discharge performance of primary and secondary batteries. Primary batteries have a higher capacity and discharge faster than secondary batteries
Figure 4.	Potential ranges for various lithium compounds used as electrodes for lithium ion batteries. Reproduced by permission of The Electrochemical Society, Inc. ²
Figure 5.	Anatomy of a high energy density lithium battery constructed of a lithiated metal-oxide cathode and a lithium intercalated graphite anode. The two electrodes are separated by electrolyte and an electrode separator. Current is collected at the electrode terminals that reside outside of the battery package.
Figure 6.	Potential profile in an AC impedance experiment for a resistor (top curve) and a capacitor (bottom curve)
Figure 7.	The impedance is a vector comprised of two parts. The real component is resistance and the imaginary component is capacitance. θ is the phase angle between current and potential.
Figure 8.	Example of a typical Nyquist plot obtained from AC impedance spectroscopy
Figure 9.	Planar zig-zag structure of PEO
Figure 10.	3D pictures of the side and top views of the 7 ₂ helix of PEO23

Figure 11.	Arrhenius plot of the temperature-dependent conductivity of PEO-LiClO ₄ (O:Li = 6)24
Figure 12.	Schematic showing the segment-assisted diffusion of Li ⁺ through the PEO matrix. The circles represent the ether oxygens of PEO. Reproduced with permission from reference 55
Figure 13.	Various polymer architectures designed to decrease crystallization of PEC in SPEs
Figure 14.	Mesogenic polymers synthesized by Ingram and coworkers. Both 1 and 2 have predominantly poly(ethylene oxide) backbones. Structures 1 and 2 differ in that in 1, pendant mesogenic groups are attached to the chain via flexible alkyl spacers
Figure 15.	PPP(EO) _{x/y} reported by Wegner and Meyer in reference 92
Figure 16.	Extrapolation of dn/dc of PPP-EO _m as a function of PPP weight fraction to obtain dn/dc of PPP-EO ₀
Figure 17.	Comparison of calculated values of dn/dc for PPP-EO _m with experimentally obtained data
Figure 18.	The extinction coefficient (ε) of PPP-EO _m as a function of PPP weight fraction
Figure 19.	Plot of the ratio of molecular weights obtained by GPC to those obtained by LS as a function of the number of ethylene oxide units in the side chains of PPP-EO _m polymers
Figure 20.	DSC scans of PPP-EO _m (7 < m > <45>); PEG-dm-2000 is shown for comparison. The data are second heating scans, taken at 10 °C/min after quenching the sample from 180 to -100 °C. The arrows mark the T_g transitions
Figure 21.	The relationship between T _g and the weight fraction of PEO in the side chains. The dashed line is a least squares fit to the data

Figure 22.	TGA scans of PPP-EO _m polymers. Polymer samples were dried under vacuum at 100 °C overnight, equilibrated under N ₂ at 80 °C for 12 hrs, and then heated under N ₂ at 10 °/min
Figure 23.	Room temperature X-ray powder diffraction scans of PPP-EO _m polymers. All scans were collected at a rate of 0.05 2θ /min over a range of $2\theta = 1-50^{\circ}$
Figure 24.	Fluorescence spectra of PPP-EO _m and their corresponding monomers (inset). Data were collected at room temperature in chloroform using an excitation wavelength of 313 nm
Figure 25.	Solid-state Raman spectra of PPP-EO _m polymers. Data shown were obtained at room temperature and are the average of 20 scans of 6 seconds in duration
Figure 26.	Cross polarized optical micrographs of PPP-EO ₂ at 140 °C a) after 5 minutes at 140 °C b) after shearing the sample and c) 1 minute after shearing showing break-up of the elongated domains
Figure 27.	The relationship between T _g and the length (m) of the ethylene oxide side chain in PPP-EO _m polymers. The data were acquired through MDSC. The line is a guide
Figure 28.	DSC scans of neat PPP-EO _m (dashed) and LiClO ₄ /PPP-EO _m composites (solid). The scans shown are the first heating scans after quenching the sample from 180 °C. The samples were heated at 10 °C/min under He 78
Figure 29.	X-ray powder diffraction patterns of PPP-EO _m /LiClO ₄ composites. The data were collected at room temperature at a rate of 0.05 2θ /min over a range of $2\theta = 1-50^{\circ}$
Figure 30.	Temperature-dependent conductivities for selected PPP-EO _m /LiClO ₄ composites. The data are derived from AC impedance data, with all samples having an O:Li ratio of 20
Figure 31.	A cross-section of the conductivity data at 30 °C, indicating a conductivity maximum at $m = <16>$. Decreases in σ for $m = <45>$ and PEO-dm-2000 reflect partial crystallization of the samples.

Figure 32.	Diffuse reflectance IR spectra of A200 silica nanoparticles, the sulfonimide-modified silica (A200-C5NHTf), and its lithiated form (A200-C5NTfLi). Data were obtained from samples prepared in a 2:1 ratio of sample to dry KBr
Figure 33.	IR spectra comparing the starting material (C5NHTf) and formation of the lithium salt (C5NTfLi). Data were collected as thin films sandwiched between NaCl plates
Figure 34.	Thermogravimetric analysis of A200 and A200-C5NHTf measured in air from 30 °C to 800 °C at a rate of 10 °C/min. The weight loss at 700 °C corresponds to 36 % coverage of the silica nanoparticle surface
Figure 35.	Conductivity of PEG-dm-500/A200-C5NTfLi composites. The data are derived from AC impedance measurements taken after equilibration for 20 min
Figure 36.	Cross section of conductivity at 40 °C. The data are obtained from the Arrhenius conductivity plot
Figure 37.	DSC scans of PEG-dm-500, 10, 20, and 40 wt% of PEG-dm-500/A200-C5NTfLi composite polymer electrolytes. Data were collected under He at a rate of 10 °C/min
Figure 38.	Comparison of the heat of fusion for the various composite polymer electrolytes as a function of weight percentage of A200-C5NTfLi. The data were obtained by integrating the areas under the curve for the melting transition for each DSC scan

List of Schemes

Scheme I.	A proposed mechanism ³⁴ for the reduction of ethylene carbonate to for passivating layers at the solvent electrode interface	
Scheme II.	Synthesis of monomers 4a – 4k	1 5
Scheme III.	Synthesis of A200-C5NTfLi)0
Scheme IV.	Proposed synthetic scheme for increasing the concentration of lithium ion per particle	

List of Tables

Table 1.	Some common small molecule hosts for electrolytes and their properties
Table 2.	Structures of potential host polymers for use in solid polymer electrolyte lithium polymer batteries
Table 3.	Example of SPE polymers and their conductivities
Table 4.	Ionic conductivities of representative gel polymer electrolytes. Taken from reference 70
Table 5.	Some examples of composite polymer electrolytes. ⁷⁰
Table 6.	Examples of early polymer systems with immobilized anions designed to bring about single cation conductivity
Table 7.	Properties of PPP-EO _m polymers. a) Molecular weight data were obtained from GPC measurements in CHCl ₃ using a light scattering and a refractive index detector. b) T_g and T_m values were obtained from MDSC and DSC measurements. c) The brackets < > indicate samples with polydisperse EO chains with average degrees of polymerization = m
Table 8.	Properties of PPP-EO _m polymers
Table 9.	Lithium concentrations of various composite polymer electrolytes and their measured ionic conductivities at 30 and 80 °C
Table 10.	An example of the saved data. The format is the complex impedance, phase angle, frequency

List of Abbreviations

A200 Aerosil® 200

A200-C5NHTf triethoxysilyl N-pentane trifluoromethane sulfonimide bound to

Aerosil® 200

A200-C5NTfLi lithium salt of A200-C5NHTf

AC alternating current

ATRP atom transfer radical polymerization

bp boiling point

CPE composite polymer electrolyte

DC direct current DEA diethylamine

DRIFTS diffuse reflectance infrared Fourier transform spectroscopy

DSC differential scanning calorimetry

EO ethylene oxide fs fumed silica

FTIR Fourier transform infrared GPC gel permeation chromatography

 I_0 initial current I_{ss} steady state current

IR infrared

j imaginary number
LS light scattering
m multiplet

M_n number-average molecular weight

mp melting point

M_W weight-average molecular weight

MDSC modulated differential scanning calorimetry

n number of repeat units

NMR nuclear magnetic resonance

PDA photodiode array detector

PDI polydispersity index

PEG poly(ethylene glycol)

PEGDME poly(ethylene glycol) dimethyl ether

PEG-dme-500 poly(ethylene glycol) dimethyl ether ca. 500 g/mol PEG-dme-2000 poly(ethylene glycol) dimethyl ether ca 2000 g/mol

PEO poly(ethylene oxide)

PPP-EO_m poly(p-phenylene) with ethylene oxide side chains of length m

PPP poly(p-phenylene)

q quartet s singlet

 $\begin{array}{ll} \text{SPE} & \text{solid polymer electrolyte} \\ T_c & \text{crystallization temperature} \\ T_g & \text{glass transition temperature} \end{array}$

TEA triethylamine

TGA thermogravimetric analysis

T_m melting temperature

t triplet

 t_{Li}^{+} lithium ion transport number

UV-vis ultraviolet-visible VI virtual instrument

X_n degree of polymerization

XRD X-ray diffraction Z complex impedance

Z' real part of the complex impedance Z

Z" imaginary part of the complex impedance Z

Chapter 1

1 Introduction

1.1 Introduction

The need for high energy density rechargeable lithium batteries for portable electronic devices and for electric vehicle propulsion has driven research on solid polymer electrolytes. Rechargeable lithium batteries containing polymer electrolytes should have longer lifetimes, higher efficiencies and higher capacities than batteries based on liquid electrolytes. A polymer based device is expected to be lightweight and flexible, two properties that are attractive in terms of design and manufacture. The purpose of this research is to examine two types of solid polymer electrolytes. The first is a comb-like polymer based on a rigid poly(p-phenylene) backbone substituted with flexible oligo(ethylene oxide) teeth. The second is a single ion conductor prepared from silica nanoparticles in poly(ethylene oxide).

1.2 General

A battery is a device that transforms stored chemical energy into electrical energy. The fundamental design of a battery consists of two electrodes inserted in an ion conducting medium, usually a salt or a salt solution. Connecting a load between both electrodes completes the circuit, allowing electrons to flow from one electrode to the other, and consequently, chemical reactions at each electrode generate a flow of ions from one electrode to the other through the electrolyte. Electrons are generated at one electrode (anode)

through oxidation reactions, and consumed at the other electrode (cathode) through reduction of species in the electrolyte. As shown in **Figure 1** the anions move towards the anode and the cations move in the opposite direction towards the cathode. Their movement is dictated by the concentration gradient and electromotive field generated at the beginning of battery use.

The driving force for the flow of electrons is the difference in the electrochemical potentials of the two redox reactions. **Figure 1** is a simple representation of a Zn/Cu battery with a zinc anode and a copper cathode. The net electrochemical reaction is oxidation of Zn⁰ to Zn²⁺ at the anode, and reduction of Cu²⁺ to Cu⁰ (plating) at the cathode. The electromotive force of this cell, defined in equation (1.1), is the difference between the standard reduction potentials for the two half-cell reactions..

$$E_{cell} = E_{cuthode} - E_{anode} \tag{1.1}$$

The relevant reduction potentials at 25 °C are:

anode
$$Zn^{2+} + 2e^{-} \rightarrow Zn -0.76V$$

cathode $Cu^{2+} + 2e^{-} \rightarrow Cu 0.34V$

and thus $E_{cell} = 0.34 - (-0.76) = 1.10 V$ The free energy for the cell reaction (ΔG) is defined in equation (1.2) where F is Faraday's constant and n is the number of equivalents (electrons) involved in the reaction.

$$\Delta G = -nFE_{cell} \tag{1.2}$$

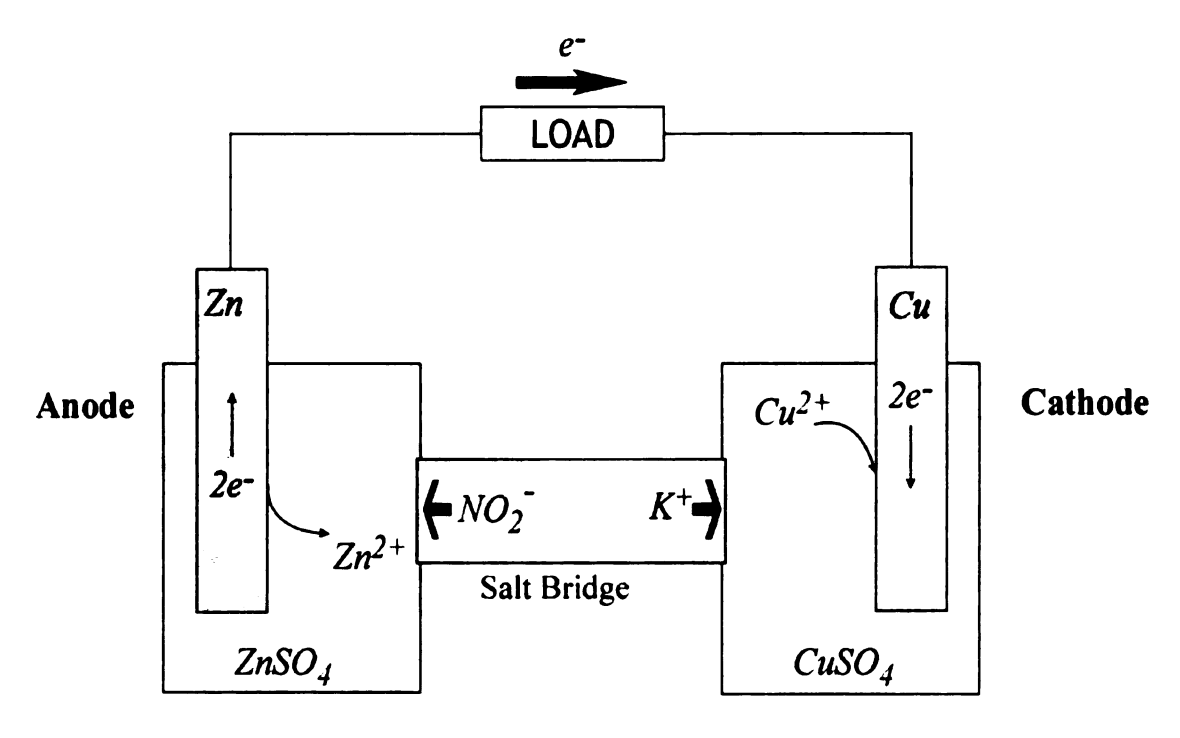


Figure 1. Zn/Cu electrochemical cell.

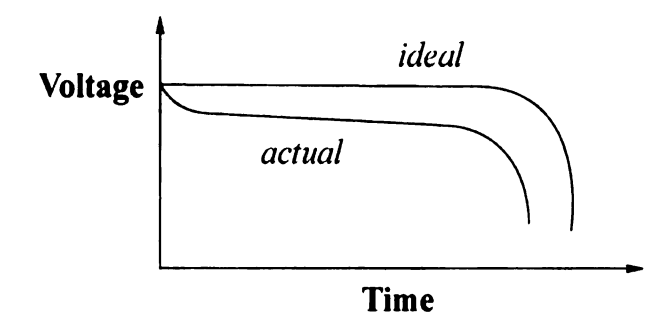


Figure 2. Ideal versus actual discharge curves for electrochemical cells.

When ΔG in equation (1.2) is negative (discharge conditions) the reaction is spontaneous. If the cell reaction was reversed then E_{cell} is negative and an external source of energy (charging) is needed to drive the chemical reaction.

The theoretical capacity of a cell is the total charge in ampere-hours involved in the electrochemical reaction per gram of electrode materials. The theoretical energy density of a battery takes into account both voltage and theoretical capacity and is commonly expressed in Watt-hours per gram (Wh/g) or Watt-hours per liter (Wh/L). The calculation of energy density is shown in equation (1.3).

Energy density =
$$V \times Ah/g = Wh/g$$
 (1.3)

In reality, the theoretical energy density is never realized. Figure 2 compares a typical experimental discharge curve¹ with the ideal case. In an ideal system, the battery discharges at the theoretical voltage until the capacity is fully utilized (all active materials are depleted) at which point the voltage falls to zero. In a real cell, the voltage drops to some stable value at the onset of discharge after which the voltage drops to zero. Discharge at less than the theoretical voltage reflects an internal resistance in the cell, usually from polarization of active materials. Depending on the active materials and conditions of use, the practical capacity of a cell ranges from is 25-70% of the theoretical capacity.

Batteries are classified as primary or secondary batteries. In a primary battery, the chemical changes that occur during the discharge process are irreversible, while those of

secondary batteries are reversible. Thus, primary batteries are disposed of after discharge, while secondary batteries may be recharged. The difference in performance between a primary and a secondary cell can be illustrated as in **Figure 3**, where a high discharge rate is characteristic of secondary cells and high capacity of primary cells.

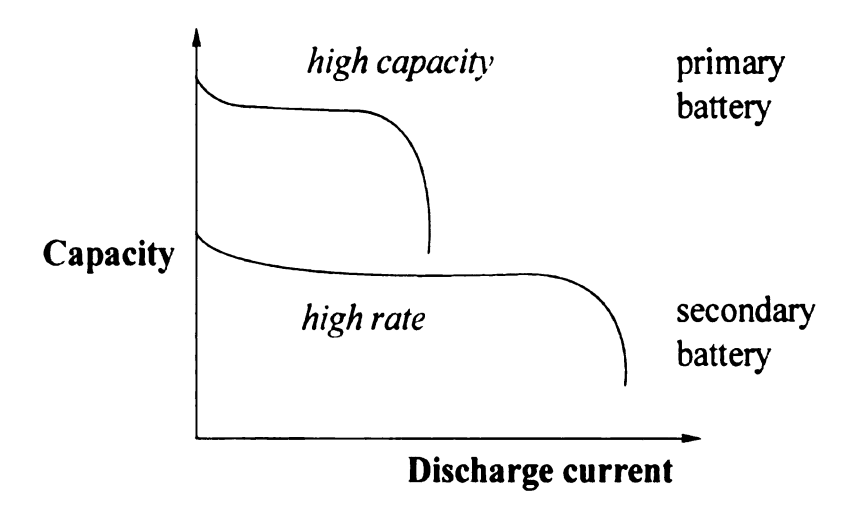


Figure 3. Comparison of discharge performance of primary and secondary batteries.

Primary batteries have a higher capacity and discharge faster than secondary batteries.

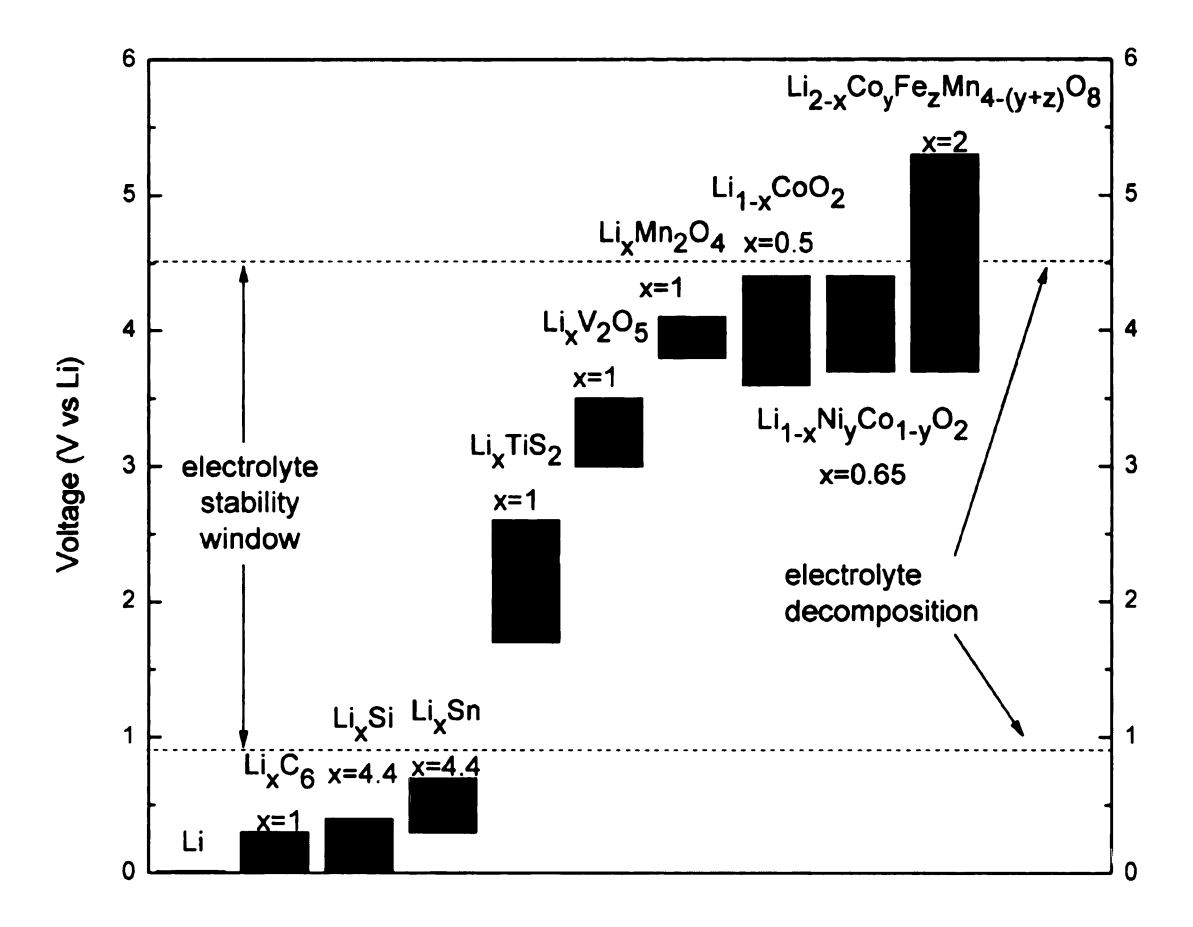


Figure 4. Potential ranges for various lithium compounds used as electrodes for lithium ion batteries. Reproduced by permission of The Electrochemical Society, Inc.²

Lithium batteries currently are available as primary and secondary cells. The reduction potential of lithium (-3.04 V) and its low atomic mass make it an attractive element for high energy density batteries, which are critical for applications in portable electronic devices and for electric vehicle propulsion. In a lithium battery, the cathode is typically a metal oxide such as a manganese oxide or cobalt oxide while the anode is either lithium metal or lithium intercalated graphite. Such combinations lead to an electrochemical potential of 3 to 4 V. The chemical reactions that take place at the electrodes are oxidation of Li⁰ at the anode, and intercalation of Li⁺ into the channels and layers of the metal ox-

ide cathode. When lithium intercalated graphite is used as the anode, the anode reaction is de-intercalation of Li⁺. The coupling of the de-intercalation/intercalation reactions yields what is described as a "rocking chair" cell, where ions are shunted from one anode to cathode. This design avoids the use of metallic lithium, which can lead to catastrophic failure of cells (**Figure 5**). A critical feature of the cell is the electrolyte, which must physically separate the cathode and the anode and provide a highly conductive medium for transport of lithium cations. Since most electrolytes are liquids, inert polymer screens are often inserted between the electrodes.

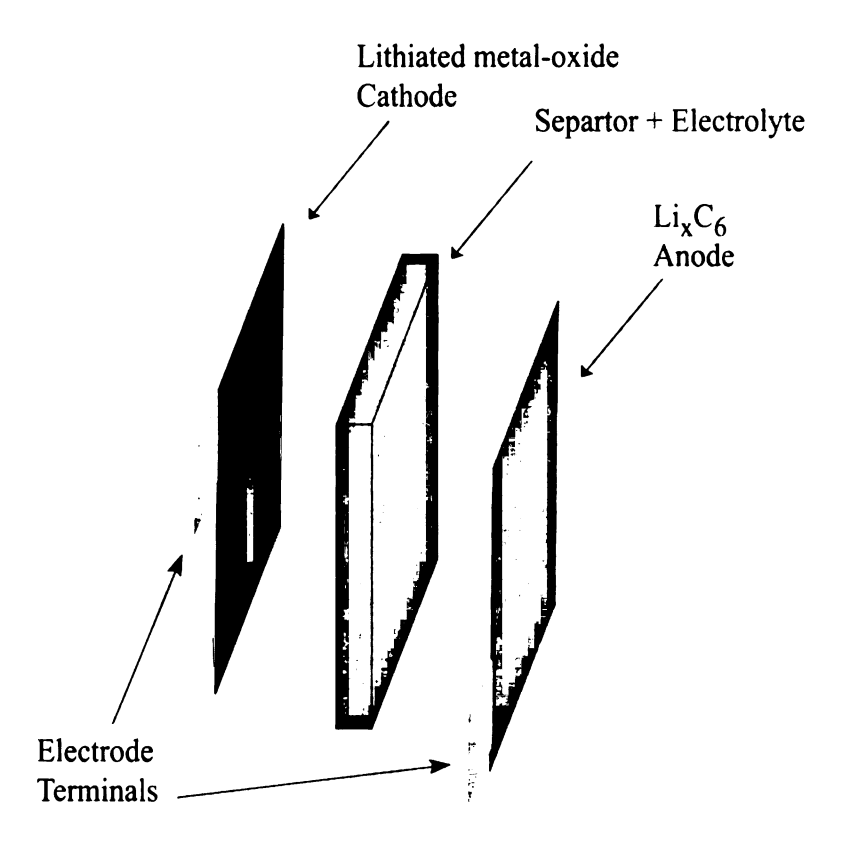


Figure 5. Anatomy of a high energy density lithium battery constructed of a lithiated metal-oxide cathode and a lithium intercalated graphite anode. The two electrodes are separated by electrolyte and an electrode separator. Current is collected at the electrode terminals that reside outside of the battery package.

A major problem that limits applications of lithium batteries is that most electrolytes decompose at such high electrochemical potentials. New electrolytes are needed that have sufficient mechanically stability to separate the electrodes, possess high ionic conductivities and are compatible with the high electrochemical potentials of lithium batteries.

1.3 Ionic Conductivity

The ionic conductivity (σ) of a material represents contributions from mobile cations and anions, and as shown in equation (1.4) can be described in terms of the number of charge carriers per unit volume (n_i), the carrier charge (q_i) and the mobility of each ion relative to its average velocity in an applied field of unit strength (μ_i)

$$\sigma = \sum_{i} n_{i} q_{i} \mu_{i} \tag{1.4}$$

The diffusivity of an ion depends on its size and mass, and thus it is not surprising that a small, light and electropositive metal such as Li⁺ is desirable for fast ion mobility. In addition to the charge/size ratio, ion mobility is also highly temperature dependent due to electrostatic and dipolar interactions of ions with electrolytes. High ionic conductivity is a result of ions being able to diffuse rapidly through an electrolyte medium.

Since is it is difficult for ions to move freely in a crystal lattice or a rigid solid, electrolytes are rarely used below their melting (T_m) or glass transition (T_g) temperatures where ion mobility is hindered. The temperature dependence of σ can be described by the Vogel-Tammann-Fulcher (VTF) equation (1.5).

$$\sigma(T) = A T^{-\frac{1}{2}} e^{(-E_a/k_b(T - T_0))}$$
(1.5)

where the pre-exponential factor A is proportional to the number of charge carriers, E_a is the apparent activation energy, k_b is the Boltzmann constant, and T_0 is the temperature at which the conductivity is zero and is usually taken to be the glass transition temperature (T_g) . Higher conductivity is attained as the larger the difference between T_0 and the operational temperature T, increases.

1.4 Ionic Conductivity Measurements – Impedance Spectroscopy

AC impedance spectroscopy is commonly used to measure the electrochemical properties of a material. The experiment involves sandwiching a material between two electrodes, applying a constant voltage bias across the two electrodes, and applying an alternating current as a function of frequency. The data collected are the complex impedance, the frequency, and the phase angle between current and applied bias. Information about diffusion, concentration of charged species and transference numbers can be extracted from the data. In addition, the data are commonly used to model electrochemical cells through an equivalent circuit analysis, which is a combination of capacitors and resistors arranged either in series or in parallel.

The starting point for impedance spectroscopy is Ohm's law, (equation (1.6)) which describes the potential (E) as a function of current (I) and resistance (R)

$$E = IR \tag{1.6}$$

As written, equation (1.6) is valid for one circuit element: the ideal resistor. Impedance (Z) is a more general descriptor of resistance for a variety of circuit elements

$$E = IZ \tag{1.7}$$

In AC impedance spectroscopy the potential is varied in a sinusoidal fashion and can be expressed as

$$\dot{E} = E \sin(\omega t) \tag{1.8}$$

It follows from Ohm's law that current is then

$$\dot{I} = \frac{\dot{E}}{R} \tag{1.9}$$

$$\dot{I} = \frac{E\sin(\omega t)}{R} \tag{1.10}$$

Where the magnitude of current $I = \frac{E}{R}$. In terms of impedance (Z) equation (1.10) can be

written as

$$\dot{E} = \dot{I}Z \tag{1.11}$$

$$Z = \frac{\dot{E}}{\dot{I}} \tag{1.12}$$

$$Z = \frac{E\sin(\omega t)}{\frac{E}{R}\sin(\omega t)}$$
 (1.13)

In the case of a resistor Z = R. The charge of a capacitor (q) is defined as q = CE where C is the capacitance of the capacitor. Since current is the amount of charge passed per unit time

$$i = \frac{dq}{dt} \tag{1.14}$$

Using the same treatment to define impedance for a resistor, the impedance for a capacitor is

$$\dot{q} = C\dot{E} \tag{1.15}$$

$$\frac{d\dot{q}}{dt} = \frac{d}{dt}C\dot{E} \tag{1.16}$$

$$\frac{d}{dt}C\dot{E} = C\frac{d}{dt}E\sin(\omega t) \tag{1.17}$$

$$\dot{I} = C\omega E \cos(\omega t) \tag{1.18}$$

and since $\cos(\omega) = \sin(\omega + \frac{\pi}{2})$

$$\dot{I} = C\omega E \sin(\omega t + \frac{\pi}{2}) \tag{1.19}$$

Using equation (1.12) the impedance is then

$$Z = \frac{E \sin(\omega t)}{C\omega E \sin(\omega t + \frac{\pi}{2})}$$
 (1.20)

$$Z = -j\frac{1}{\omega C} \tag{1.21}$$

The complex number (j) takes into account the phase angle between current and potential in the complex plane as shown in the phasor diagrams of **Figure 6**. Most electrochemical cells can be represented by a combination of resistors and capacitors in which Z has two components, a resistive and a capacitive component. This means that Z is a complex value, the magnitude of which can be expressed as

$$Z = \sqrt{R^2 + (-j\frac{1}{\omega C})^2}$$
 (1.22)

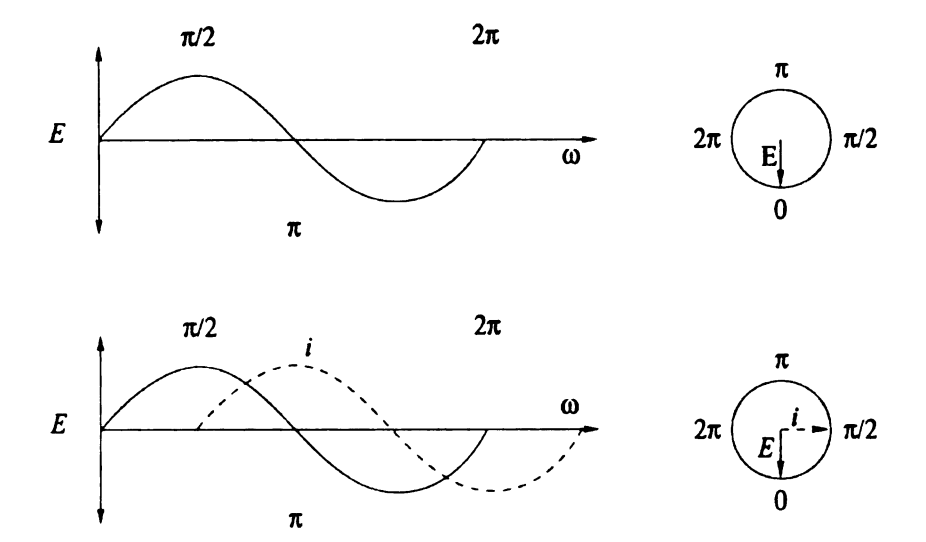


Figure 6. Potential profile in an AC impedance experiment for a resistor (top curve) and a capacitor (bottom curve)

Qualitatively impedance can be represented as shown in **Figure 7**. Mathematically, it is commonly expressed as

$$Z = Z' - jZ'' \tag{1.23}$$

where Z' is the real component $(Z'=Z\cos(\theta))$ and Z'' is the imaginary component $(Z''=Z\sin(\theta))$. Data are often plotted on a complex impedance diagram called a Nyquist plot, where the vector quantity Z at each frequency is represented by a point in the complex plane, as shown in **Figure 8**. The real bulk resistance of the material (R_b) can be extracted from the Nyquist plot at the specific frequency where the capacitive component is zero and the applied bias and resulting current are in phase. This corresponds to the point where the plotted curve intercepts the real axis as shown in **Figure 8**.

Conductivity (σ) is directly related to Ohm's law in that it is the reciprocal of resistivity (ρ) in Ω cm as in equation (1.24)

$$\sigma = 1/\rho \tag{1.24}$$

and

$$\rho = R_b(A/l) \tag{1.25}$$

where A (cm²) is the area and l (cm) is the thickness of the sample. Equation (1.24) becomes

$$\sigma = l/R_b A \tag{1.26}$$

The intercept R_b is then measured directly to calculate the ionic conductivity (σ) of the electrolyte sample.

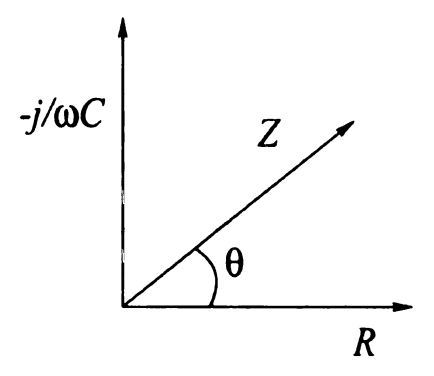


Figure 7. The impedance is a vector comprised of two parts. The real component is resistance and the imaginary component is capacitance. θ is the phase angle between current and potential.

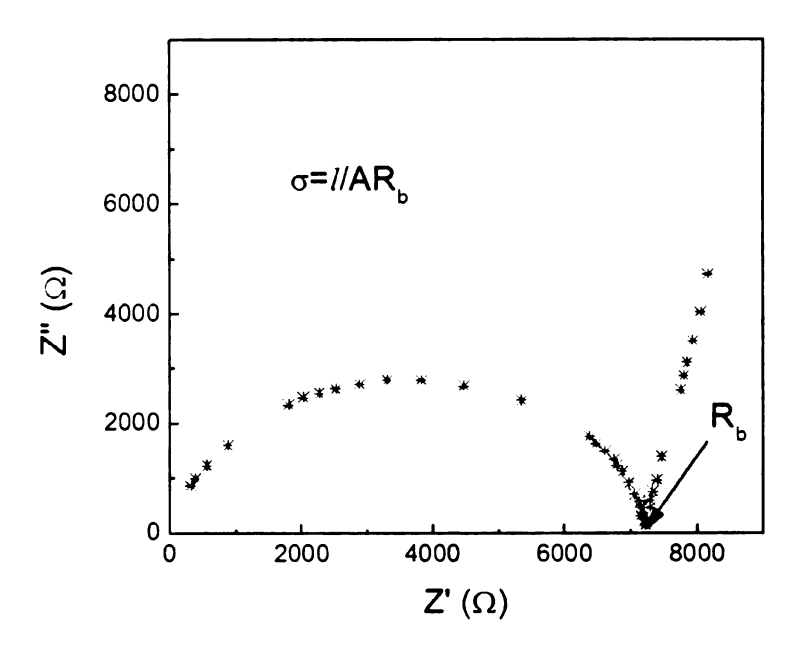


Figure 8. Example of a typical Nyquist plot obtained from AC impedance spectroscopy.

1.5 Electrolytes for Lithium Batteries

Electrolytes for lithium ion batteries are prepared by dissolving lithium salts such as LiPF₆, LiAsF₆, LiBF₄, LiPF₃(C₂F₅)₃, LiN(CF₃SO₂)₂, LiCF₃SO₂ and LiClO₄ in a polar organic medium.² While the choice of a particular salt is based on its thermal, chemical and electrochemical stability, a fundamental requirement is that the salt possesses a low lattice energy to ensure easy dissociation in solvents. Conversely, the solvent should have a high dielectric constant to overcome the lattice energy of the salt to favor dissolution of the ions. An ideal medium would dissolve a wide range of salts and be chemically, thermally and electrochemically stable throughout the voltage window of a lithium battery, typically 0 to 4.5 V vs. Li⁰. The conductivity of an electrolyte at a given temperature de-

pends on the ability of the ions to move freely between the electrodes. This depends on ion size, the charge distribution of the anions, and the degree to which ions aggregate. Lithium salts with large charge delocalized anions have been shown to form electrolytes with the highest conductivities. For example lithium imide, $LiN(CF_3SO_2)_2$, with its large sulfonimide anion has a room temperature conductivity in poly(ethylene oxide) (PEO, M_n = 2000, O:Li = 27) of 1.8×10^{-5} S/cm vs. 6.6×10^{-6} S/cm for LiClO₄.³

Many studies have been undertaken to understand the mechanism of lithium transport in electrolytes, and the interaction of lithium cations, anions and their ionic aggregates. These studies range from molecular simulations⁴⁻⁸ to experimental NMR.⁹⁻¹² Raman^{5,13,14} and impedance studies. 14-18 In PEO, the fraction of dissociated ions has been shown to decrease at low temperature, and at high salt concentrations due to the formation of large immobile aggregate species. Under such conditions, it has been established that anions and aggregates are responsible for a large fraction of current in most electrolytes. 19 The fraction of current carried by a given species is the transference number. Anion and cation transference numbers, t+ and t., can be measured through a number of electrochemical and diffusion based techniques.²⁰⁻²³ Typical experimental values for lithium ion transference numbers are in the range of $t_{+} = 0.2 - 0.4$, depending on temperature, solvent, the specific anion, and concentration.²¹ Increasing transference numbers to near unity is important for minimizing polarization at electrode surfaces, which leads to overall improvement in battery lifetime and efficiency, and not surprisingly, improvement in the lithium ion transference number has been the focus of many research projects. The general approach to the problem has been to immobilize anions by tethering the anion to a polymer or an inorganic particle.

In summary, an ideal electrolyte for secondary lithium batteries should be electrically insulating, have a high ionic conductivity (preferably a single ion conductor to minimize polarization effects at electrodes), be thermally stable, electrochemically stable through the working potential range and compatible with other cell components.²⁴

1.5.1 Small molecule electrolytes

Electrolytes in commercial lithium ion batteries are typically solutions of lithium salts in low molecular weight organic compounds. Their low viscosity leads to ionic conductivities that range from 10⁻³ to 10⁻² S/cm,²⁵ about an order of magnitude lower than aqueous and alkaline electrolytes (10⁻² to 0.1 S/cm), and their electrochemical stability results in good long-term cycling characteristics. Shown in

Table 1 are common solvents used in electrolyte formulation and their physical properties. Most electrolytes are binary or ternary combinations design for good conductivity and minimization of crystallinity.²⁶⁻²⁸ For example, combining ethylene carbonate with dimethyl carbonate in a 1:1 mixture yields a liquid with good dielectric properties at room temperature.

	Structure	mp (°C)	bp (°C)	Dielectric Constant (ε @25°C)	Conductivity σ (S/cm), 1M LiAsF ₆
ethylene carbonate		36.4	248	89.78	6.97×10^{-3}
propylene carbonate		-48.8	240	66.14	5.28 × 10 ⁻³
dimethyl carbonate		4.6	91	3.12	1.1×10^{-2}
γ-butyrolactone		-43	203	39.0	1.01×10^{-2}
tetrahydrofuran	\bigcirc	-109	66	7.75	1.29×10^{-2}

Table 1. Some common small molecule hosts for electrolytes and their properties.

These solvents are attractive due to their electrochemical stability, which can be as high as 5.1 V vs. Li/Li⁺ for carbonates and 4.0 V for ethers. They are also capable of rapidly forming stable passivating layers at the solvent electrode interface,²⁹ which are important for the stabilization of the electrochemical cell and its longevity. These layers have been

extensively studied and are thought to be made of lithium carbonate and various alkoxides from the decomposition of electrolyte at the electrode (Scheme I). 30-32 However, since liquid electrolytes do not have sufficient mechanical stability to separate electrodes, polypropylene or polyethylene mesh separators must be incorporated into the design of a battery, adding to the cost and decreasing the energy density of the battery. A major disadvantage of liquid electrolytes are safety concerns such as electrolyte leaking from improperly sealed cells, pressure build up due to formation of volatile decomposition products, and the flammability of organic solvents. Another complication with small molecule electrolytes is their ability to co-intercalate with lithium into the electrodes. Particularly common with propylene carbonate electrolytes, co-intercalation leads to electrode volume changes, cracking, and eventually battery failure. 33

Scheme I. A proposed mechanism³⁴ for the reduction of ethylene carbonate to form passivating layers at the solvent electrode interface.

1.6 Polymer Electrolytes

In 1973 Wright and coworkers first reported the ionic conductivity of PEO blended with alkali metal salts.³⁵⁻³⁷ M. Armand soon followed with his seminal work on the use of PEO as a solid electrolyte system.⁸ Their work initiated an explosion of research in polymer electrolytes. The advantages of a solid polymer electrolyte (SPE) are derived from their elastomeric strength and flexible mechanical properties.

Polymers usually exhibit excellent adhesive properties that allow for almost complete electrode coverage. More importantly, polymers do not intercalate with lithium into the electrodes which enhances cell performance and overall lifetime of the battery. Further advantages are their low volatility, ease of handling and higher viscosities. These properties circumvent issues with leaking, pressure build-up due to evolution of gases, the need for an electrode separator and allow for the manufacture of thin films (~50 µm). 38

For a polymer to be used as an SPE, the solvation energy of ions within a polymer must exceed the lattice energy of the ionic salt.³⁹ For a polymer to be considered a suitable candidate for use in an SPE, it must meet the following criteria 1) be able to coordinate to ions, 2) have a low cohesive energy and 3) have a high degree of flexibility.^{24,40} The ability for a polymer to coordinate to ions is determined by the number of atoms within the polymer chain or pendant groups which possess available lone pairs such as oxygen or nitrogen. This ability in turn is manifested as a high enough dielectric constant to separate ions. A low cohesive energy in a polymer indicates a lack of intermolecular interactions such as hydrogen bonding. The last requirement is often expressed as the need for a

low T_g . In line with these requirements, several polymers have been identified based on polyamines and polyethers; among them PEO is the most suitable candidate. It is important to note that under most circumstances, a high T_g for a polymer that sufficiently solvates ionic salts would render it unacceptable for use in solid polymer electrolytes. Listed in **Table 2** are some of the important polymers that have been studied.

Polymer	Structure
poly(ethylene oxide)	<i>(○✓)</i>
poly(propylene oxide)	to-1
poly(trimethylene oxide)	⟨० ✓✓ ⟩
poly(siloxanes)	R R +Si-o+
poly(phosphazenes)	(N=P) R
poly(β-propiolactone)	₹ ~ \ ° >
poly(acrylates)	
poly(ethylene succinate)	(°~°)
poly(ethylene imine)	(N~)
poly(N-propylaziridine)	\(\frac{1}{N}\)
poly(alkylene sulfides)	$\{st\}_n$

Table 2. Structures of potential host polymers for use in solid polymer electrolyte lithium polymer batteries.

1.6.1 Poly(ethylene oxide)

Poly(ethylene oxide) is the most successful host for polymer electrolytes. PEO is synthesized by cationic or anionic ring opening polymerization of ethylene oxide, which results in molecular weights ranging from 200 to 5×10^6 g/mol.^{22,27,41,42} The lower molecular weight oligomers are often termed polyethylene glycols. PEOs with number-average molecular weight (M_n) <600 are viscous liquids, but at higher molecular weights they are waxy solids with a T_g near -65 °C and a T_m of about 65 °C. As shown in **Figure 10**, pure PEO crystallizes in a 7_2 helix, with seven ethylene oxide repeat units completing two turns in a fiber period of 19.3 Å. A planar zigzag conformation (**Figure 9**), has also been observed for polymer crystallized under tension.^{43,44} Other structural features have been studied using X-ray analysis and various spectroscopic methods.^{24,45-53} At room temperature, typical samples of PEO are semicrystalline with a degree of crystallinity of ~60%.



Figure 9. Planar zig-zag structure of PEO.



Figure 10. 3D pictures of the side and top views of the 7_2 helix of PEO.

Typical conductivity data for a PEO-LiClO₄ electrolyte are plotted in **Figure 11**. Depending on the concentration of dissolved salt, the conductivity usually ranges from 10^{-3} to 10^{-4} S/cm at 100 °C, dropping to $\sim 10^{-6}$ to 10^{-8} S/cm at room temperature. For a given temperature, a maximum in conductivity is observed at a particular salt concentration. Usually lithium salt concentrations are expressed as a the molar ratio of ether oxygens to lithium ions, and the concentration for maximum conductivity in PEO has been observed to be at O:Li = 20 or approximately 0.4M of LiCF₃SO₃ or LiClO₄. This effect can be explained by considering equation (1.4). At low salt concentrations, the number of charge carriers, n_s is small leading to low values for σ . As the salt concentration increases, the conductivity also increases. Molecular dynamics simulations show that lithium ions

complex to four or five ether oxygens of the PEO chain,⁵⁴ and as a result, lithium cation mobility is related to the segmental motion of the PEO chain as shown in **Figure 12**. Thus complexation increases the T_g of the electrolyte, and decreases the carrier mobility (μ) leading to the observed maximum in σ .

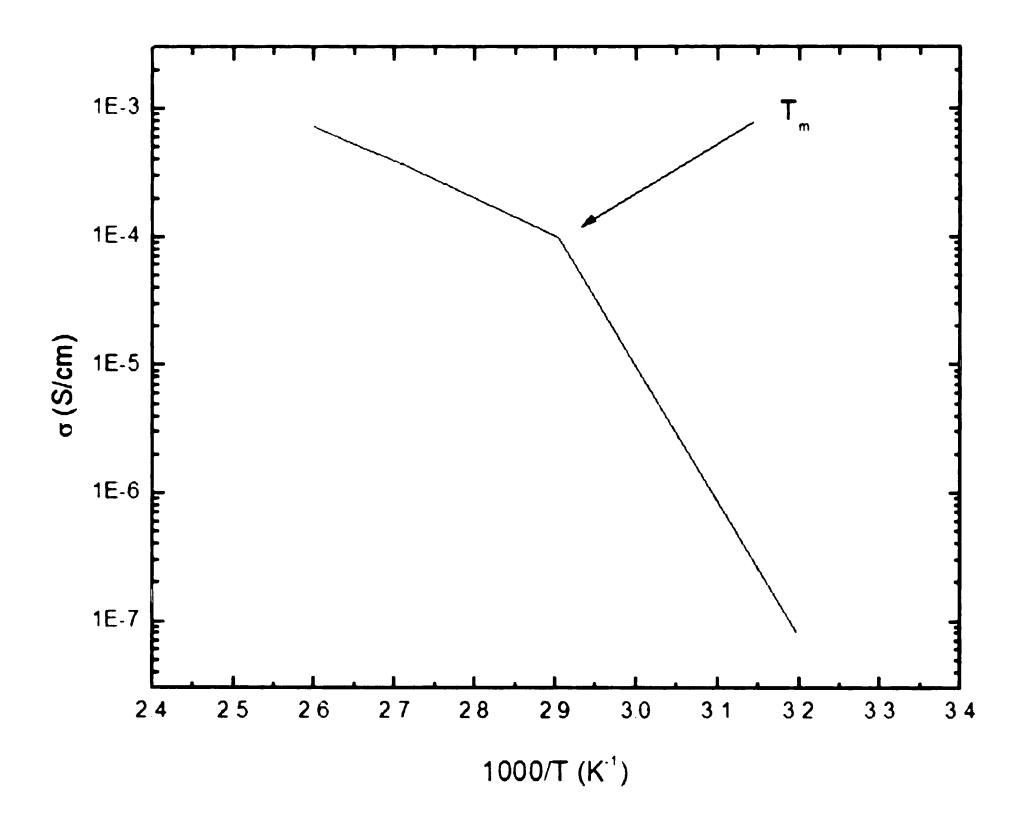


Figure 11. Arrhenius plot of the temperature-dependent conductivity of PEO-LiClO₄ (O:Li = 6).

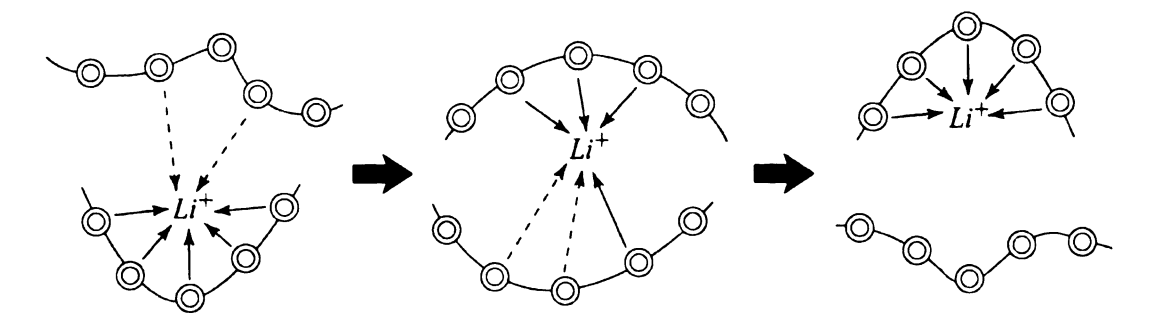


Figure 12. Schematic showing the segment-assisted diffusion of Li⁺ through the PEO matrix. The circles represent the ether oxygens of PEO. Reproduced with permission from reference 55.

1.7 Advances in PEO Based SPE

Despite PEO being an excellent solvent for alkali metal ions, SPEs based on pure PEO-metal salt complexes have poor ionic conductivities at ambient temperatures due to the partial crystallization of PEO. There are several well-explored strategies that reduce the crystallinity of PEO and enhance ionic conductivity at room temperatures, including the addition of solvents or plasticizers to high molecular weight PEO, the use of large anions that inhibit crystallization, and structural modification of PEO. ⁵⁶⁻⁵⁸ **Figure 13** is cartoon representation of several PEO architectures that have been investigated.

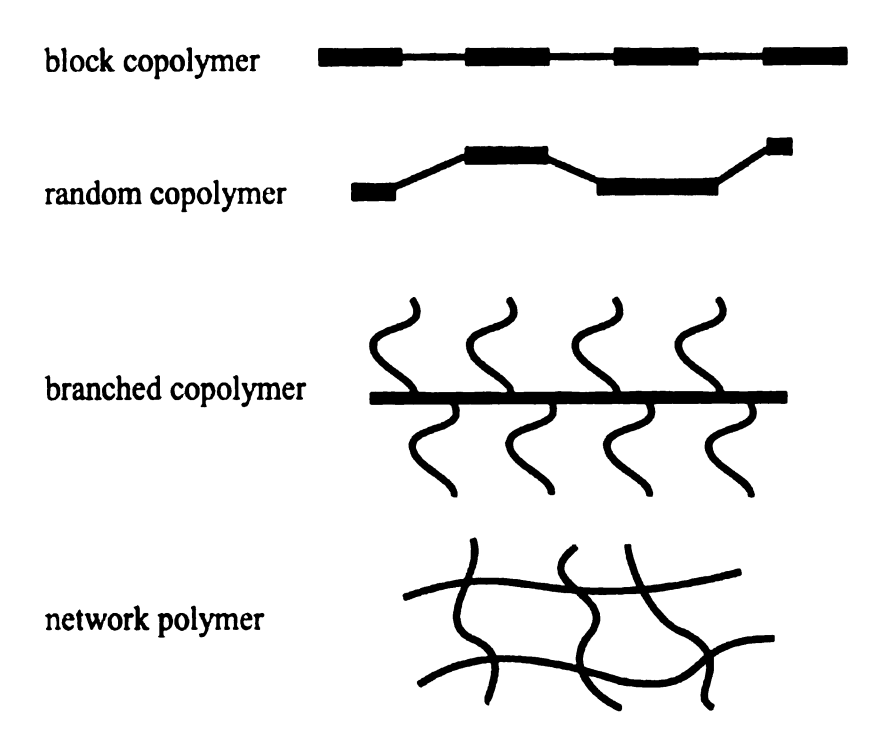


Figure 13. Various polymer architectures designed to decrease crystallization of PEO in SPEs.

These polymer architectures typically include PEO segments, which function as the conducting medium, linked to a highly flexible segment (very low T_g , < -60 °C) or a rigid segment (high T_g). In both cases the added segment must be thermally, chemically and electrochemically stable. For example poly(phosphazene) ($T_g = -70$ °C)⁵⁹ and poly(dimethyl siloxane) ($T_g = -123$ °C)⁶⁰ have been used as the backbone in comb polymers. Room temperature conductivities of 10^{-4} S/cm were observed with poly(methoxyethoxyethoxy phosphazene) (MEEP).⁶¹ Cross-linking⁶² or blending⁶³ of MEEP with PEO resulted in a stable free standing material with no change in conductivity. Use of poly(methyl disiloxanes)^{60,64} and poly(ethylene)s⁶⁵ resulted in conductivities

of 5×10^{-4} S/cm but at the expense of mechanical stability. In addition, the polysiloxane bonds are vulnerable to hydrolysis. Examples of other copolymers and their conductivities are shown in **Table 3**.

		Conductivity	Ref
-{si-o-(CH ₂ CHO) ₄ -}	LiClO ₄	1.5 ×10 ⁻⁴ S/cm	60
$O^{(CH_2CH_2O)_2CH_3}$ P=N+ $O^{(CH_2CH_2O)_2CH_3}$	LiClO ₄	8×10^{-5} S/cm	66
RO PN POR OR RO OR R= (CH ₂ CH ₂ O) ₂ CH ₃	LiSO ₃ CF ₃	7.5 × 10 ⁻⁵ S/cm @55 °C	67

Table 3. Example of SPE polymers and their conductivities.

1.7.1 Gel polymer electrolytes

The preparation of gel electrolytes is much the same as for polymer electrolytes, except that the polymer is swollen in an organic electrolyte. In these two-component systems, the polymer, usually an insulator, provides the desired mechanical properties while ionic conductivity is governed by the organic electrolyte. Feuillade and Perche first demonstrated the use of an aprotic solution containing alkali metal salts as a polymer plasticizer. The resulting gels had ionic conductivities rivaling those of liquid electrolytes. Since then, a wide variety of combinations of polymeric hosts and liquid electrolytes have been described that exhibit dimensional stability and liquid-like ionic conductivities as shown in **Table 4**. An example of a commercialized gel electrolyte is Bellcore's Plion technology, a copolymer of vinylidene difluoride and hexafluoropropylene (PVdF-HFP) swollen in an ethylene carbonate or dimethyl carbonate/LiPF₆ electrolyte. Unlike other systems, the PVdF-HFP polymer is insoluble and relatively rigid and tends to form two phase systems with other solvents or polymers.

Polymer system	polymer host	polymer electrolyte	conductivity (S/cm), 20°C	
plasticized linear PEO	poly(ethylene oxide)	(PEO) ₈ -LiClO ₄ (EC:PC, 20 mol%)	10 ⁻³	
cross linked PEO	poly(ethylene oxide)	(PEO) ₈ -LiClO ₄ (PC, 50 mol%)	8 × 10 ⁻⁴	
PVdF	poly(vinylidene fluoride)	PVdF-LiN(CF ₃ SO ₂) ₂ (EC:PC, 75 wt%)	1.5×10^{-3}	
PEGA	poly(ethylene glycol acrylate)	PEGA/ (LiClO ₄ :PO, 1M)	10-3	
PEI	poly(ethylene imine)	PEI-LiClO ₄	10-3	
PPTA	poly(p-phenylene teraphthalimide)	PPTA- (PC:EC:LiBF ₄), 25:25:0.8 mol%)	2.2×10^{-3}	
acrylates	ethylene glycol dimethacrylate (EGDMA)	EGDMA- (LiClO ₄ :PC, 1M)	2×10^{-3}	
PAN	poly(acrylonitrile)	PAN (EC:PC:LiClO ₄), 38-33:21:8 mol%	10-3	

Table 4. Ionic conductivities of representative gel polymer electrolytes. Taken from reference 70.

Other gel polymer electrolytes can be constructed from hosts such as poly(acrylonitrile) (PAN),⁷¹⁻⁷³ poly(vinylidine fluoride) (PVdF),^{11,15,74} poly(methyl methacrylate) (PMMA),⁷⁵⁻⁷⁷ cellulose ether polymers⁷⁸ and PEO.^{9,19,79} In all of these polymers a small organic molecule is responsible for high ionic conductivity, while the network polymer provides the mechanical support. Although the conductivities of gel electrolytes can exceed 10⁻³ S/cm there are mechanical stability issues at elevated temperatures due to the large volume fraction of liquid electrolyte, which can be as high as 85%.⁸⁰

1.7.2 Filler based electrolytes

Improvements in the mechanical properties of amorphous polymers can be achieved through the addition of inert inorganic fillers. Weston and Steele described the addition of α-Al₂O₃ to PEO/LiClO₄ composites.⁸¹ The primary effect in PEO was inhibition of crystallization, which led to enhanced room temperature conductivity. Additional inert particulate fillers such as ZrO₂, TiO₂, hydrophobic fumed silica, and fiber glass have been introduced into polymer electrolytes. The resulting composite polymer electrolytes show similar effects, decreased levels of polymer crystallinity.⁸² Examples of composite polymer electrolytes are listed in **Table 5**.

Composite	Polymer electrolyte	Conductivity (S/cm), 20 °C
glass polymer composites	$(0.56 \text{ Li}_2\text{S} - 0.19 \text{ B}_2\text{S}_3 - 0.25 \text{ LiI})$ - $((\text{PEO})_6\text{-LiN}(\text{CF}_3\text{SO}_2)_2)$ (18:13 vol.%)	10-4
gel polymer composites	PAN-(PC:EC:LiAsF ₆)-zeolite	10-2
nanocomposites (ceramic composites)	(PEO) ₈ -LiBF ₄ -alumina (10 wt%)	10-4
nanocomposites (ceramic composites)	PEG ₂₀₀ -LiCF ₃ SO ₃ -silica, 20 wt.%	1.5×10^{-3}

Table 5. Some examples of composite polymer electrolytes. ⁷⁰

Raghavan and Khan investigated the rheological properties of hydrophobic fumed silica dispersed in poly(ethylene glycol) dimethyl ethers.⁸³ They found that these composites have weak physical bonds between the silica particles and are shear sensitive. Shearing caused a sharp drop in the viscosity of the composite, which recovered with time. This thixotropic behavior can be an advantage when considering the processing of thin film electrolytes. In another study, Krawiec investigated the relationship between conductivity and the particle size of alumina fillers in PEO/LiBF₄ composites.⁸⁴ The ionic conductivity increased from 10⁻⁵ S/cm for micrometer-sized Al₂O₃ to 10⁻⁴ S/cm for the nanometer-sized particles. These results were ascribed to Lewis acid sites on the particles interacting with the BF₄ anions. Other composites such as glass in PEO₆-LiC(CF₃SO₂)₂ exhibited good mechanical stability and a conductivity of 10⁻⁴ S/cm at room temperature.⁸⁵ More dramatic improvements in mechanical stabilities have been realized using polymerizable alkyl acrylate groups onto the surface of fumed silica nanoparticles. These enable forma-

tion of a permanent three dimensional network throughout a low molecular weight poly(ethylene oxide) matrix, leading to liquid-like ionic conductivities in dimensionally stable electrolytes.⁸⁶

1.8 Proposed Solid Polymer Electrolyte Systems

1.8.1 Molecularly reinforced electrolytes

Flexible polymers assume a coiled conformation in melts and solutions. For crystallization to occur from a polymer melt, the coils must disentangle to be included in the crystal lattice. Because the dynamics of polymer chains is typically slower than the crystallization rate, flexible polymers generally yield semicrystalline materials. In contrast, rod like polymers do not entangle, and instead the steric effects between rigid linear polymers lead to a parallel arrangement in which a transition to an order liquid crystalline system may occur.⁸⁷ Such a transition may be induced by a flow process which forms macroscopically oriented solutions or melts with order that is preserved in the solid state.

Because of their shape, rigid-rod polymers cannot assume the wide range of conformations characteristic of flexible polymers in melts or solutions. Not surprisingly, most such polymers have high melting points and are poorly soluble, making processing and study of these rigid polymers difficult.⁸⁷ Consequently, dissolution into a solvent or melting the polymer requires the disruption of intermolecular interactions. However, the melting points and solubility of rod-like polymers can be depressed by one of the following: 1) Insertion of flexible comonomer units such as an *n*-alkylene chain that acts as a

spacer, 2) Inclusion of bent units of different size which leads to a disruption of the crystal structure, or 3) Addition of flexible side chain substituents to the rigid main chain. In the latter case, the side chains act as bound solvent, decreasing interactions between main chains which leads to a large increase in entropy when dissolving or melting the polymer.⁸⁷⁻⁸⁹

Solid polymer electrolyte materials of high mechanical strength have been obtained using rigid molecules. Ingram and coworkers reported the use of side chain liquid crystal polymer electrolytes based on rigid segments separated by hexa(ethylene oxide) as shown in Figure 14.90

OCHCH₂)₆

Figure 14. Mesogenic polymers synthesized by Ingram and coworkers. Both 1 and 2 have predominantly poly(ethylene oxide) backbones. Structures 1 and 2 differ in that in 1, pendant mesogenic groups are attached to the chain via flexible alkyl spacers.

The T_g of 1 is 5 °C while that of 2 is -36 °C. As expected polymer 1 exhibits liquid crystalline behavior and undergoes a smectic-isotropic transition at 44 °C while polymer 2 does not exhibit any transitions other than T_g . Upon addition of LiClO₄ the T_g of both polymers increases by 20 °C and the clearing temperature of polymer 1 increases to 52 °C. Both polymers have similar conductivities (~10⁻⁷ S/cm at 30 °C), however the ionic conductivity of polymer 2 shows a greater temperature dependence.

Wegner and Meyer reported SPEs based on rigid polymers shown **Figure 14c.**^{91,92} The poly(*p*-phenylene) main chain is highly rigid due to the 1,4 linkages of the aromatic rings. As shown in **Figure 15** each repeating unit consists of a disubstituted aromatic ring and an unsubstituted phenyl ring that acts as a spacer.

$$\begin{array}{c|c} OR_x & OR_y \\ \hline R_xO & R_yO \end{array}$$

$$R_x = (CH_2CH_2O)_xCH_3 \qquad 2 \le x \ge 6$$

$$R_y = (CH_2CH_2O)_yCH_3 \qquad 2 \le y \ge 6$$

Figure 15. PPP(EO)_{x/y} reported by Wegner and Meyer in reference 92.

Through temperature dependant X-ray powder diffraction studies, they demonstrated that these polymers adopt a planar comb structure in which the PPP backbones are arranged in layers separated by the liquid ethylene oxide matrix. The resulting lamellar phases, described as a smectic B-type structure, remains unaltered to 150 °C, at which point a phase

transition leads to a lower order liquid-crystalline phase.⁵⁵ When cast from solution, the PPP layers orient parallel to the film plane in small local domains. As mentioned previously, the side chains act as bound solvent, and so it is not surprising that these polymers have low $T_g s$ (~ -50 °C) which decrease as the side chains increase in length. The resulting ionic conductivities are on the order or 10^{-4} S/cm at room temperature.

1.8.2 Syntheses of rigid polymer systems

Controlled synthetic methods are necessary to produce ideal rigid polymer structures. Since any defects or side reactions can lead to a dramatic decrease in the desired properties, the methods employed must be regiospecific and lead to stable products. As shown earlier, flexible links in a rigid rod backbone can dramatically alter the polymer characteristics. The solubilities of most rigid polymers decrease as the degree of polymerization increases. Traditionally, poor solubility has made it difficult to synthesize poly(p-phenylenes) (PPP). For PPP, the synthetic route must employ methods that allow for exclusive formation of the para aromatic linkages and high molecular weights.

One synthetic route to these polymers utilized an electrochemical coupling of aromatic monomers to afford polyphenylenes on inert electrodes such as platinum. 93,94 The oxidative coupling and reduction of aryl halide monomers affords small quantities of polymer that are structurally irregular, containing a substantial mixture of *ortho*, *meta* and *para* aromatic linkages. While many catalytic methods such as Friedel-Crafts synthesis and polymerization of p-dibromobenzene with lithium quickly yield polyphenylenes, these materials are fraught with defects in the aromatic linkages affording nonlinear polymers.

Improvements were obtained through the use of the Ullmann homocoupling of 1,4diiodobenzene using activated copper powder affording the correct 1,4 substitution pattern throughout the polymer chain. 95-97 However, the severe conditions for this reaction limited its scope of application to monomers that contained functional groups that can tolerate the prolonged reaction temperatures, > 200 °C. Milder conditions and greater chemoselectivity have been realized through the use of transition metal catalysts. 98-104 These methods afford PPP in high yields and the para linkage with a high degree of fidelity. Specifically, palladium and nickel catalyzed aryl coupling reactions are tolerant of a wide variety of functional groups which allows for the synthesis of a wide range of substituted PPPs. The catalytic polymerization involves three major steps: oxidative addition of the arylhalide onto the active metal center, a transmetallation step to add a second aryl group and eliminate the halides, and reductive elimination to form the aryl – aryl bond of the product. Due to the high efficiency and number of turnovers, these polymerizations can often be conducted at ~5 mol% catalyst loadings. However, these systems are sensitive due to the in-situ formation of zero valent metals. Thus impurities such as moisture, air and protic substances must be excluded from the reaction mixture.

1.8.3 Single ion solid polymer electrolytes

Solid polymer electrolytes prepared by dissolving lithium salts in a host suffer from cell polarization and loss of conductivity at high concentrations. These effects contribute to decreased lifetime and efficiency of the electrochemical cell. It is widely accepted that the formation of ion clusters are the cause of both phenomena.^{2,19,80} These aggregates of anions and cations form ionic crosslinks between polyether chains by strongly coordinat-

ing to the ether oxygens. Indeed the observed ionic conductivity is not simply due to the mobility of single ions, but includes contributions from triple and higher ionic aggregates with unequal numbers of positive and negative charges. Formation of aggregates at high salt concentrations reduces the number of charge carriers available to carry current and lowers efficiency. These drawbacks can be averted by a) immobilizing the anion within the electrolyte, b) increasing the size of the anion such that its mobility is significantly reduced, or c) adding Lewis acids, usually in the form of a ceramic filler that binds to anions and reduces their mobility. However immobilizing the anion causes an approximately order of magnitude loss in conductivity, 106-108 which reflects the participation of the anion in the conduction mechanism. This is better understood through consideration of ion transference numbers, the fraction of the total ion current carried by a charged species. Mathematically the transference number is defined as

$$t_{+} = 1 - t_{-} = \frac{z_{+}D_{-}}{z_{-}D_{-} - z_{-}D_{-}}$$
 (1.27)

where z_i is the charge of the carrier and D_0^i is the diffusion constant associated with that species. In any given system $\sum [t_+ + t_-] = 1$. Typical experimental results for the lithium ion transference numbers in polymer electrolytes range from 0.2 to 0.4, and thus the majority of the current is carried by anions during discharge of a battery. Since the anions do not intercalate into the electrodes, they deposit at the electrodes and form a space charge, thereby inducing polarization of the cell. Obviously, immobilization of the anions eliminates a large fraction of the ionic conductivity directly leading to the decreased ionic conductivity observed in single ion conductive polymer electrolytes. In many cases, however, increased cell life and efficiency outweigh the loss in conductivity.

The earliest examples of anion immobilization in electrolytes was reported by McIntyre et al., 109 Tsuchida et al. 110 and Shriver et al. 111 McIntyre reported ionic conductivities of poly(lithium 2-sulphethyl methacrylate) (PSEM-Li) and poly(lithium 2-(4-carboxyhexafluoro-butanoyl-oxy) ethyl methacrylate) (PCHFEM-Li) in comparison with dilithium hexafluoroglutarate (LiHFG). Tsuchida reported single ion conduction in poly(oligo(oxyethylene methacrylate)-co-(alkali-metal methacrylates), while Shriver investigated poly(styrene sulphonates) to achieve single ion conduction. In all cases the ionic conductivities ranged from 10-6 to 10-5 S/cm at 30 °C, however, Tsuchida was able to report lithium ion transport numbers of 0.99. Since then, there have been many investigations aimed at achieving higher ionic conductivities (> 10-5 S/cm at room temperature) in single ion conductor SPEs. 112

Polymer name	Polymer Structure			
poly(lithium 2-sulphethyl methacrylate)	sO ₃ -Li+			
poly(lithium 2-(4-carboxyhexafluoro-butanoyloxy) ethyl methacrylate)	O (CF ₂) ₃ COO Li ⁺			
dilithium hexafluoroglutarate/PEG	LiOOC—(CF ₂) ₃ -COOLi			
poly(oligo(oxyethylene methacrylate)-co- (lithium methacrylates)	O OLi O			
poly(sodium styrene sulphonate)	SO ₃ Na			

Table 6. Examples of early polymer systems with immobilized anions designed to bring about single cation conductivity.

One class of electrolytes that has received a great deal of attention are those described as composite polymer electrolytes (CPEs) which incorporate inorganic or ceramic particulates in a polymer electrolyte. Aside from increased mechanical stability and ionic conductivity, the addition of such particles stabilizes the electrode/electrolyte interface. Incorporating a small molecule solvent as a plasticizer in a polymer electrolyte increases

the segmental motion of the host polymer and the addition of nanoparticles appears to do the same, giving rise to an straight line Arrhenius-type plot. 112-114 It is thought that the nanoparticles inhibit the reorganization of the polymer chains through Lewis acid - base interactions between the surface of the nanoparticles and the polymer chains. 115 Scrosati et al. suggested that the enhancement of the ionic conductivity and lithium ion transference number is due to the formation of pathways at the surfaces of the nanoparticles along which the lithium ions would follow. 116 Furthermore, these CPEs can achieve lithium ion transference numbers that approach unity if the inorganic nanoparticles are negatively charged. For example, Shriver et al. 117-120 reported the use of siloxyaluminate polymers capable of achieving 10⁻⁵ S/cm at 25 °C and lithium ion transport numbers of The material is comprised of a siloxyaluminate polymer main chain, with oligo(ethylene oxide) side chains. It is thought that due to the delocalization of anionic charge over the Si-O $(p-d)\pi$ system and the presence of substituents that the lithium cations would be inhibited from tightly pairing with the negatively charged backbone and thus have a higher conductivity. 121 However, plots of conductivity versus 1000/T (K⁻¹) revealed that these systems behave no differently that neat PEO/LiClO₄ systems when the side chains were relatively long, 1000 and 2000 g/mol. The conductivity in these cases decreases in a linear fashion until crystallization occurs, at which point the conductivity dramatically reduces to 10⁻⁸ S/cm⁻¹. Crystallization was not observed for side chains with molecular weights of 400 or 600 g/mol.

Fedkiw et al. 108 reported recently lithium hectorite based CPEs in which they achieved lithium ion transference numbers of 0.98 and a conductivity of 2×10^{-4} S/cm⁻¹ at room

temperature. Hectorite belongs to a class of layered clays known as smectites and are characterized as a sandwich structure of cations trapped between negatively charged plates. These platelets are well known to disperse in water and other solvents to create a gelled system. By dispersing lithium hectorite in carbonates such as ethylene carbonate or propylene carbonate a mechanically stable system with high ionic conductivities was achieved.

A similar approach would be to disperse modified inorganic fillers as a lithium salt in low molecular weight poly(ethylene oxide). By doing so, issues of electrolyte decomposition are avoided. Baker and Fedkiw *et al.* ¹²² demonstrated that incorporation of surface modified silica nanoparticles into poly(ethylene glycol) dimethyl ether of 500 g/mol) (PEG-dm 500) forms CPEs with a high degree of mechanical stability, electrolyte – electrode interfacial stability, and high ionic conductivities on the order of > 10⁻³ S/cm at room temperature. In a similar fashion to the lithium hectorite CPE system, silica nanoparticles were modified by attaching a lithium sulfonamide salt onto the surface and dispersing in PEG-dm 500. The details of this study are examined in chapter 4.

Chapter 2

2 Synthesis of Substituted Poly(p-phenylene)s with Oligo(ethylene oxide) Side Chains

2.1 Introduction

Our interests in novel solid polymer electrolytes have led us to consider ethylene oxide substituted poly(p-phenylene)s (PPPs), since the rigid backbone of PPP would endow an electrolyte with thermal and mechanical stability, and the pendant ethylene oxide segments would support ionic conductivity. Although PPP itself is insoluble and unprocessable, the addition of flexible side chains to PPP's rigid backbone has proven to be an extremely effective procedure for obtaining tractable and fusible materials. Such materials often exhibit properties such as pronounced thermochromism and solvatochromism, 123 thermotropic and lyotropic liquid crystallinity, 124-128 and structural self-assembly. 129-132 Because of the strict 1,4 connectivity of the benzene ring in PPP and the ability to vary the length of the oligo(ethylene oxide) side chains, the ethylene oxide substituted poly(p-phenylene)s are an ideal system for studying the structure property relationships of rigid macromolecules. If we view the rigid PPP backbone as a reinforcing element and the oligo(ethylene oxide) side chains as bound solvent, these materials can be regarded as "molecular composites" of two components dispersed at the molecular level. 92,133-137

There have been several reports of the synthesis of poly(p-phenylene)s substituted with ethylene oxide side chains. Most recently Lère-Porte et al. used a Stille coupling to synthesize a thienylene-dialkoxyphenylene copolymer with diethylene glycol monomethyl ether side chains. Johansson et al used palladium-catalyzed coupling to prepare a related system, oligo(ethylene oxide) substituted polythiophenes. These high molecular weight polymers were used for light emitting electrochemical cells. Wegner et al. reported the synthesis of poly(p-phenylene)s with oxyethylene side chains via a Stille-like palladium mediated coupling reaction. These high molecular weight polymers self assemble into lamellar sheets in which the rigid backbones are aligned with respect to each other.

PPP-EO_m

Colon et al.¹⁴¹ first reported the use of Ni(0) to synthesize biaryls from aryl chlorides in quantitative yield at mild temperatures and in short reaction times. They extended this catalytic method to the polymerization of bis(aryl chlorides) to give poly(arylene ether sulfone)s.¹⁴² Udea et al. used the same method to synthesize poly(arylene ether ketone)s¹⁴³ and poly(thiophene)s.¹⁴⁴ Ni(0)-catalyzed coupling reactions have also been used to prepare soluble substituted polyphenylenes. Sheares et al.^{145,146} synthesized substituted poly(2,5-benzophenone)s, while Percec et al.^{147,148} reported the synthesis of various soluble aryl and alkyl substituted polyphenylenes.

Since esters are stable under the conditions of the Ni(0)-catalyzed coupling reaction, a series of ethylene oxide substituted poly(p-phenylene)s are readily available by the polymerization of the corresponding oligo(ethylene oxide) 2,5-dichlorobenzoates. The modular synthesis of the monomers and the ready access to their polymers via Ni(0) catalyzed coupling encouraged us to investigate a series of poly(p-phenylene)s (PPP-EO_m) substituted with oligo(ethylene oxide) monomethyl ethers with various degrees of polymerization (m). The purpose of this study is to understand the effect of side chain length on the mechanical, thermal and chemical properties of these polymers. Herein, we report the results of the synthesis and characterization of our monomers and their corresponding polymers.

2.2 Results and Discussion

2.2.1 Monomer synthesis

The monomers were easily synthesized from 2,5-dichlorobenzoic acid. This modular route offers the flexibility of preparing a series of monomers by simply using various ethylene glycol monomethyl ethers. Only alcohols 3a-3d are commercially available in monodisperse form, and thus alcohols 3e-3h were synthesized using a modified version of a literature procedure. The monomers were purified by different methods depending upon their boiling points. Monomer 4a was recrystallized from methanol, and short side chain monomers 4b-4d with lower boiling points were vacuum distilled to yield clear oils. Since monomers with longer side chains thermally decomposed prior to boiling, monomers 4e-4h were purified by column chromatography.

Scheme II. Synthesis of monomers 4a - 4k

2.2.2 Polymerization

The monomers were polymerized utilizing a nickel-catalyzed aryl coupling reaction to yield substituted poly(p-phenylene)s **5a-5k**. Originally proposed as an inexpensive, high-yield route to substituted biphenyls^{142,150,151} without terminating side reactions, and with tolerance to a variety of functional groups, it provided an efficient method for the polymerization of dichloro aromatic compounds.^{104,142,151} p-Phenyl linkages in the resulting polymers were ensured by starting with p-dichloro-substituted aryl monomers. The ac-

tive catalytic species, a Ni(0) complex, is generated *in situ* by the reduction of NiCl₂ using finely granulated zinc. Upon mixing of all reaction components, the polymerization solution becomes pink and develops into a dark red color shortly after heating due to the formation of Ni(0). Contamination of the polymerization by oxygen causes the developing color to change to green within the first minutes of the reaction, indicating oxidation of active Ni(0) catalyst to form black NiO. Proton sources terminate the growing polymer chain and can be present as residual moisture in solvent, solvent decomposition products, and in monomers which may contain high boiling alcohols carried over from the synthesis of the monomer. Water was eliminated by vacuum distillation of solvent over 3Å molecular sieves prior to use, while residual alcohol in the monomers was removed by running toluene solutions of the monomer monomers through a short pad of oven-dried silica gel inside the dry box, and/or through an azeotropic reflux of the monomer in benzene.

2.2.3 Polymer characterization

Molecular weights obtained by size exclusion chromatography and calibrated relative to polystyrene standards may afford misleadingly high molecular weights due to the difference in the hydrodynamic volumes (volume occupied by the polymer in a solvent) for chemically different polymers of the same molecular weight. For a random coil such as polystyrene and the linear, rod-like PPP-EO_m system, the difference in hydrodynamic volumes is a consequence of the different end to end distances of the two polymers. For a random coil, the end to end distance is $\sqrt{nl^2}$ where n is the number of repeat units and l is the length of each repeat unit, while that of a rigid linear rod is simply nl. Hence the

volume occupied by a rod-like polymer in solution is larger than that of a random coil of the same molecular weight.¹⁵²

Light scattering provides an absolute measure of M_w , the weight average molecular weight. Experimentally, the excess scattering, I_{θ} , (scattering corrected for scattering by solvent) of a polymer solution per unit volume at angle θ is measured as a function of concentration and angle. The Raleigh ratio, defined as I_{θ}/I_{0} where I_{0} is the intensity of the incident light, can be expressed in terms of M_{w} as shown in equation (2.1)

$$R(\theta) = K * c(1 + \cos^2 \theta) M_{w}$$
 (2.1)

where c is the concentration of the solute molecules (g/mL) and K* is a constant. $K^* = 4\pi^2 (dn/dc)^2 n_0^2 / (N_A \lambda_0^4)$, where n_0 is the refractive index of the solvent, N_A is Avogadro's number, λ_0 is the vacuum wavelength of the incident light, and dn/dc is the specific refractive index increment, which describes the change in refractive index of the polymer solution with solute concentration.

The data from a light scattering experiment are usually analyzed using a Zimm plot where the quantity $K*c/R(\theta)(1+\cos^2\theta)$ is plotted as a function of both concentration and θ . Simultaneous extrapolation of the data to zero θ and zero concentration gives $1/M_w$ as the y-intercept. When light scattering is used as a detector in size exclusion chromatography, a concentration detector such as refractive index or UV-vis detector provides the concentration information as well as the molecular weight distribution. The molecular weight distribution can be analyzed to give the polydispersity index (PDI), M_w/M_n Since

 M_w is directly measured by light scattering, M_n can be easily calculated. The definitions of M_n and M_w are shown below in equations (2.2) and (2.3)

$$M_{n} = \frac{\sum_{i} n_{i} M_{i}}{\sum_{i} n_{i}} = \frac{\sum_{i} c_{i}}{\sum_{i} c_{i} / M_{i}}$$
(2.2)

$$M_{w} = \frac{\sum_{i} n_{i} M_{i}^{2}}{\sum_{i} n_{i}} = \frac{\sum_{i} c_{i} M_{i}}{\sum_{i} c_{i}}$$
 (2.3)

The only polymer-specific quantity that must be known for light scattering is dn/dc, the specific refractive increment. Values of dn/dc for several polymers are reported in the literature, however since the PPP-EO_m had not been synthesized previously, the value of dn/dc must be determined experimentally. dn/dc was measured for PPP-EO_m where m = 0,1, 3, 5, <12> and <45>. The dn/dc values for the rest of the polymers in the series were calculated from the weighted average of PEO and PPP-EO₀ in the polymer, as shown in equation (2.4)

$$\frac{dn}{dc} = W_A \frac{dn}{dc} + W_B \frac{dn}{dc}$$
(2.4)

$$A = - CH_3$$

$$B = (OCH_2CH_2)_m$$

where component A is defined as PPP-EO₀ and component B is PEO. A plot of the experimentally determined values of dn/dc as a function of the weight fraction of PPP-EO₀

in the polymer (**Figure 16**) yields a line where the left and right y-intercepts correspond to the dn/dc of PPP-EO₀ and PEO, respectively. The linearity of the data validates the use of equation (2.4). **Figure 17** compares the experimental dn/dc values with those calculated using equation (2.4).

As noted above, a UV-vis detector provides the concentration of polymer analyte in solution for the calculation of M_w . The extinction coefficient (ϵ) of each polymer can be obtained in the same manner as the specific refractive increment as shown in equation (2.5)

$$\varepsilon_{AB} = W_A \varepsilon_A + W_B \varepsilon_B \tag{2.5}$$

using the same definitions for A and B as in equation (2.4). Since ε for ethylene oxide is zero in the visible part of the spectrum, ε should simply reflect the weight fraction of the PPP component in PPP-EO_m polymers. Values of ε were measured for PPP-EO_m where m = 0,1,3,5,<12> and <45>. A plot of ε of the polymer versus the weight fraction of PPP in each polymer (**Figure 18**) was linear with an intercept of zero and the extinction coefficient of PPP as the slope. The ε values for the rest of the polymers in the series were calculated from the weighted average of PEO and PPP-EO₀ in the polymer, using equation (2.5).

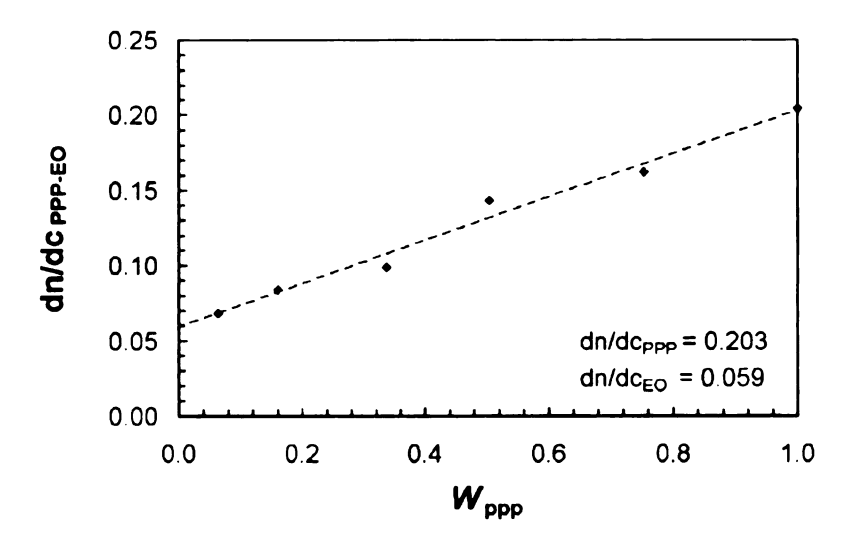


Figure 16. Extrapolation of dn/dc of PPP-EO_m as a function of PPP weight fraction to obtain dn/dc of PPP-EO₀.

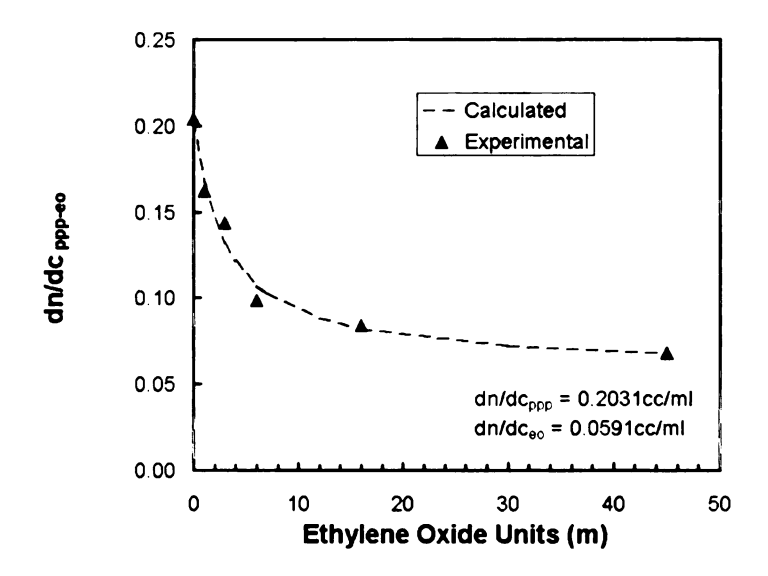


Figure 17. Comparison of calculated values of dn/dc for PPP-EO_m with experimentally obtained data.

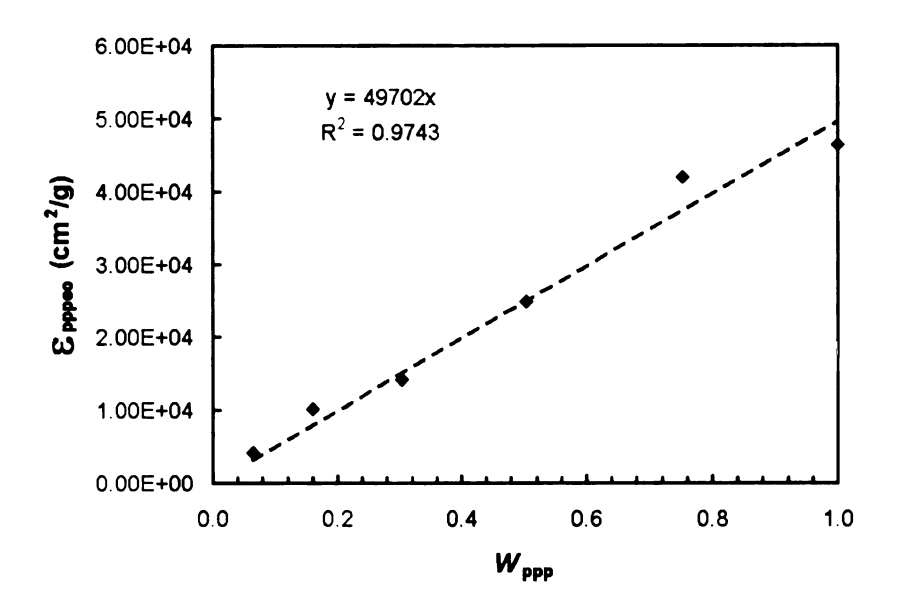


Figure 18. The extinction coefficient (ϵ) of PPP-EO $_m$ as a function of PPP weight fraction

	GPC ^a				Light Scattering*				DSCb	
m	M _w	X _n	PDI	dn/dc	M _w	X _n	PDI	Tg	T _m	
0	17,613	68	1.9	0.203	6,124	32	1.43	37		
1	59,207	117	2.8	0.168	30,120	135	1.25	33		
2	19,330	59	1.5	0.146	15,520	52	1.34	-5		
3	65,795	94	2.6	0.132	48,790	107	1.71	-34		
4	22,738	37	2.0	0.121	15,430	41	1.21	-29		
5	23,008	29	2.2	0.114	18,570	35	1.48	-30		
6	32,782	33	2.5	0.108	31,710	61	1.30	-44		
7	20,324	22	2.1	0.103	17,870	29	1.40	-51		
<12>°	29,079	21	2.1	0.088	25,770	22	1.73	-43		
<16>°	22,776	15	1.8	0.082	20,920	19	1.29	-54	22	
<45>°	46,860	13	1.8	0.068	46,590	18	1.20	-53	49	
	1									

Table 7. Properties of PPP-EO_m polymers. a) Molecular weight data were obtained from GPC measurements in CHCl₃ using a light scattering and a refractive index detector. b) T_g and T_m values were obtained from MDSC and DSC measurements. c) The brackets < > indicate samples with polydisperse EO chains with average degrees of polymerization = m.

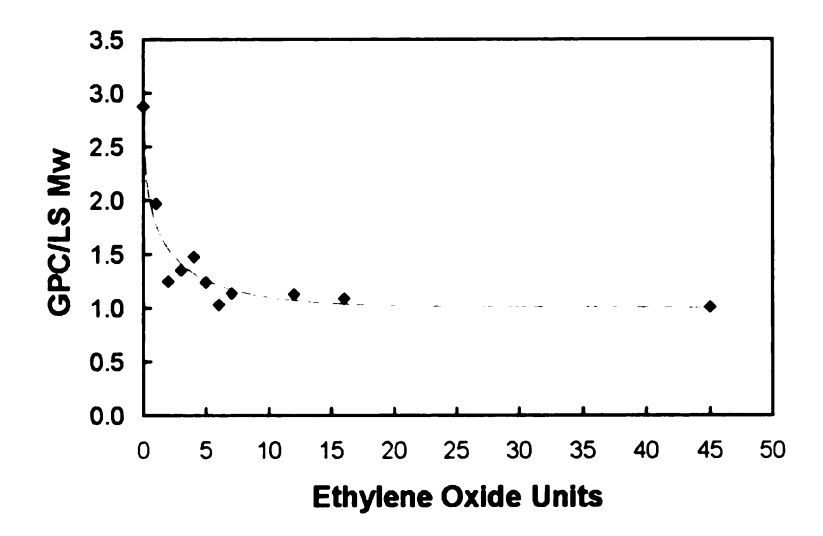


Figure 19. Plot of the ratio of molecular weights obtained by GPC to those obtained by LS as a function of the number of ethylene oxide units in the side chains of PPP-EO_m polymers.

Table 7 presents representative molecular weights obtained from size exclusion chromatography coupled with a light scattering detector. As noted previously, the GPC values obtained for PPP-EOm polymers with short side chains should be higher than those obtained from light scattering. However, both techniques begin to agree at approximately m = 6 where the ratio of the M_w values is almost 1. This suggests that in dilute solution, the polymers with long side chains behave as a random coil of poly(ethylene oxide) with a rigid core. These results agree with characterization data from similar PPP based polymers. 153,154

2.2.4 Differential scanning calorimetery (DSC)

Related PPP systems with short ethylene oxide chains are reported to show glass transition (T_g), melting (T_m) and in some cases crystallization (T_c) transitions. These polymers differ from the those of this study in that the PPP backbone consists of disubstituted aromatic rings spaced with unsubstituted phenyl rings, and possess polydisperse oligo(ethylene oxide) chains. Shown in Figure 20 are DSC scans of the PPP-EO_m polymers with long side chains. No distinct thermal transitions were observed for polymers with m < 12 (5a-5h) using conventional DSC. However, modulated DSC did reveal glass transitions for the short side chain polymers which show a near-linear decrease in T_g from 40 to -60 °C as the side chain length increases (Figure 21). The polymer melting points show similar behavior, with the melting point of the long side chain polymers approaching that of poly(ethylene oxide). Both the T_g and T_m data indicate the increasing "PEO character" of the polymers as m increases.

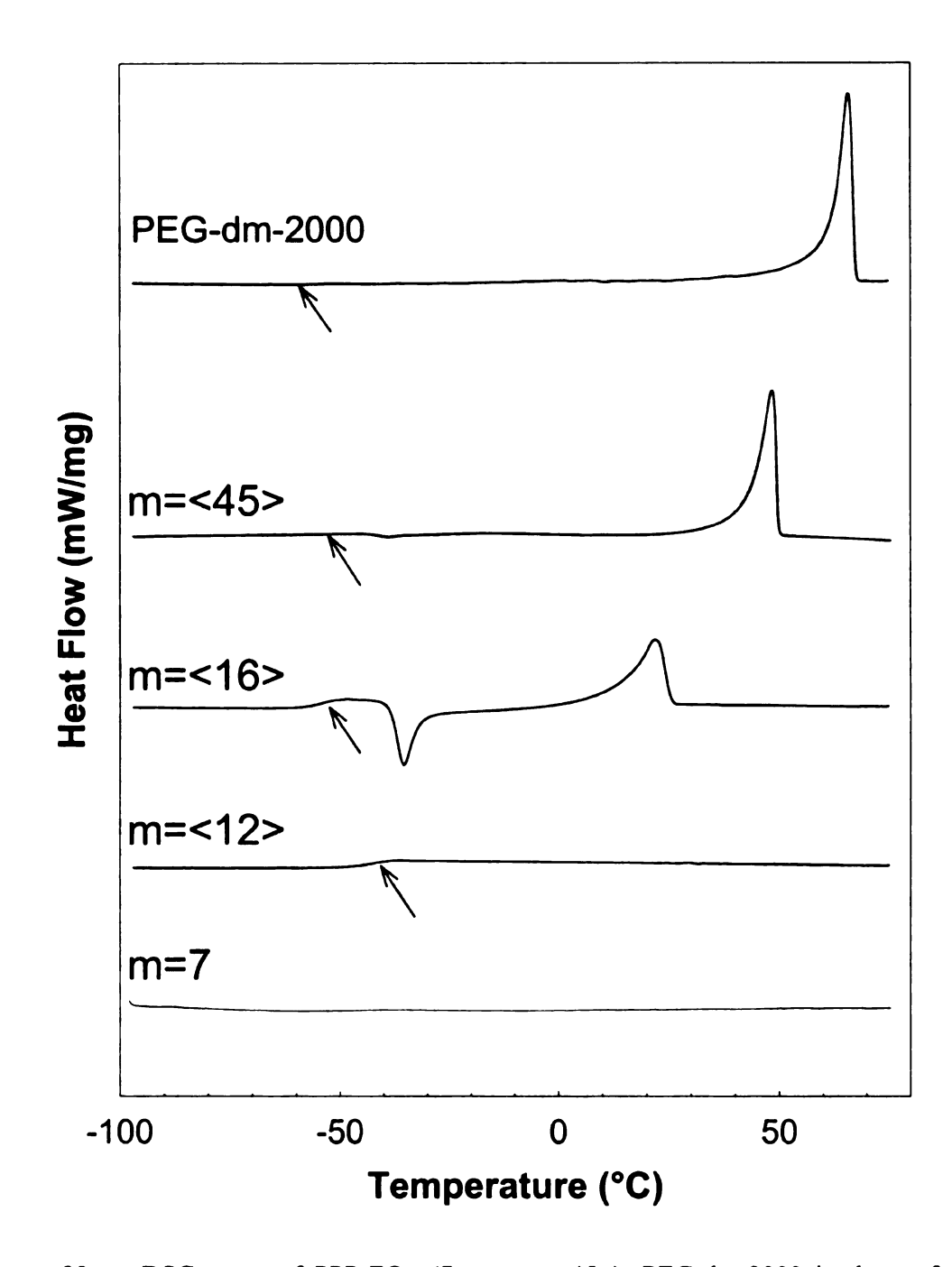


Figure 20. DSC scans of PPP-EO_m (7 < m > <45>); PEG-dm-2000 is shown for comparison. The data are second heating scans, taken at 10 °C/min after quenching the sample from 180 to -100 °C. The arrows mark the T_g transitions.

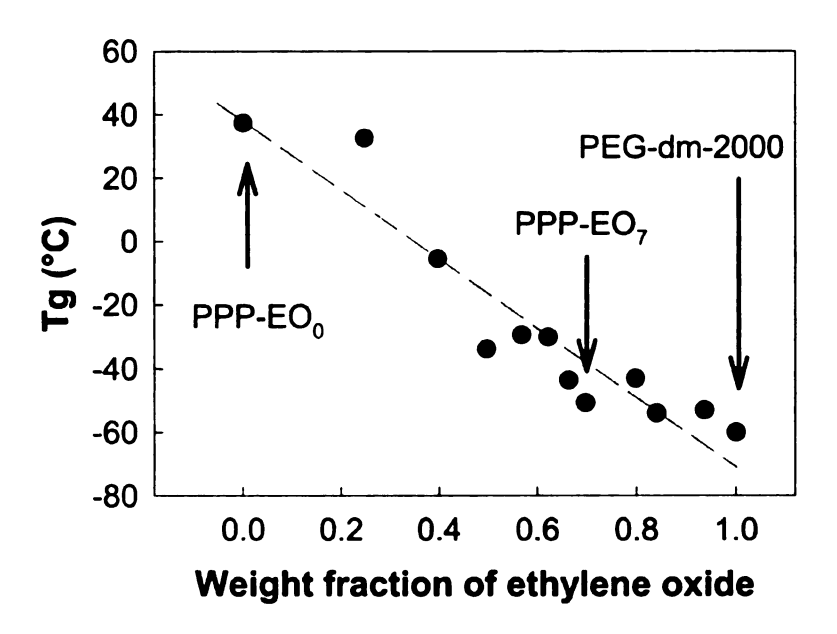


Figure 21. The relationship between T_g and the weight fraction of PEO in the side chains. The dashed line is a least squares fit to the data.

2.2.5 Thermogravimetric analysis (TGA)

Thermogravimetric analysis reveals the dual nature of the PPP-EO_m As seen in Figure 22 the PPP-EO_m polymers exhibit similar thermal profiles, however, the onset of degradation decreases as the side chains become longer. Since PPP degrades in inert atmospheres to a char that is stable to 800 °C,¹⁵⁶ the observed weight loss at T < 500 °C must correspond to the degradation of the PEO side chain. A simple model that assumes loss of the side chain and the ester group matches the weight loss data well. PEO is thought to degrade to dioxanes through a radical process, and since PPP-EO_m polymers with long side chains have a degradation profile that is nearly identical to that of PEO, they too may degrade by the same mechanism. In contrast, PPP-EO_m polymers with short side chains show enhanced stability, which may reflect the decreased number of sites to support

PEO-like degradation. Thus de-esterification and decarbonylation must be more important in the degradation of short side chain PPP-EO_m polymers.

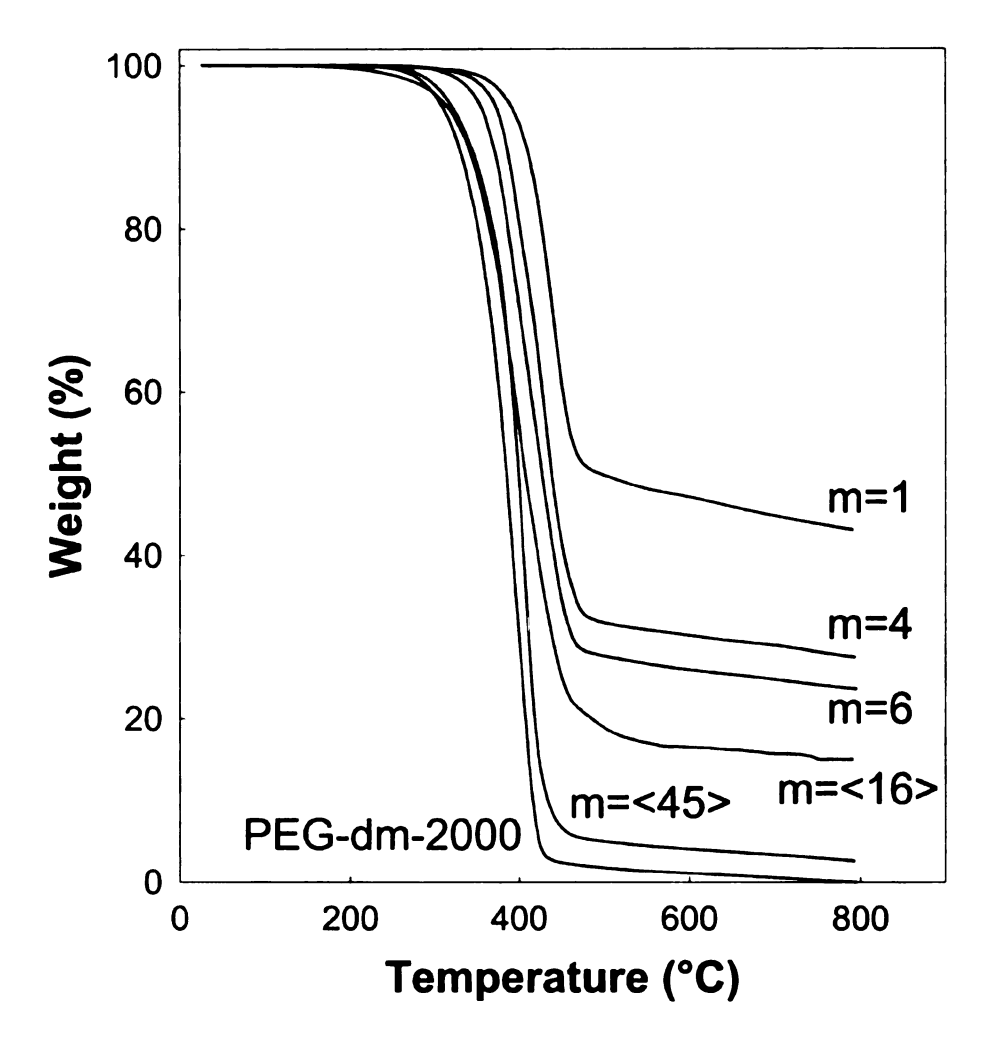


Figure 22. TGA scans of PPP-EO_m polymers. Polymer samples were dried under vacuum at $100\,^{\circ}$ C overnight, equilibrated under N₂ at $80\,^{\circ}$ C for 12 hrs, and then heated under N₂ at $10\,^{\circ}$ /min.

2.2.6 X-ray diffraction (XRD)

Figure 23 shows X-ray diffraction data for the PPP-EOm polymers. Scans of PPP-EO2 and PPP-EO3 show a peak at approximately $2\theta = 5$ (d = 15Å) that disappears as the side chain increases in length. The same peak has been observed for PPPs disubstituted with triethyleneoxide monomethyl ether side chains, and has been assigned to the spacing between the rigid polymer backbones. ^{11,13,14} The loss in structural periodicity reflects the transition from a PPP-like structure to one more characteristic of PEO. As the side chains lengthen, steric limitations to side-chain crystallization are eased and the chains eventually organize in a structure characteristic of PEO. The scattering data for PPP-EO<45> are nearly identical to that of PEO.

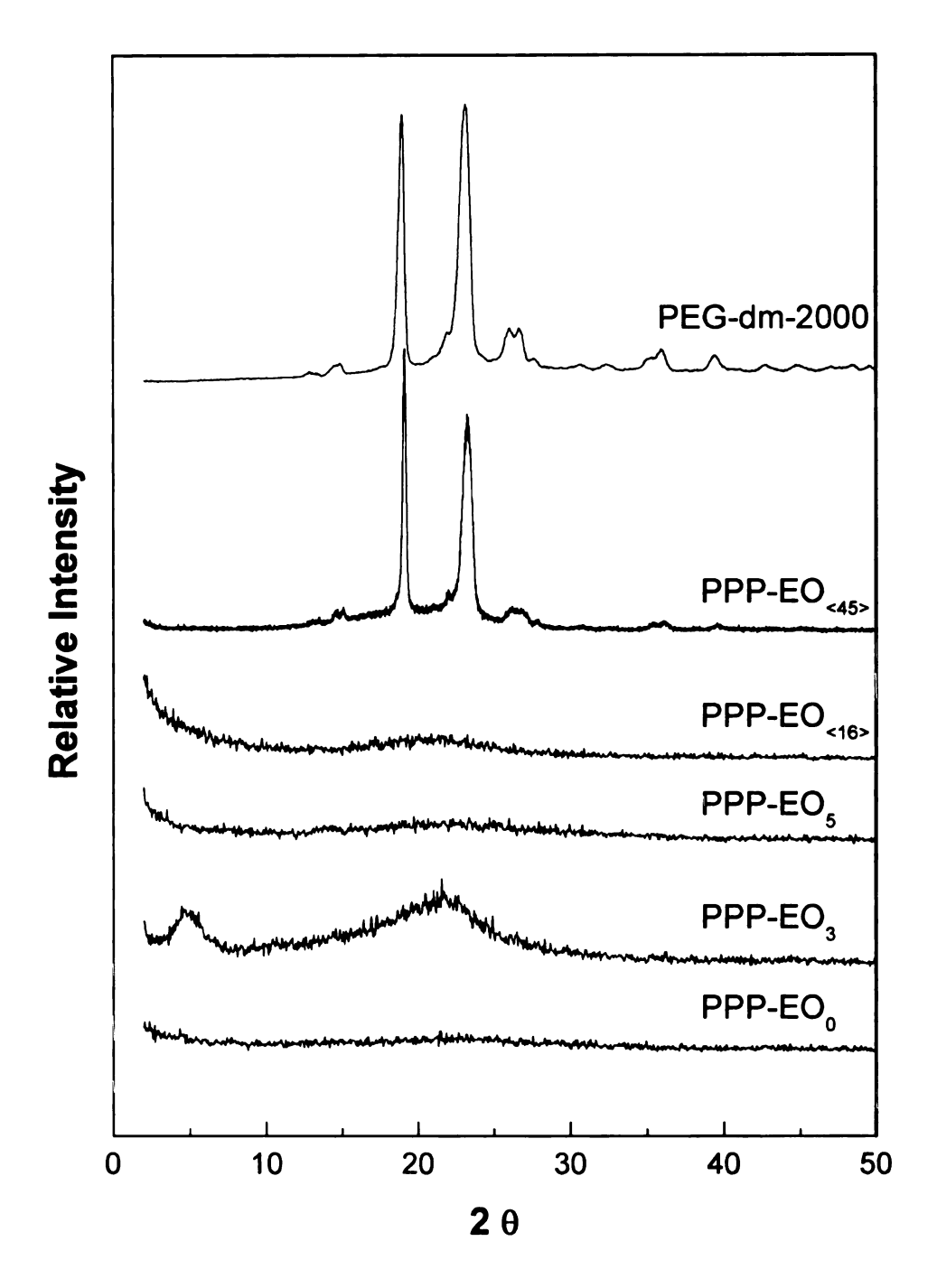


Figure 23. Room temperature X-ray powder diffraction scans of PPP-EO_m polymers. All scans were collected at a rate of 0.05 2θ /min over a range of $2\theta = 1-50^{\circ}$.

Comb and brush structures can be proposed for the structures of these polymers. In the first, the backbone phenyl rings form a nearly flat ribbon (small dihedral angle between each ring), with side chains extended from the back bone to give an overall flat structure. The comb could be either single-sided (normal comb) or double-sided (teeth project from both sides of the backbone) The second model is akin to a polymer brush, in which the dihedral angle between rings is large and the side chains radiate from that center. We propose that the dominant solid state structure must be comb-like, while a brush architecture makes more sense for the structure in solution.

The fluorescence data argue for a brush architecture in solution. Figure 24 shows that the fluorescence data for the PPP-EO_m series are similar with only small shifts in λ_{max} . Thus the effective conjugation length is the same for each polymer, and the average dihedral angle between rings in the backbone must also be similar. If we compare the shift in λ_{max} for the polymers to that of a model repeat unit, methyl benzoate (398 nm), the similar λ_{max} values argue for limited conjugation along the backbone and large dihedral angles. However, conjugation is manifested in the dramatically increased luminescence intensity for the polymers compared to the monomers. (The fluorescence intensities for the polymers and monomers are normalized such that the number of rings in each sample is constant). We also noted an increase in fluorescence intensity with increases in the length of the EO side chain (inset to Figure 10). These effects are likely due to the side chains increasingly acting as the "solvent" for the PPP backbone in the fluorescence experiments.

Raman spectroscopy provides some insight into the solid state structure. Hernandez et al. ¹⁵⁷ and Lefrant et al. ¹⁵⁸ used Raman spectroscopy to interrogate the structure of PPP polymers. **Figure 25** shows Raman spectra several PPP-EO_m polymer films and PEG-dm-2000. The prominent peak at 1608 cm⁻¹ is due to 'in plane' asymmetric bending, which is sensitive to conjugation and hence the dihedral angle between adjacent rings. According to Pimenta, Mathews et al. ¹⁵⁹ the Raman shift of the 'planar' form of PPP is 1601 cm⁻¹, while the values calculated for helical PPP with 20° and 50° twists are 1630 and 1635 cm⁻¹ respectively. The observed 1608 cm⁻¹ transition is thus consistent with a nearly planar PPP backbone.

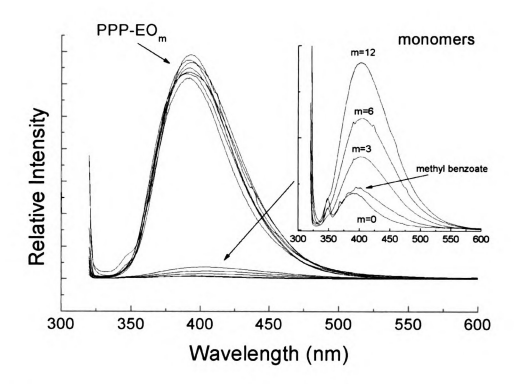


Figure 24. Fluorescence spectra of PPP-EO_m and their corresponding monomers (inset). Data were collected at room temperature in chloroform using an excitation wavelength of 313 nm.

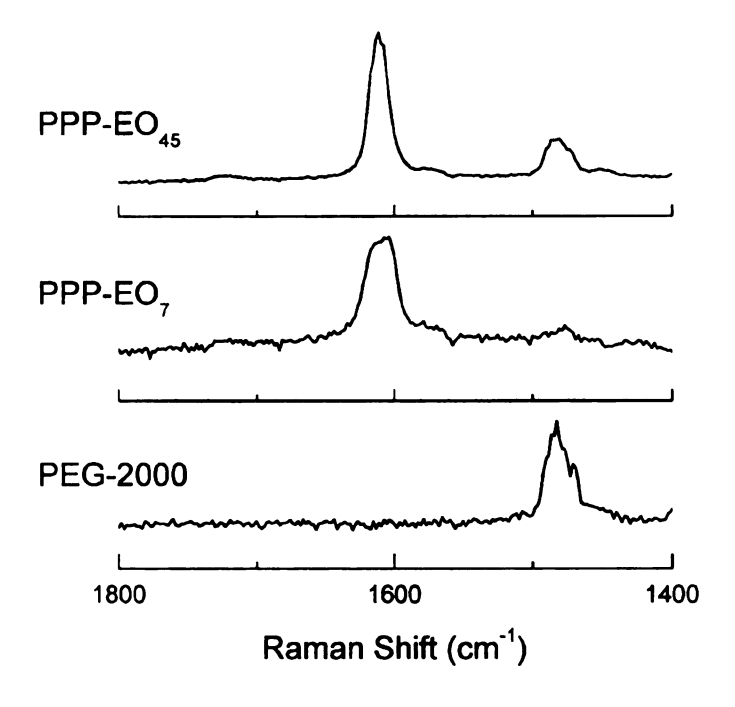


Figure 25. Solid-state Raman spectra of PPP-EO_m polymers. Data shown were obtained at room temperature and are the average of 20 scans of 6 seconds in duration.

2.2.7 Polarized light optical microscopy

Rod-like polymers often exhibit liquid crystallinity. Preliminary tests show that some members of the PPP-EO_m family are thermotropic and orient under shear. Examination of PPP-EO₂ at 140 °C under cross-polarizers (**Figure 26**) shows that the polymer melts into small circular domains that retain some degree of order. Upon shearing the sample, these domains elongate, maintain their alignment, and return to their original state after the relief of shear stress. This behavior disappears for m = 5-12. Instead, these polymers sim-

ply soften and show no birefringence. Samples with m > 12 are crystalline, and as expected from the X-ray data, exhibit melting and recrystallization similar to PEO.

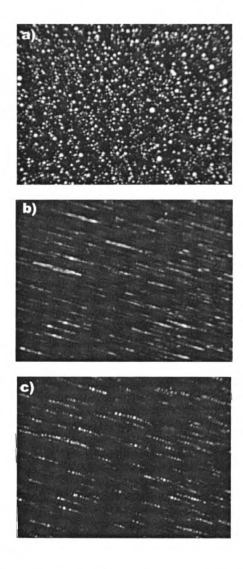


Figure 26. Cross polarized optical micrographs of PPP-EO₂ at 140 °C a) after 5 minutes at 140 °C b) after shearing the sample and c) 1 minute after shearing showing breakup of the elongated domains.

2.2.8 Conclusions

The Ni(0) mediated polymerization of ethylene oxide substituted 2,5-dichlorobenzoate monomers produces high molecular weight polyphenylenes with pendant ethylene oxide side chains. As shown by T_g, T_m, and X-ray data, the characteristics of these polymers evolve from PPP-like to that of PEO as the length of the side chains increase. With the exception of PPP-EO₀, PPP-EO₁, and PPP-EO_{45>}, all polymers are amorphous at room temperature and have T_gs below 0 °C. The T_gs of EO₀ and PPP-EO₁ are 37 and 33 °C, respectively, while PPP-EO_{45>} exhibits PEO-like crystallinity at room temperature. Simple changes in the length of the side chains enable tuning the physical properties of these polymers to match applications in display devices or as solid polymer electrolytes. Further investigation into the lithium ion conductivity of the PPP-EO_m polymers will be described elsewhere. ¹⁶⁰

2.3 Experimental

Materials. Reagent grade nickel chloride hydrate was heated (250 °C) under vacuum to give a fine, orange powder with constant weight. Triphenylphosphine was recrystallized from ethanol (95%), dried over CaSO₄, and after removing the ethanol, dried under vacuum. Granulated zinc was purified by stirring in acetic acid, filtered, rinsed thoroughly with diethyl ether, and dried under vacuum. It was then crushed with a mortar and pestle to increase its surface area. The polymerization solvent, N,N-dimethyl formamide (DMF), was stirred over molecular sieves (3Å, activated by heating ~300 °C under vacuum), and distilled under vacuum. Poly(ethylene oxide) dimethyl ether (PEO-dm-2000, ca. 2000 g/mol) was obtained from Aldrich and was dried by azeotropic distillation of

benzene, followed by removal of the solvent *in vacuo*. Unless otherwise specified, all other materials and solvents were ACS reagent grade and were used as received from commercial suppliers without further purification.

Characterization. Proton nuclear magnetic resonance (¹H NMR) spectra were measured using a Varian Gemini-300 spectrometer at 300 MHz. All samples were run at room temperature in CDCl₃. Chemical shifts were calibrated using residual CHCl₃ and are reported in ppm (δ) relative to tetramethylsilane. Molecular weights of polymers were determined using a Wyatt Technologies miniDAWN light scattering detector, and a Waters 410 Differential Refractive Index detector. CHCl₃ was used as the eluting solvent at a flow rate of 1 mL/min. DSC data were obtained under helium using a Perkin-Elmer DSC 7 instrument at a heating rate of 10 °C/min. The DSC 7 temperature was calibrated with an indium standard. The reported DSC results from polymer samples are the second heating scan, taken after flash cooling the sample from the melt to erase the thermal history. TGA were run under nitrogen and air at a heating rate of 10 °C/min on a Perkin-Elmer TGA 7 instrument. Elemental analyses were performed using a Perking-Elmer 2400 Series II Analyzer. X-ray diffraction patterns were measured using a computer controlled Rigaku 200B rotating anode diffractometer operating in reflective mode at 45kV/100 mA, with graphite monochromatized Cu (K_α) radiation. Fluorescence spectra were obtained at room temperature using a computer controlled JobinYvon Spex Fluorolog-3 spectrometer utilizing a 450W Xe lamp at an excitation wavelength of 313 nm, and a slit width of 5.0 nm, scanning from 320 to 600 nm. Raman spectra were collected at room temperature using a computer controlled Chromex RAMAN 2000 spectrometer

(Chromex, Inc.) utilizing a diode-pumped, frequency doubled CW Nd:YAG Laser (500 mW at 532 nm, Coherent), a Chromex 500is spectrometer (f/4, 600 grooves/mm holographic grating), and a thermoelectrically cooled 1024 × 256 charge coupled device (CCD) detector by Andor Tech. Ltd. Typically, 20 6-second scans were collected for each spectrum with an incident power density of ca. 500 kW/cm² (100 mW at the sample at 5 μm diameter spot size).

Ethanol, 2-[2-[2-(2-hydroxyethoxy)ethoxy], 1-(4-methylbenzenesulfonate) Ts(OCH₂CH₂)₄OH] (6)

An aqueous solution of KOH (67.79 g, 1.21 mol, in 200 mL H₂O) was added to a solution of tetra(ethylene glycol) (469.30 g, 2.42 mol) in THF (200 mL) at 0 °C. While stirring at 0 °C, a solution of tosyl chloride (114.93 g, 0.60 mol) was added dropwise. The reaction mixture was allowed to warm to room temperature and stir overnight. The reaction mixture was then dissolved in 1500 mL of water and extracted with chloroform (2 × 1500 mL). The combined organics were washed with saturated aqueous NaHCO₃ (2 × 1500 mL) and water (2 × 1500 mL), then dried over MgSO₄, filtered and the solvent removed under reduced pressure. The crude mixture was then dissolved in methanol (1200 mL) and allowed to cool in a freezer overnight. The mixture was filtered and solvent removed to afford a yellow oil (163.0 g, 78 % yield) with spectral data that match those previously reproted. H NMR (300 MHz, CDCl₃) 8 2.4 (s, 3H, 3.4-3.8 (14 H), 4.1 (t, 2H), 7.3 (d, 2H), 7.8 (2H).

Ethanol, 2-[2-[2-[(tetrahydro-2H-pyran-2-yl)oxy-]ethoxy]ethoxy]-, 1-(4-methylbenzenesulfonate) [Ts(OCH₂CH₂)₄OTHP] (7).

p-Toluenesulfonic acid (8.9 g, 0.05 mol) and 3,4-dihyrdo-2H-pyran (129.86 g, 1.55 mol) were added to a stirred solution of compound **6** (163.0 g, 0.46 mol) dissolved in dioxane (700 mL) and allowed to stir at room temperature overnight. The reaction mixture was then neutralized with triethylamine and concentrated under reduced pressure. The crude product was dissolved in chloroform (600 mL), washed with saturated aqueous NaCl (3 × 400 mL), dried over MgSO₄, filtered and the solvent removed under reduced pressure to afford the crude product as a brown oil with spectral data that match those previously reported. The product was used without further purification. H NMR (300 MHz, CDCl₃) δ 2.4 (s, 3H), 3.4-3.9 (m, 14H), 4.1 (t, 2H), 4.6 (t, 1H), 7.3 (d, 2H), 7.8 (d, 2H).

Alcohols 3e-3h: General Procedure. The appropriate alcohol (0.18 mol) was added as a THF solution (30 mL) to a stirred suspension of NaH (12.67 g, 0.34 mol) in THF (50 mL) at 0 °C, and stirred for an additional 30 min. A solution of compound 7 (70.83 g, 0.16 mol in THF 200 mL) was then added dropwise and the reaction mixture was heated to reflux for 6 hrs. Upon cooling, the reaction mixture was filtered and solvent removed under reduced pressure. The crude material was dissolved in a mixture of ethanol (400 mL) and 2N HCl (200 mL). The solution was refluxed overnight, and was then concentrated under reduced pressure to yield a dark brown oil, which was purified as indicated below.

2,5,8,11-Tetraoxatetradecan-14-ol [CH₃(OCH₂CH₂)₄OH] (3f). Reaction of methanol with 7 gave compound 3f as a clear colorless oil. Vacuum distillation (120 °C / 200

mtorr) yielded 8.63 g (25%) with spectral data that match those previously reported.⁹² ¹H NMR (300 MHz, CDCl₃) δ 3.35(s, 3H), 3.48-3.75(m, 16H).

2,5,8,11,14-Pentaoxahexadecan-16-ol [CH₃(OCH₂CH₂)₅OH] (3g). Reaction of 2-methoxy ethanol with 7 gave compound 3g as a clear colorless oil, which was purified by column chromatography (silica gel) with a gradient eluent from hexane to chloroform/methanol (9:1) to yield 6.00 g (14.5%) with spectral data that match those previously reported. ⁹² H NMR (300 MHz, CDCl₃) δ 3.35(s, 3H), 3.48-3.75(m, 20H).

2,5,8,11,14,17-Hexaoxanonadecan-19-ol [CH₃(OCH₂CH₂)₆OH] (3h). Reaction of 2-methoxy diethylene glycol with 7 gave compound **3h** as a clear colorless oil, which was purified by column chromatography (silica gel) with a gradient eluent from hexane to chloroform/methanol (9:1) to yield 1.42g (15%) with spectral data that match those previously reported. ^{92 1}H NMR (300 MHz, CDCl₃) δ 3.35(s, 3H), 3.48-3.75(m, 24H).

2,5,8,11,14,17,20-Hexaoxadocosan-22-ol [CH₃(OCH₂CH₂)₇OH] (3i). Reaction of 2-methoxy triethylene glycol with 7 gave compound 3i as a clear colorless oil, which was purified by column chromatography (silica gel) with a gradient eluent from hexane to chloroform/methanol (9:1) to yield 1.83g (23%) with spectral data that match those previously reported. ¹⁶³ ¹H NMR (300 MHz, CDCl₃) δ 3.35(s, 3H), 3.48-3.75 (m, 28H).

Monomer synthesis: General procedure. The alcohol (3a-l, 37 mmol) and 2,5-dichlorobenzoyl chloride (5.16 g, 24.6 mmol) were dissolved in pyridine (50 mL) and

heated (50-60 °C) overnight. Upon cooling, methylene chloride (100 mL) was added and the solution was washed three times with 50 mL of 1N HCl (aq) and once with 50 mL of H₂O. The combined organics were dried over magnesium sulfate, filtered, and the solvent removed under reduced pressure. The compounds were dried by refluxing in benzene using a Dean-Starke trap and purified by recrystallization (4a), vacuum distillation (4b-4d) or column chromatography (4e-4l) inside a drybox.

Methyl-2,5-dichlorobenzoate (4a). Compound 4a was purified by recrystallization from methanol to yield 4.74 g (94%). mp 35 °C (DSC) lit. 164 (mp 38-39 °C). 1H NMR (300 MHz, CDCl₃) δ 3.9(s, 3H), 7.4(d, 2H), 7.8(t, 1H).

3-Oxybutyl-2,5-dichlorobenzoate (4b). Compound **4b** was purified by vacuum distillation at 105 °C/80 mtorr to yield 5.63 g (92%). ¹H NMR (300 MHz, CDCl₃) δ 3.4(s, 3H), 3.7(t, 2H), 4.45(t, 2H), 7.4(d, 2H), 7.8(t, 1H). Anal. Calcd. for C₁₀H₁₀Cl₂O₃: C, 48.22; H, 4.05. Found: C, 48.26; H, 4.03.

3,6-Dioxyheptyl-2,5-dichlorobenzoate (4c). Compound **4c** was purified by vacuum distillation at 170 °C/130 mtorr to yield 5.98 g (83%). ¹H NMR (300 MHz, CDCl₃) δ 3.4(s, 3H), 3.55(t, 2H), 3.7(t, 2H), 3.85(t, 2H), 4.5(t, 2H), 7.4(d, 2H), 7.8(t, 1H). Anal. Calcd. for $C_{12}H_{14}Cl_2O_4$: C, 49.17; H, 4.81. Found: C, 49.01; H, 4.50.

3,6,9-Trioxydecyl-2,5-dichlorobenzoate (4d). Compound 4d was purified by vacuum distillation at 195 °C/200 mtorr to yield 6.55 g (79%). ¹H NMR (300 MHz, CDCl₃) δ

3.35(s, 3H), 3.5(t, 2H), 3.65(m, 6H), 3.8(t, 2H), 4.45(t, 2H), 7.4(d, 2H), 7.8(t, 1H). Anal. Calcd. for C₁₄H₁₈Cl₂O₅: C, 49.87; H, 5.38. Found: C, 49.75; H, 5.39.

3,6,9,12-Tetraoxytetradecyl-2,5-dichlorobenzoate (4e). Compound 4e was purified by column chromatography (silica gel) with hexane/ethyl acetate (2:1) as the eluting solvent to yield 7.83g (54%). ¹H NMR (300 MHz, CDCl₃) δ 3.35(s, 3H), 3.5(t, 2H), 3.65(b, 10H), 3.8(t, 2H), 4.45(t, 2H), 7.4(d, 2H), 7.8(t, 1H). Anal. Calcd. for C₁₆H₂₂Cl₂O₆ C 50.41; H 5.82. Found C 50.29; H 5.64.

3,6,9,12,15-Pentaoxyhexadecyl-2-5-dichlorobenzoate (4f). Compound **4f** was purified by column chromatography (neutral alumina) with hexane/ethyl acetate (2:1) to yield 3.39g (37%) 1 H NMR (300 MHz, CDCl₃) δ 3.35(s, 3H), 3.5(t, 2H), 3.65(b, 14H), 3.8(t, 2H), 4.45(t, 2H), 7.4(d, 2H), 7.8(t, 1H). Anal. Calcd for C₁₈H₂₆Cl₂O₇ C 50.83; H 6.16. Found C 50.59; H 6.99.

3,6,9,12,15,18-Hexaoxynonadecyl-2-5-dichlorobenzoate (4g). Compound **4g** was purified by column chromatography (neutral alumina) with hexane/ethyl acetate (2:1) to yield 1.24g (55%) 1 H NMR (300 MHz, CDCl₃) δ 3.35(s, 3H), 3.5(t, 2H), 3.65(b, 18H), 3.8(t, 2H), 4.45(t, 2H), 7.4(d, 2H), 7.8(t, 1H).) Anal Calcd C₂₀H₃₀Cl₂O₈ C 51.18; H 6.44. Found C50.83; H 6.75.

3,6,9,12,15,18,21-Heptaoxyicosyl-2,5-dichlorobenzoate (4h). Compound 4h was purified by column chromatography (neutral alumina) with hexane/ethyl acetate (2:1) to yield

1.83g (74%) ¹H NMR (300 MHz, CDCl₃) δ 3.35(s, 3H), 3.5(t, 2H), 3.65(b, 22H), 3.8(t, 2H), 4.45(t, 2H), 7.4(d, 2H), 7.8(t, 1H). Anal Calcd C₂₂H₃₄Cl₂O₉ C 51.47; H 6.68. Found C 51.78; H 6.93

3,6,9,12,15,18,21,24,27,30,33,36-Dodecaoxyheptacontyl (average) -2,5-dichlorobenzoate (4i). Compound 4i was purified by column chromatography (silica gel) with hexane/ethyl acetate (2:1) as the eluting solvent to yield 15.12 g (85%). ¹H NMR (300 MHz, CDCl₃) δ 3.35(s, 3H), 3.5(t, 2H), 3.65(b, 40H), 3.8(t, 2H), 4.45(t, 2H), 7.4(d, 2H), 7.8(t, 1H). Anal. Calcd. for C₃₂H₅₄Cl₂O₁₄: C, 52.39; H, 7.42. Found: C, 51.15; H, 7.17.

3,6,9,12,15,18,21,24,27,30,33,36,39,42,45,48-Hexadeca-oxynonatetracontyl (average) -2,5-dichlorobenzoate (4j). Compound 4j was purified by column chromatography (silica gel) with hexane/ethyl acetate (2:1) as the eluting solvent to yield 18.39 g (81%). 1 H NMR (300 MHz, CDCl₃) δ 3.35(s, 3H), 3.5(t, 2H), 3.65(b, 58H), 3.8(t, 2H), 4.45(t, 2H), 7.4(d, 2H), 7.8(t, 1H). Anal. Calcd. for C₄₀H₇₀Cl₂O₁₈: C, 52.80; H, 7.75. Found: C, 51.04;H, 7.15.

3,6,9,12,15,18,21,24,27,30,33,36,39,42,45,48,51,54,57,60,63,66,69,72,75,78,81,84,87,90, 93,96,99,102,105,108,111,114,117,120,123,126,129,132,135-Pentatetraconta-oxyhexacontahectyl (average) -2,5-dichlorobenzoate (4k). Compound 4k was purified by column chromatography (silica gel) with hexane/ethyl acetate (2:1) as the eluting solvent to yield 32.07 g (60%). ¹H NMR (300 MHz, CDCl₃) 8 3.35(s, 3H), 3.5(t, 2H),

3.65(b, 174H), 3.8(t, 2H), 4.45(t, 2H), 7.4(d, 2H), 7.8(t, 1H). Anal. Calcd. for C₉₈H₁₈₆Cl₂O₄₇: C, 53.81; H, 8.57. Found: C, 53.80;H, 8.73.

Nickel catalyzed polymerization, General procedure: Inside a helium atmosphere drybox, the monomer (1.8 mmol) was added to NiCl₂ (23.3 mg, 0.18 mmol), 2,2'-bipyridine (28.1 mg, 0.18 mmol), triphenylphosphine (283.3 mg, 1.08 mmol), zinc powder (0.71 g, 1.08 mmol), and DMF (1.0 mL) and pre-heated for 30 min. at 80 °C in a 10 mL vial with a Teflon septum cap. The vial was then immersed in an oil bath set for 85 °C. The pink solution became red after 10 minutes, eventually turning deep red-brown after 30 minutes. The mixture was stirred overnight. Upon cooling, the solution was transferred into a flask containing 200 mL of 2N HCl/MeOH (1:1) and stirred until the excess zinc dissolved. The polymer was extracted from the HCl/MeOH mixture with methylene chloride (3 × 50 mL). The combined organic layers were dried over MgSO₄, filtered, and the solvent removed under reduced pressure to yield a pale yellow film. The polymer was then purified via precipitation of a concentrated chloroform solution of the polymer into MeOH, filtered and dried.

Chapter 3

3 Lithium Ion Conductivity of Substituted Rigid Rod Solid Polymer Electrolytes

3.1 Introduction

Solid polymer electrolytes (SPE) have been the focus of intense research because of their importance to applications such as lithium batteries and electrochromic devices. Since Fenton³⁶ and Armand⁸ first reported the use of poly(ethylene oxide) (PEO) as a polymer electrolyte, polyether matrices have been the most studied due their ability to dissolve inorganic salts. In such systems the metal cations coordinate to the ether oxygens and thus their mobility is strongly coupled to the segmental motion of the polymer. In PEO, a semi-crystalline polymer, this limits ion transport to the amorphous regions of the polymer host.

A number of approaches have been reported that limit crystallinity and increase the segmental chain motion and mechanical stability of polyether matrices. These include the use of graft and block copolymers, comb architectures, crosslinked systems and blending polyethers with plasticizing additives. 58,136,165-167 To this end, Meyer and Wegner reported comb polymers that have rigid backbones and flexible oligo(ethylene oxide) side chains as teeth. In such structures the rigid backbone contributes thermal and mechanical stability, while the side chains provide a highly conductive medium for ions. 91,92,136,140 They reported good conductivities and provided proof that their system formed a lamellar structure composed of comb polymers.

Khan described the synthesis and characterization of a related system, a family of poly(thiophene) copolymers that contain thiophene units substituted with a single PEG-me-350 side chain (H(OCH₂CH₂)_nOCH₃, n~7).¹⁶⁸ Room temperature conductivities of 10^{-6} S/cm were reported for the homopolymer that has one PEG 350 chain per repeat unit. The rigid backbone comb polymers prepared to date generally contain polydisperse ethylene oxide units, and no systematic study of the effect of the side chain length on the thermal and conductive properties of these molecularly reinforced solid polymer electrolytes has been reported.

The poly(*p*-phenylene) system provides one of the best frameworks for studying the properties of rigid combs. The parent polymer lacks significant thermal transitions below 400 °C^{169,170} and is electrochemically stable.¹³⁸ Attaching pendent ethylene oxide side chains to the rigid backbone provides a conductive medium for ion transport.^{91,92,136,140} These "hairy rod" molecules⁸⁷ can be regarded as "molecular composites"⁹² of two components, a rigid polymer and PEO, that are dispersed at the molecular level.^{92,133-136} Steric interactions between substituents at the ortho positions increase the torsional angle between the phenyl rings. ^{137,171,172} Twisting of adjacent rings out of planarity introduces an element of disorder and creates an environment in which the side chains have a larger spatial separation than for a planar conformation, thereby enhancing segmental chain motion. However, in the limit of long oligo(ethylene oxide) side chains, the steric limits introduced by the twisting rings would be less important and the side chains would be expected to associate and crystallize. Understanding the ionic conductivity of these copolymers as a function of side chain length is the goal of this investigation.

$$\begin{array}{c} 0 & 0 & 0 \\ \hline \\ - & \\ \end{array}$$

PPP-EO_m

We report herein the characterization of a series of poly(p-phenylene)s (PPP-EO_m) substituted with various length (m) ethylene side chains. We believe that a systematic study of the structure property relationships of these polymers can provide insight into how to balance high segmental motion with the need to maintain dimensional stability.

3.2 Results and Discussion

3.2.1 Thermal properties

The glass transitions of comb polymers depend on the rigidity of the polymer backbone and the length and stiffness of the teeth of the comb. For the PPP-EO_m system, we expected that for short teeth, the physical properties would be dominated by the PPP backbone, but in the limit of very long teeth, the properties of the comb would converge to those of PEO. The most interesting material from a conductivity perspective would be when the teeth are long enough to have high segmental motion, but still too short to crystallize.

DSC and MDSC were used to measure the T_gs and T_ms of the PPP-EO_m polymers. As shown in **Figure 27**, the T_gs decreased as the lengths of the PEO segment increased,

eventually converging to the T_g of PEO for side chains of m = <45>. The glass transitions for polymers with short side chains were particularly weak, and could only be detected by MDSC. Crystallization was first observed at m = 16, which melts at 22 °C, and increasing m to 45 increased T_m to 42 °C. It is interesting to compare these data with PEO homopolymers of comparable molecular weights. For example, PEG-dm-500 (m~10) has a melting point of 15 °C, while PEO-dm-2000 (m=<45>) melts at 49 °C. Ignoring crystallization, polymers with the longest side chains should exhibit the highest conductivities because of their low T_g .

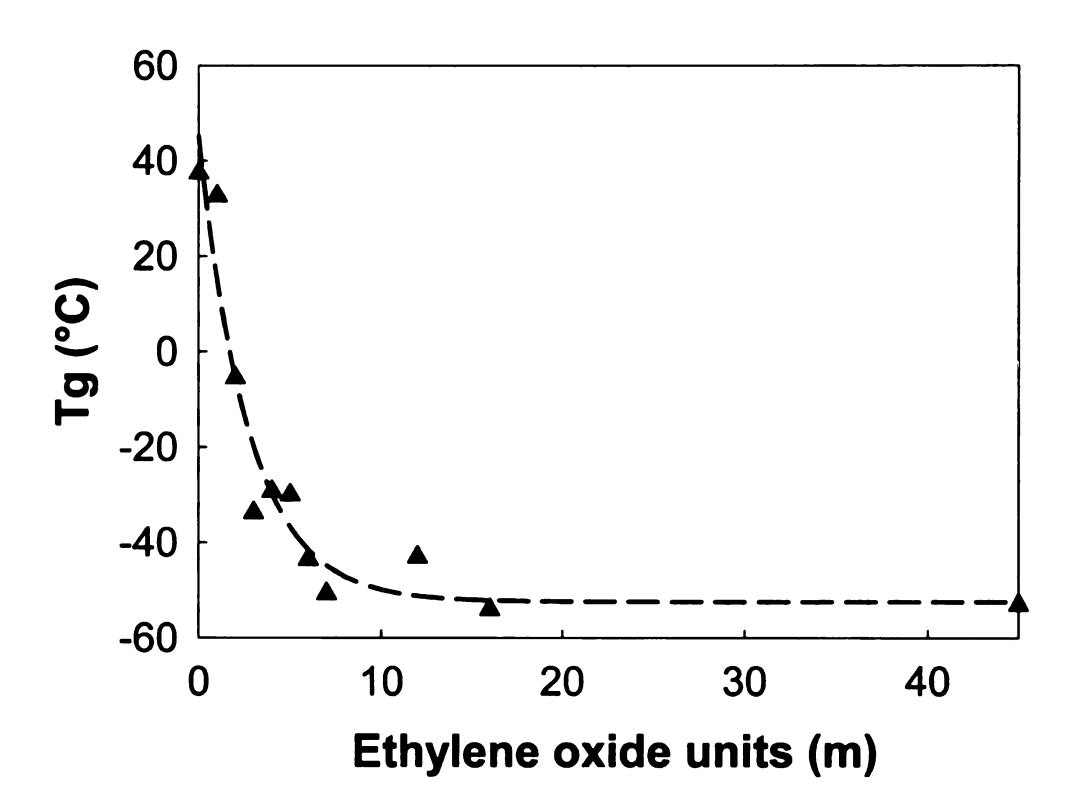


Figure 27. The relationship between T_g and the length (m) of the ethylene oxide side chain in PPP-EO_m polymers. The data were acquired through MDSC. The line is a guide.

m	M _n	PDI	Neat		Composite	
			Tg	T _m	Tg	T _m
3	48,800	1.71	-34	-	-	-
7	17,900	1.40	-51	-	-	-
<16>	20,900	1.29	-54	22	-41	-
<45>	46,600	1.20	-53	49	-26	42
PEG-dm-2000	~2000	-	-60	66	-26	48

Table 8. Properties of PPP-EO_m polymers

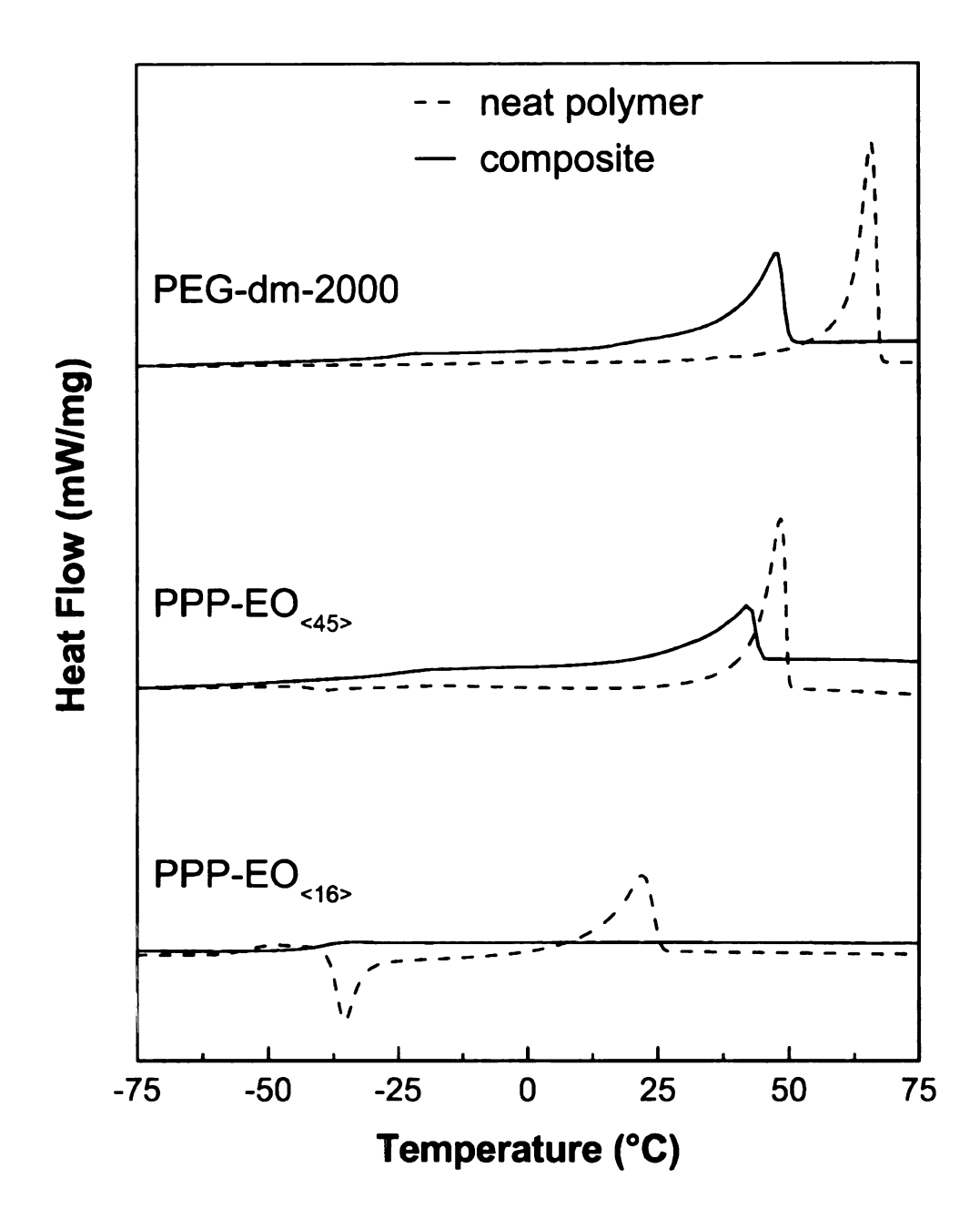


Figure 28. DSC scans of neat PPP-EO_m (dashed) and LiClO₄/PPP-EO_m composites (solid). The scans shown are the first heating scans after quenching the sample from 180 °C. The samples were heated at 10 °C/min under He.

Dissolution of salts in polyethers generally results in a decrease in crystallinity and a parallel increase in T_g . The initially formed amorphous state is often a kinetic product; crystallization of PEO salt complexes is well-known. The data for the polymer/LiClO₄ complexes (O:Li = 20) are shown in **Figure 28**. The addition of LiClO₄ depresses both the melting point and the crystallinity, as indicated by the decrease in ΔH_{fus} . PPP-EO_{<16>}/LiClO₄ is rendered amorphous, while the corresponding PPP-EO₄₅ complex shows a slight decrease in T_m , and a more substantial decrease in crystallinity. These results predict that PPP-EO₁₆/LiClO₄ should have the highest conductivity at room temperature. It is useful to note that the behavior of m = 45 and PEO-dm-2000 are qualitatively the same, pointing out the transition in physical properties from PPP-like to PEO as the side chains lengthen. The addition of LiClO₄ to PPP-EO_{<16>} and PPP-EO_{<45>} leads to an increase in T_g . Increases in T_g are usually ascribed to transient cross-links, the coordination of lithium cations with neighboring polyether chains. These ties between chains also inhibit crystallization by decreasing chain mobility.

3.2.2 X-ray diffraction

The XRD data of the composites (**Figure 29**) reveal that the solubility of the lithium salt in PPP-EO_m polymers depends on the length of the side chains. Despite all samples shown in **Figure 29** having the same O:Li ratio, the XRD patterns for PPP-EO₃ and PPP-EO₇ show evidence of undissolved LiClO₄, while longer chains completely solubilize LiClO₄. This effect is easily understood by considering the consequences of anchoring one end of a PEO oligomer to a rigid backbone. Ethylene oxide segments directly attached to the polymer have limited ability to coordinate effectively with ions due to the

inflexibility of PPP. Once the chains are sufficiently long, the effect of the PPP backbone is ameliorated and dissolution of LiClO₄ is facile. We previously observed a similar effect in (AB)_n multiblock copolymers, where the A block is an exact length EO segment and the B block is an alkylene chain.⁶⁵ The ionic conductivity in this system had low conductivities when the A block length was short, but it rapidly increased as the length of A increased. The dependence on A was traced to the need for two segments to solubilize each LiClO₄ in short A blocks, but in polymers with longer A blocks, one segment was sufficient.

3.2.3 AC impedance spectrscopy

Since the solubility of the lithium perchlorate salt in the PPP-EO_m polymers increases with an increase of side chain length, it is clear that the conductivities of these solid polymer electrolytes should follow in similar fashion. Figure 30 shows the conductivity data for the composites, plotted as σ vs. 1000/(T-T₀) where T₀ was set at -60 °C, the T₈ of PEO. At 30 °C, the PEO and PPP-EO₃ composites both have poor conductivities, ~10⁻⁶ S/cm. The conductivity of PPP-EO₃ is low over the entire temperature range as a result of the poor solubility of LiClO₄ in the polymer, while the low conductivity of the PEO complex reflects its crystalline nature. The conductivities of the other composites follow the trends predicted by the XRD data. The increases in conductivity seen for PPP-EO₇ and PPP-EO₁₆ parallel the increasing solubility of LiClO₄ in the composites, while the appearance of diffraction peaks for PEO in PPP-EO₄₅ is consistent with a slight drop in conductivity relative to PPP-EO₁₆. A slice through the conductivity data at 30 °C (Figure 31) shows a maximum conductivity of 3×10⁻⁵ S/cm for PPP-EO₁₆. The activa-

tion energies for ion transport extracted from the conductivity data were 0.52 (PEO), 0.49 (PPP-EO_{<45>}), 0.64 (PPP-EO_{<16>}), 0.84 (PPP-EO₇) and 0.93 KJ/mol (PPP-EO₃

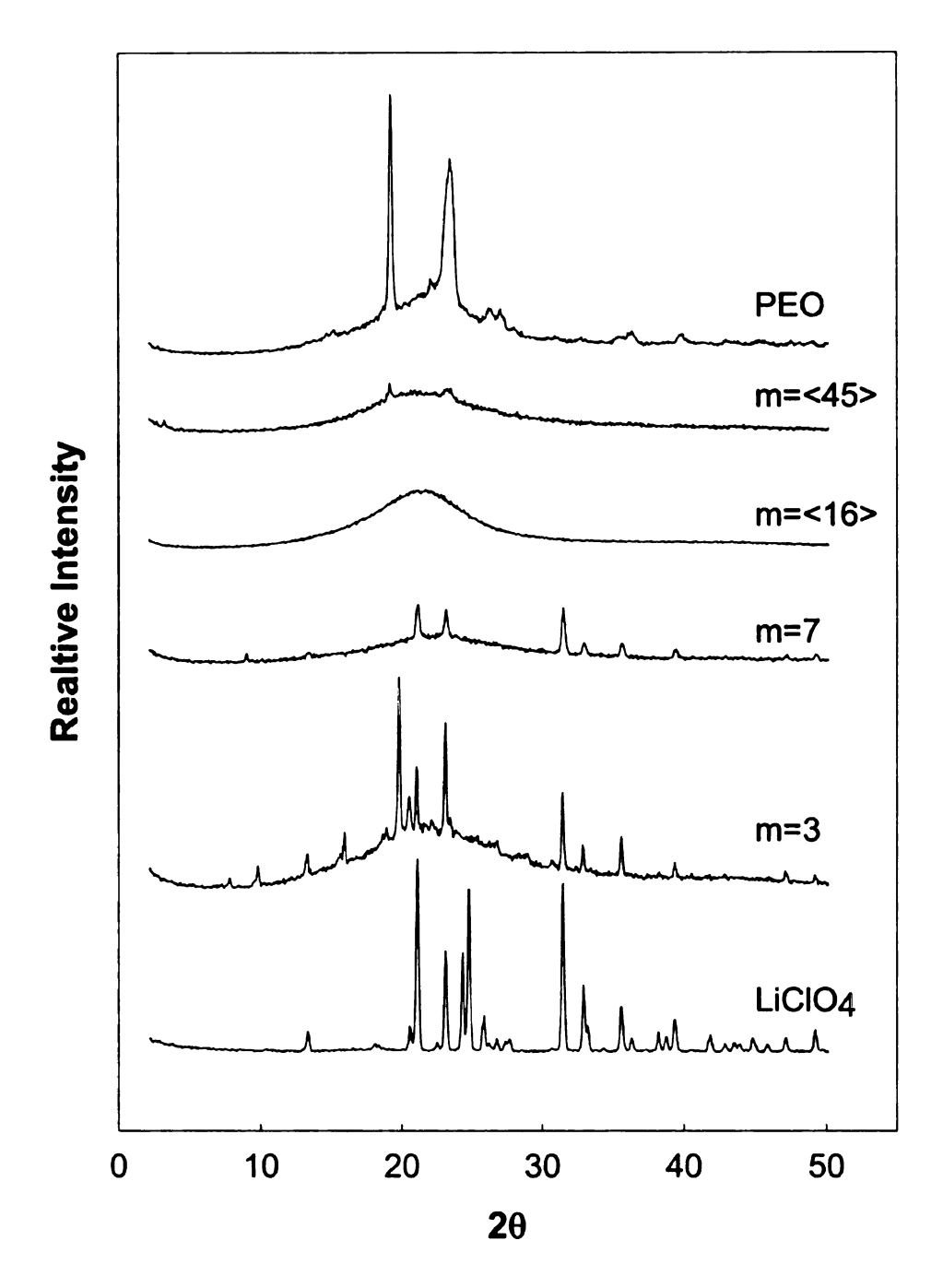


Figure 29. X-ray powder diffraction patterns of PPP-EO_m/LiClO₄ composites. The data were collected at room temperature at a rate of 0.05 2θ /min over a range of $2\theta = 1$ -50°.

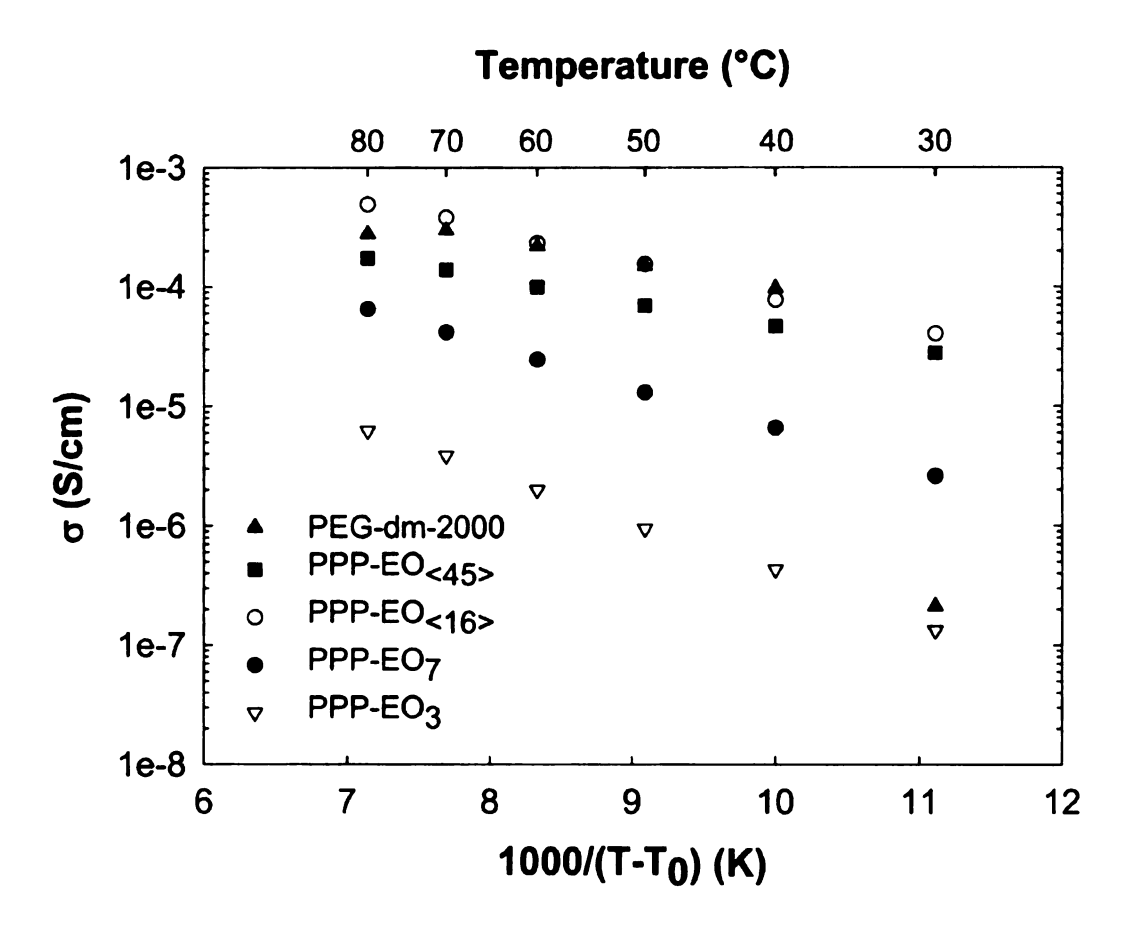


Figure 30. Temperature-dependent conductivities for selected PPP-EO_m/LiClO₄ composites. The data are derived from AC impedance data, with all samples having an O:Li ratio of 20.

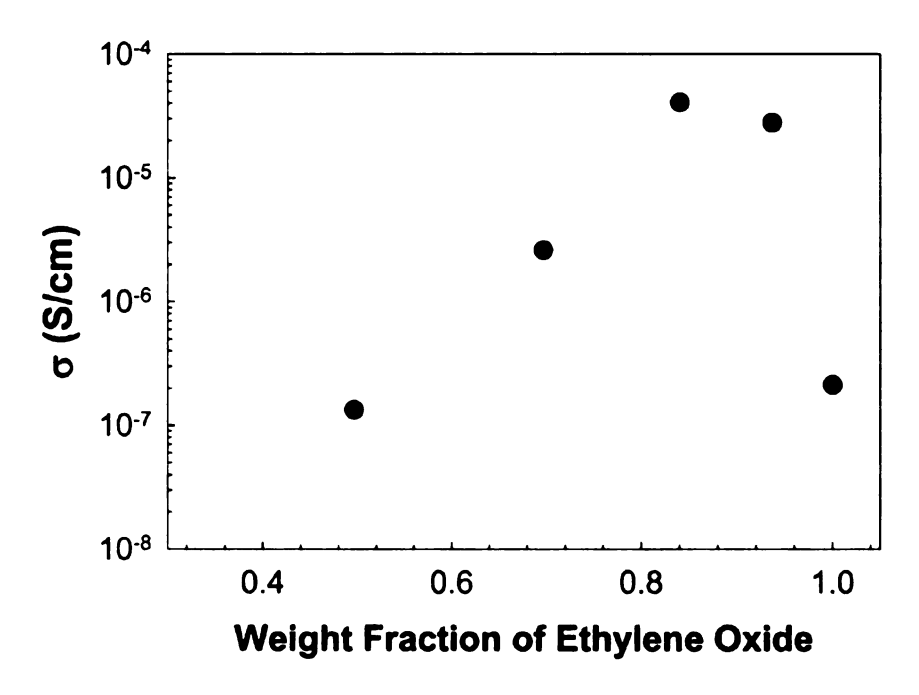


Figure 31. A cross-section of the conductivity data at 30 °C, indicating a conductivity maximum at m = <16>. Decreases in σ for m = <45> and PEO-dm-2000 reflect partial crystallization of the samples.

3.3 Conclusions

Solid polymer electrolytes based on PPP substituted with oligo(ethylene oxide) side chains and lithium perchlorate exhibit conductivities ranging from 10^{-6} S/cm to 10^{-4} S/cm at 30 °C. The conductivity is dependent on the length of the EO chain attached to each ring. When the EO chain is short, the solubility of LiClO₄ is low leading to undissolved salt and low conductivities. Lengthening the EO chains increases the solubility of LiClO₄ and chain mobility, causing a more than two order of magnitude increase in the room temperature conductivity when m = <16>. For longer side chains, crystallization begins

to suppress the ionic conductivity, an effect that can be minimize by using branched chains that inhibit crystallization.

3.4 Experimental

Synthesis and characterization of the PPP-EO_m polymers are reported elsewhere. Solvents used in the preparation of the composite electrolytes were vacuum distilled from molecular sieves and stored in a helium filled dry box. Poly(ethylene oxide) dimethyl ether (PEO-dm-2000, ca. 2000 g/mol) was obtained from Aldrich and was dried by azeotropic distillation of benzene, followed by removal of the solvent *in vacuo*. All electrolytes were prepared in a helium filled dry box by mixing acetonitrile solutions of LiClO₄ and the desired polymer. The samples were then concentrated under reduced pressure to afford a viscous solution which was directly cast into the sample holder used for impedance analysis. All composites had an O:Li ratio of 20. Only the oxygen atoms of the polyether chain were included in calculating the O:Li ratio; the carbonyl oxygen was not counted.

AC impedance spectroscopy was conducted over a frequency range of 5 Hz to 13 MHz using an HP 4192A LF Impedance Analyzer, with an applied voltage of 10 mV. Conductivity measurements were taken at 30, 40, 50, 60, 70 and 80 °C. Prior to each measurement, samples were held at temperature for at least 20 minutes under a flow of nitrogen. The sample cell was constructed of stainless steel disks separated by a Teflon collar. The sample films had a thickness of 0.053 cm and an area of 1.27 cm². Differential Scanning Calorimetry (DSC) data were obtained under He using a Perkin-Elmer DSC 7 instrument

at a heating rate of 10 °C/min, with the temperature calibrated with an indium standard. Reported DSC results are second heating scans, taken after flash cooling the samples from an isotropic melt. Modulated Differential Scanning Calorimetry (MDSC) data were obtained under N_2 using a TA Instruments Q1000 fitted with a refrigerated cooling system. Samples were scanned from -70 to 200 °C at a scanning rate of 1 °C/min. X-ray powder diffraction patterns were obtained using a computer controlled Rigaku 200B rotating anode diffractometer operating in reflective mode at 45 kV/100 mA, with graphite monochromatized Cu (K_{α}) radiation.

Chapter 4

4 Self-assembled Silica Nano-composite Polymer Electrolytes

4.1 Introduction

Solid polymer electrolytes based on poly(ethylene oxide) (PEO) and lithium salts have been extensively studied due to their potential application in secondary lithium ion batteries. 38,40,80 Most electrolytes are prepared by dissolving a lithium salt such as LiPF₆ or Li-ClO₄ in PEO or a structural analog of PEO, however, the performance of such systems suffer from low lithium ion transference numbers (t_{Li}^{\dagger}) and cell polarization. The reason for the low $t_{i,i}^{\dagger}$ values is due to coordination of lithium cations to the oxygen atoms of polyethers, and thus the ionic mobility becomes dominated by the more mobile anions.^{2,80} Bruce and co-workers estimated that in such systems the t_{Li}^+ can be as low as 0.1. A recent investigation by Scrosati and co-workers reported a t_{Li}^+ of 0.28 using a lithium dicyanotriazolate salt, a typical value for PEO/salt systems. 189 Higher transference numbers for Li⁺ may be attained by reducing the mobility of anions. Several strategies have been investigated, including tethering anions to the polymer host in polymer electrolytes, increasing the size of the anion, and addition of Lewis acids, usually in the form of ceramic particles, that complex with anions. In cases where the anions are fully immobilized, losing the contribution of anions in binary salt electrolytes depresses the conductivity to ~1/10th of its original conductivity. 106-108

Early investigations of composite polymer electrolytes demonstrated the advantages of incorporating inorganic fillers into a PEO host matrix. 81,82,190 When the particle size of such fillers was small ($< 5 \mu m$) they suppressed crystallization and substantially improved the conductivity. 82 Incorporation of nanoparticles also were shown to enhance the mechanical and electrochemical properties of electrolytes. 191,192 For example, the addition of silica nanoparticles to poly(ethylene glycol) dimethyl ether (PEG-dm)/LiClO₄ systems yielded electrolytes with conductivities of ~10⁻³ S/cm at 25 °C, and elastic moduli of > 10⁶ dynes/cm². However, the applications of particles described above do not resolve the problems associated with low t_{Li}^{\dagger} values in polymer electrolytes. More recently, negatively charged inorganic fillers such as montmorillonites and other silica-aluminates have been used as anions. 108,193,194 Since the anions are massive, their mobilities are minimal and t_{Li}^+ was measured to be ~0.9. Another particle-based approach to immobilization of anions would be to tether them to the surface of nanoparticles. When incorporated in a PEO matrix, such particles may serve multiple purposes, including providing mechanical stability, 83,122 improving the stability of the electrode-electrolyte interface. 195,196 and immobilization of the anions allowing the lithium cation to be the only mobile species.

In this report, we explore the tethering of lithium trifluoromethane sulfonimide to fumed silica and the properties of electrolytes prepared by dispersing the silica in a low molecular weight polyether. Our goal is to take advantage of the high surface area of fumed silica to immobilize sufficient numbers of anions to support single ion conductivity by cations.

4.2 Results and Discussion

4.2.1 Synthesis

The ease in which perfluoroalkyl sulfonimides can be synthesized¹⁹⁷ along with the good conductivity and cycling characteristics¹⁹⁸ of lithium perfluoroalkyl sulfonimides identifies them as attractive candidates for anchoring to surfaces. Furned silica is a suitable nanoparticle support because it has a high surface area (200 m²/g), and the silanol groups that decorate its surface can be readily functionalized in high yield by reaction with chloro- or alkoxysilanes. The synthetic sequence shown in **Scheme I** was used to anchor the salts to furned silica. A five carbon tether simplifies the synthesis and places the salt a reasonable distance from the surface. The synthesis involves standard chemical transformations, a Gabriel synthesis to generate the pentenyl amine, formation of the trifluoromethylsulfonimide using triflic anhydride, and hydrosilylation of the resulting alkene with triethoxysilane using Karstedt's catalyst. Each intermediate product was characterized by standard spectroscopic methods.

Scheme III. Synthesis of A200-C5NTfLi

i) Et₃N, CHCl₃, *p*-toluene sulfonic acid, 98%; ii) potassium phthalimide, DMF, 80%; iii) hydrazine hydrate, EtOH, 60°C; iv) HCl, EtOH, reflux, 52%; v) (CF₃SO₂)₂O, CH₂Cl₂, Et₃N, 58%; vi) (EtO)₃SiH, Karstedt's catalyst, benzene; vii) Et₂NH, **A**; viii) BuLi, toluene.

4.2.2 Infrared spectroscopy

The imide was attached to the silica surface using diethylamine as a catalyst. DRIFTS IR spectra of the modified silica demonstrate successful anchoring of the sulfonimide (**Figure 32**). The IR spectrum of A200 exhibits a sharp peak at 3750 cm⁻¹ corresponding to the free Si-OH stretching. Near-complete loss of the O-H band and the appearance of bands for the imide at 2800-3000 cm⁻¹ (CH stretching) and at 1443 and 1369 cm⁻¹ (sul-

fonyl asymmetric and symmetric stretching) confirm attachment of the imide. The expected CF₃ band was obscured by intense bands from the fumed silica. We also were unable to observe the N-H stretch of the sulfonimide, a problem previously reported by others for similar systems. Jezorek et al. characterized alkyl amines bound to silica surfaces and they found it difficult to observe the amine stretch.¹⁹⁹ Only after the amine was chemically modified did evidence of the amine become apparent. In a similar manner, the existence of the amine is supported by the appearance of a broad peak at 1470 cm⁻¹ after lithiation, which is attributed to the SO₂ asymmetric and symmetric stretches of the sulfonimide salt.^{200,201} Conditions for deprotonation of the imide were developed by reacting the N-pentenylsulfonimide with butyllithium in toluene. As shown in **Figure 33**, the N-H stretch at 3250 cm⁻¹ is lost upon reaction with methyllithium under these conditions. The ease in which the salt is formed assures the formation of the bound sulfonimide salt.

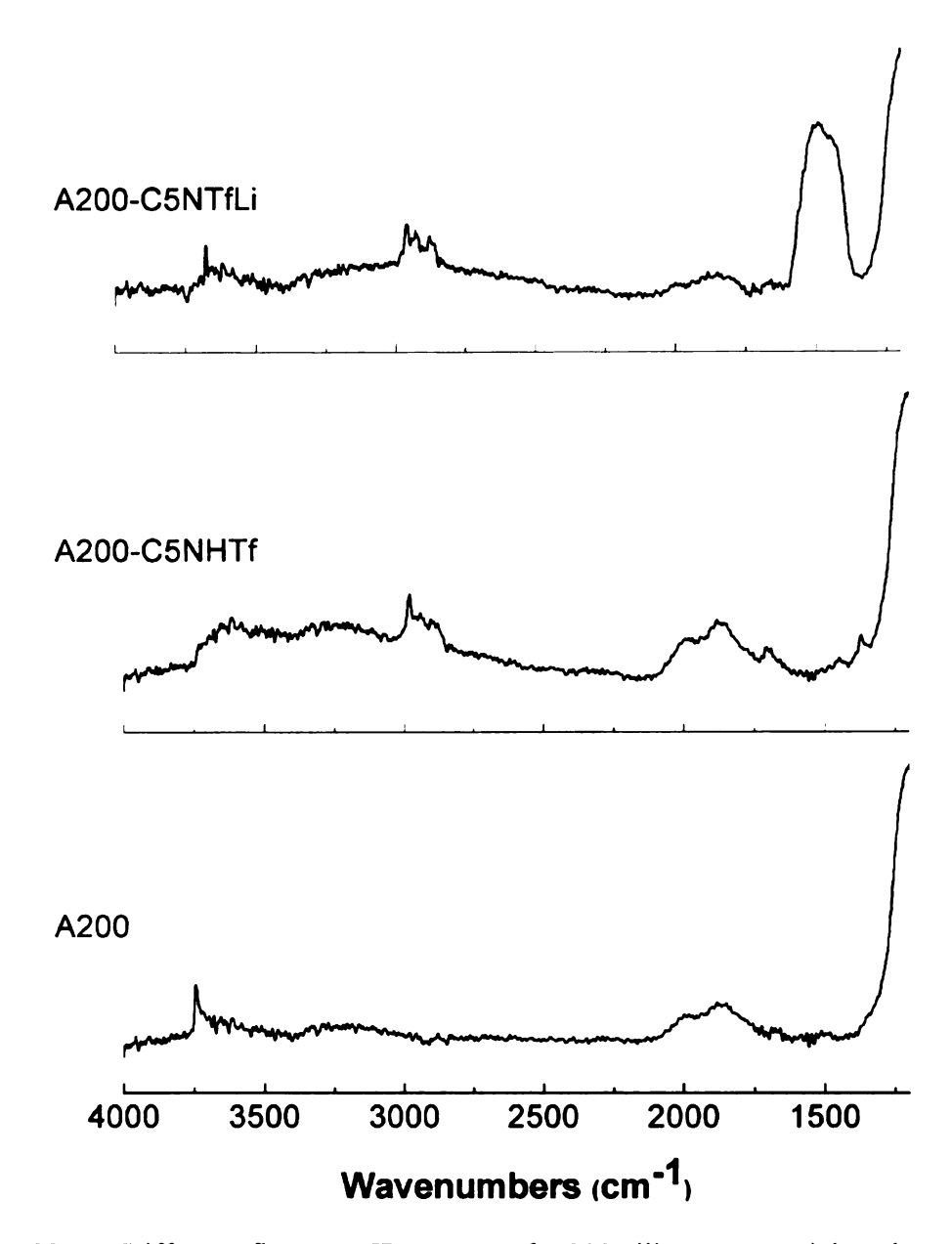


Figure 32. Diffuse reflectance IR spectra of A200 silica nanoparticles, the sulfonimide-modified silica (A200-C5NHTf), and its lithiated form (A200-C5NTfLi). Data were obtained from samples prepared in a 2:1 ratio of sample to dry KBr.

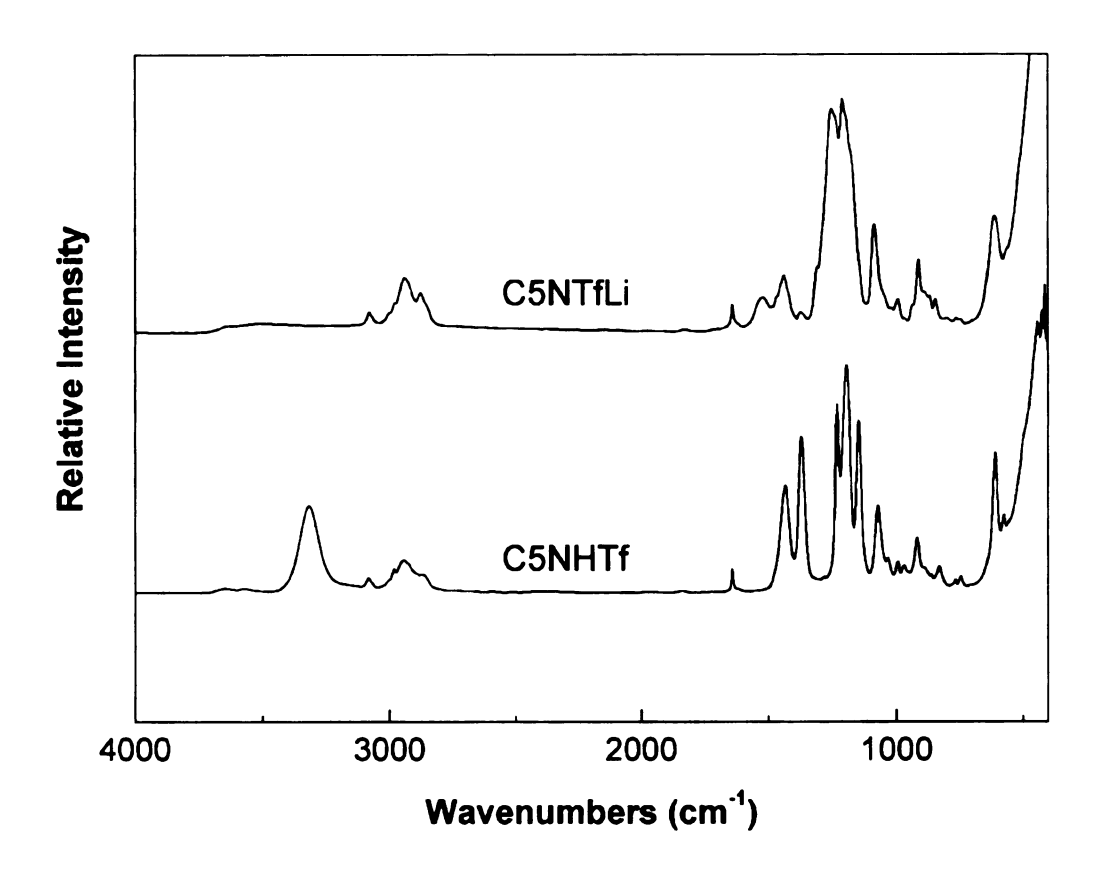


Figure 33. IR spectra comparing the starting material (C5NHTf) and formation of the lithium salt (C5NTfLi). Data were collected as thin films sandwiched between NaCl plates.

4.2.3 Thermogravimetric analysis

The surface coverage of silanol groups on A200 is ~1.0 mmol/g. ²⁰² Assuming the alkyl sulfonimide is attached to the silica through each of the alkoxy groups, complete coverage of the nanoparticles with 0.33 mmol of imide (81 mg), would give modified silica with 7.9% of the mass as the bound imide. The extent of surface coverage can be probed by thermogravimetric analysis (TGA) experiments run in air. Assuming all decomposi-

tion products of the imide are volatile, the resulting weight loss should be at most 7.9%. The measured weight loss for the functionalized silica was 2.6 % corresponding to 36 % surface coverage, or 0.12 mmol/g silica (**Figure 34**) If each sulfonimide is converted to the corresponding lithium salt upon reaction with butyl lithium, then the maximum lithium carrier concentration in an electrolyte would be 0.12 mmol/g of silica.

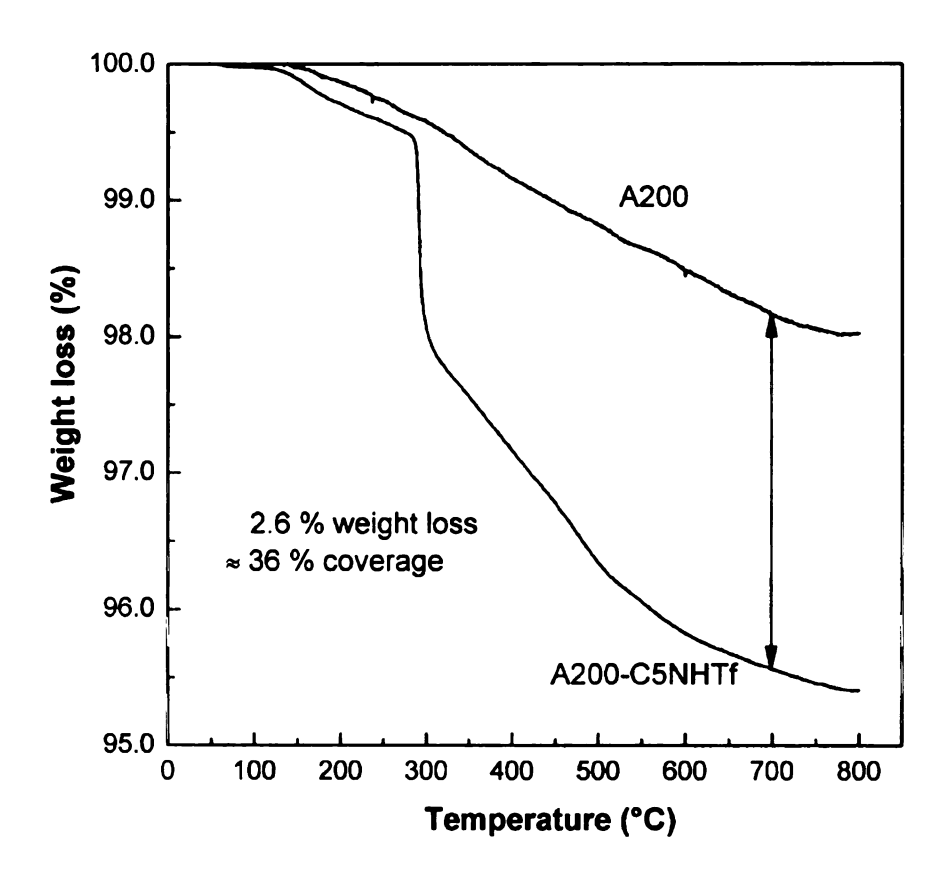


Figure 34. Thermogravimetric analysis of A200 and A200-C5NHTf measured in air from 30 °C to 800 °C at a rate of 10 °C/min. The weight loss at 700 °C corresponds to 36 % coverage of the silica nanoparticle surface.

4.2.4 AC impedance spectroscopy

Polymer composites of A200-C5NTfLi and poly(ethylene oxide) dimethyl ether were prepared by mixing an acetonitrile solution of the polymer with a dispersion of silica in acetonitrile, removing the solvent under reduced pressure, and mechanically mixing the composite to obtain a paste. The weight fraction reported was based on the total mass of the composite, as opposed to the mass of the polymer, the protocol commonly used for polymer electrolytes. Composites with low silica loadings (10 – 25 wt%) are pastes while higher loadings (30 – 50 wt%) are powders that become pastes upon shearing. The conductivity data for the samples appear in **Table 9** and in **Figure 35**. The conductivities at 30 °C for the 19, 24, 30 and 35 wt% composites of were $\sim 10^{-6}$ S/cm. The conductivities of the 10, 15, and 50 wt% composites could not be determined due to the low concentration of charge carriers (Li⁺) in the case of the first two samples. For samples > 45 wt%, the low conductivity stems from poor connectivity, i.e. the volume fraction of PEG-dm-500 is too low to be continuous throughout the electrolyte. The conductivity of 40 wt% composites could only be determined at 80 °C and 70 °C due to the high resistance of the material, exceeding the operational limits of the impedance analyzer, again likely due to poor connectivity. Similar effects have been observed with R805/PEG-dm electrolytes (R805 is an octyl modified hydrophobic fumed silica) at comparable silica loadings.^{86,122} Data for the R805/LiClO₄/PEG-dm-500 system are shown in Figure 35. As expected, the conductivities of the A200-C5NTfLi composites were more than an order of magnitude difference lower than the binary salt system.

Lithium concentrations in polyether electrolytes are often expressed as the ratio of ether oxygens to lithium ions. For electrolytes prepared from binary salts, the conductivity usually increases with decreases in the O:Li ratio, reaching a maximum at ~20. For the current system, the O:Li ratios reported in **Table 9** are an order of magnitude lower than the optimum O:Li ratio of 20. Shriver, et al. previously reported that for an O:Li ratio of 26, the ionic conductivity of polysiloxane – trifluoromethyl sulfonamide polyelectrolytes was 1.3×10^{-6} S/cm at 25 °C. Similarly Tominaga, et al. reported conductivities of ~10⁻⁵ S/cm at room temperature in a poly(propylene oxide) based sulfonimide. Given that the O:Li ratio in the PEG-dm-500/A200-C5NTfLi composites exceeds 200, increases in carrier concentration should substantially improve the conductivity, and thus we view the ionic conductivities observed for these samples as encouraging.

One concern with the measured conductivities is a potential contribution to the conductivity from residual silanols on the surface of the silica particle. These groups also should be lithiated under the conditions used to deprotonate the sulfonimide. To test for conductivity due to the lithiated silanols, A200 was treated with butyllithium using the same protocol for the synthesis of A200-C5NTfLi. A 30 wt% composite prepared from the lithiated silica and PEG-dm-500 was analyzed by impedance spectroscopy. The conductivity of the composite was < 10⁻⁸ S/cm, the detection limit of the AC impedance analyzer. Thus we conclude that the contribution from lithiated silanols can be neglected.

Sample (wt%)	O:Li ratio	σ (S/cm) 30 °C	σ (S/cm) 80 °C
19	710	1.27x10 ⁻⁶	2.49x10 ⁻⁶
24	530	8.35x10 ⁻⁷	1.36x10 ⁻⁶
30	390	1.20×10^{-6}	3.02x10 ⁻⁶
35	310	5.28x10 ⁻⁷	1.73×10 ⁻⁶
40	250	-	4.48x10 ⁻⁸

Table 9. Lithium concentrations of various composite polymer electrolytes and their measured ionic conductivities at 30 and 80 °C.

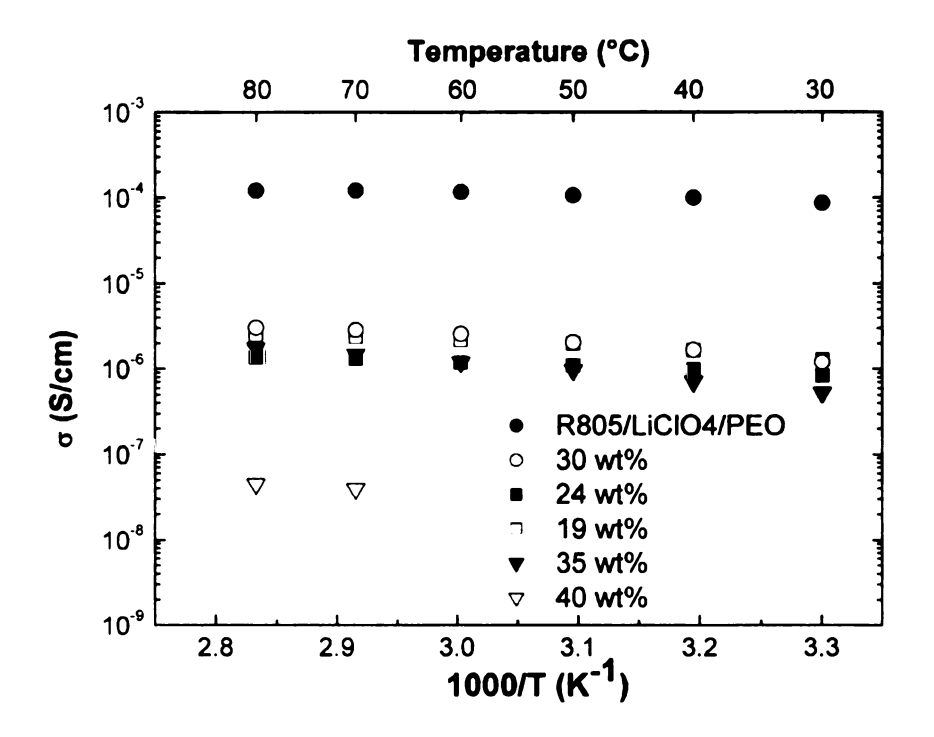


Figure 35. Conductivity of PEG-dm-500/A200-C5NTfLi composites. The data are derived from AC impedance measurements taken after equilibration for 20 min.

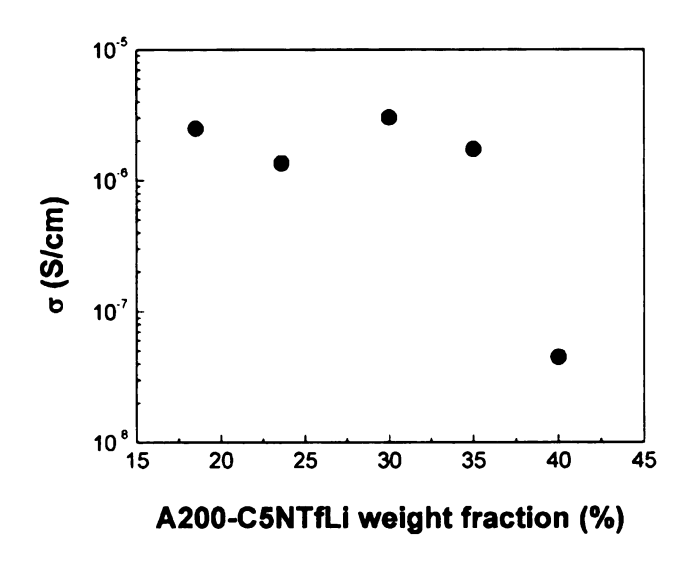


Figure 36. Cross section of conductivity at 40 °C. The data are obtained from the Arrhenius conductivity plot.

4.2.5 Transference number measurement

To support the claim that these composites are indeed single ion solid polymer electrolytes, lithium ion transference numbers were measured according to the method described by Bruce and Vincent.²³ The experiment involves the measurement of the bulk resistance of the material prior and after DC polarization. This provides the initial and the steady state interfacial resistance. The DC polarization step is conducted by application of a small bias, typically less than 10 mV, and the current decay to a steady state is monitored over time. This provides the initial and steady state current. The lithium ion transference number can then be determined using equation (4.1)

$$t_{Li^{+}} = \frac{I_{s} \left(\Delta V - I_{o} R_{o}\right)}{I_{o} \left(\Delta V - I_{s} R_{s}\right)} \tag{4.1}$$

where I_s and I_0 are the steady state and initial currents, and R_s and R_0 are the steady state and initial interfacial resistances respectively.

According to Bruce and Vincent, the interfacial resistances of an ideal electrolyte system can be ignored if the concentration of the charge carriers is small enough to create a linear concentration gradient between the electrodes. In addition the kinetics at the electrodes must be fast and the applied bias <10 mV. Since the lithium concentrations in the PEGDME500/A200-C5NTfLi composites are approximately one tenth of a typical electrolyte, we approximate this system as an ideal system, simplifying equation (4.1) to

$$t_{Li^{+}} = \frac{I_{s}}{I_{\circ}} \tag{4.2}$$

Using equation (4.2), t_{Li}^{+} was determined as described in the literature ¹⁰⁸ and was found to be 0.86 ± 0.03. In comparison, siloxyaluminate polymers containing ethylene oxide side chains exhibited t_{Li}^{+} of 0.71. ¹²¹ Whereas, the t_{Li}^{+} for PEO-LiTFSI was found to be 0.60 ± 0.03 for O:Li = 5. ²⁰⁴

4.2.6 Differential scanning calorimetry

Finally, the addition of fumed silica to PEO electrolytes is known to improve a variety of physical and electrochemical characteristics of electrolytes, including increasing their modulus and improving interfacial stability. We used DSC scans of the composites to

screen for particle-matrix interactions. In general, dissolution of salts in polyethers suppresses crystallinity. $^{19,173-178}$ For the A200-C5NtfLi composites, the charged surface of the nanoparticles suggest that their interaction with the polymer matrix will be similar to that of salts in polyethers. Shown in **Figure 37** are the DSC scans of 0, 10, 20 and 40 wt% PEG-dm-500/A200-C5NTfLi composites. The effects of the modified silica on the properties of PEG-dm-500 were minor. Only small decreases in the melting point and ΔH_{fus} temperature are seen over the entire composition range tested (**Figure 38**).

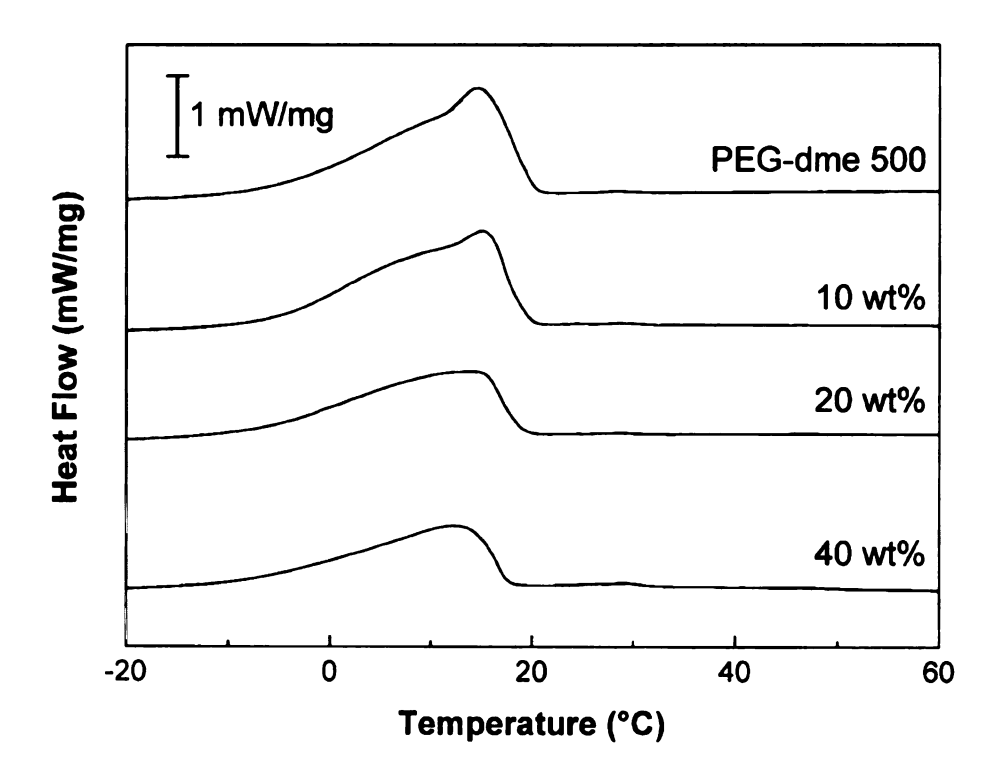


Figure 37. DSC scans of PEG-dm-500, 10, 20, and 40 wt% of PEG-dm-500/A200-C5NTfLi composite polymer electrolytes. Data were collected under He at a rate of 10 °C/min.

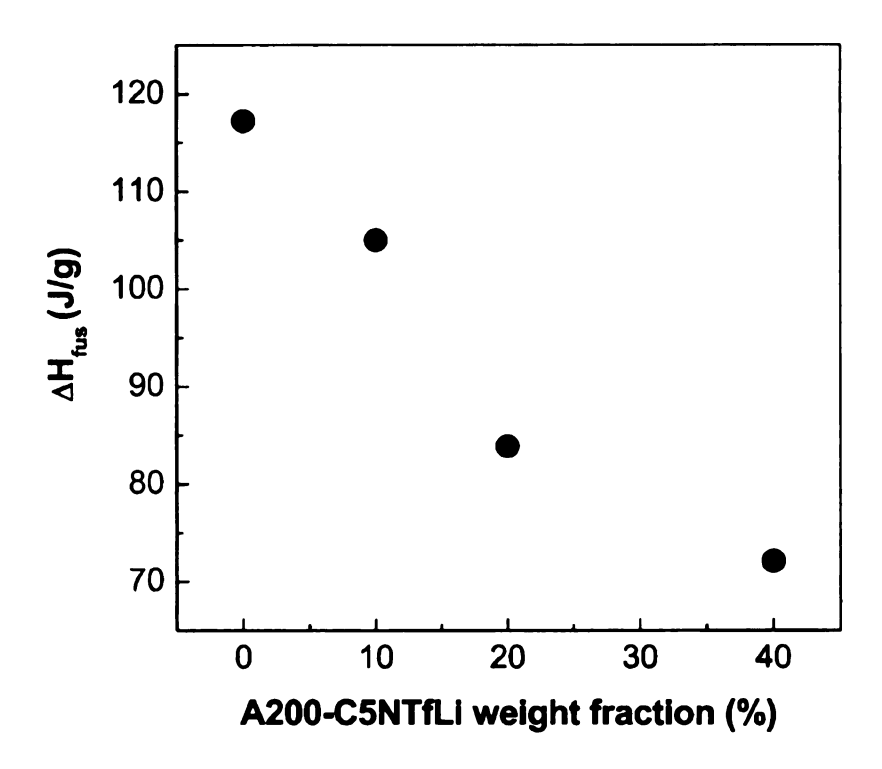


Figure 38. Comparison of the heat of fusion for the various composite polymer electrolytes as a function of weight percentage of A200-C5NTfLi. The data were obtained by integrating the areas under the curve for the melting transition for each DSC scan.

4.3 Conclusion

Lithium sulfonimide salts were successfully immobilized on the surface of nanoparticulate fumed silica. Dispersion of the particles in PEG-dm-500 gave polymer electrolytes with near unity lithium ion transference numbers. Composites containing 19-35 wt% silica had conductivities of $\sim 10^{-6}$ S/cm. The ionic conductivity of each complex was similar and exhibited a weak dependence on temperature. The conductivities of the 10, 15 and 50 wt% composites were $< 10^{-8}$ S/cm, presumably due to insufficient carriers in the case of

the first two composites, and discontinuity in the PEG-dm-500 polymer phase for the later composite. Although the lithium concentrations are too low to be of immediate practical use, improved conductivities may be obtained by grafting branched polymers to the surface of the silica nanoparticles where each branch is terminated with a lithium sulfonimide salt, thus increasing the lithium loading per nanoparticle.

4.4 Future work

Grafting branched polymers onto the silica nanoparticles can increase the ionic conductivity by increasing the lithium concentration within the composite polymer electrolytes. The termini of each branch would contain a lithium salt such as the lithium sulfonimide salt already used. The amount of lithium salt potentially delivered by each particle can be controlled by polymerizing a styrene derivative such as 4-vinylbenzoyl trifluoromethane-sulfonamide through atom transfer radical polymerization (ATRP). ATRP is a well established and widely used method to control the degree of polymerization in olefins. By controlling the reaction time and conditions one can optimize the lithium concentration per nanoparticle. Shown in **Scheme IV** is the proposed synthetic route by which this can be accomplished.

Scheme IV. Proposed synthetic scheme for increasing the concentration of lithium ions per particle.

4.5 Experimental

5-Bromopentene, triflouromethane sulfonyl anhydride, potassium phthalimide, butyllithium (1.6M in hexanes) (Aldrich) and Karstedt's catalyst (Gelest) were used as received. Aerosil 200 fumed silica, a gift from Degussa, was dried at 100 °C for 2 hours under vacuum before use. Triethyl amine was distilled over KOH pellets. Diethyl ether was dried by stirring over KOH pellets for 1 hr, and then was filtered three times through a pad of dried silica gel (Davisil, grade 633, 100-425 mesh (Aldrich). Toluene was distilled from sodium benzophenone ketyl. Poly(ethylene glycol) dimethyl ether (PEG-dm-500, ca. 500 g/mol) (Aldrich) was dissolved in dry diethyl ether, stirred over KOH pellets, and filtered four times through activated basic alumina. Diethyl ether, toluene and PEG-dm-500 were degassed immediately after purification and transferred into a helium filled drybox.

¹H NMR spectra were measured using a Varian Gemini-300 spectrometer at 300 MHz. All samples were run at room temperature in CDCl₃. Chemical shifts were calibrated using residual CHCl₃ and are reported in ppm (δ) relative to tetramethylsilane. ¹⁹F NMR spectra were measured in CDCl₃ using a Varian Inova-300 spectrometer at 282.2 MHz. The chemical shifts are reported in ppm (δ) relative to α,α,α-trifluoromethylbenzene. Infrared spectra of 1 and its lithium salt were obtained with a Mattson Galaxy Series FTIR 3000 as thin films sandwiched between NaCl plates. Diffuse reflectance infrared spectra of modified silicas were obtained from a computer-controlled Nicolet Protégé 460 equipped with a DRIFTS (diffuse reflectance infrared Fourier transform spectroscopy) Auxiliary experiment module. The samples were powders mounted on sample stubs and were mixed with potassium bromide in a 2:1 ratio of sample to salt.

All manipulations of the polymers and electrolytes were carried out in a helium drybox. AC impedance data were obtained from an HP 4192A LF Impedance Analyzer scanning from 5Hz to 13MHz with an applied voltage of 10 mV that was controlled by an in-house designed LabView application. All impedance samples have a thickness of 0.053 cm and an area of 1.27 cm². Data were taken at 30, 40, 50, 60, 70 and 80 °C, with the samples equilibrated at each temperature for at least twenty minutes prior to measurement. The sample cell was constructed of stainless steel disks separated by a Teflon collar. Differential scanning calorimetry (DSC) measurements were run under helium at a heating rate of 10 °C/min using a Perkin Elmer DSC 7 calibrated with indium. The reported DSC curves are second heating scans taken after an initial heating scan to erase the thermal history, and a fast quench to -100 °C. Thermogravimetric analyses (TGA) were run in air at a heating rate of 10 °C/min on a Perkin-Elmer TGA 7 instrument.

Synthesis of N-pentenyl triflouromethane sulfonimide, C5NHTf (1). Trifluoromethane sulfonyl anhydride (6.49 g, 23 mmol) was added dropwise to a vigorously stirred solution of N-pentenyl amine²⁰⁵ (2.00 g, 23 mmol), triethyl amine (2.56 g, 25 mmol) and freshly distilled dichloromethane (25 mL) cooled to -70 °C. After the addition was complete, the reaction mixture was allowed to warm to room temperature and stir for 2 hrs under nitrogen. The solvent was removed *in vacuo* to afford a yellow oil that was redissolved in 4N NaOH and washed with dichloromethane (2 × 50 mL). The product was then neutralized with 4N HCl and extracted with dichloromethane (8 × 50 mL). The combined organic layers were dried over MgSO₄, filtered, and the solvent removed under reduced pressure to afford a light yellow oil (2.5 g, 50 % yield) with spec-

tral data that match those reported in the literature.²⁰⁶ ¹H NMR δ 1.7 (q, 2H), 2.1 (q, 2H), 3.25 (q, 2H), 4.9 (br, 1H), 5.1 (m, 2H), 5.8 (m, 1H).

Synthesis of triethoxysilane, N-pentane trifluoromethane sulfonimide (2). Triethoxysilane (0.76 g, 4.6 mmol), compound 1 (1.0 g, 4.6 mmol) and Karstedt's catalyst (30 μ L) were dissolved in 1 mL of benzene and stirred in air overnight. The volatiles were removed under vacuum, and the residue was dissolved in diethyl ether and stirred over decolorizing carbon. Following filtration through a glass microfiber filter, the solvent was removed under vacuum to afford a mixture of compound 2, and divinyl silane (catalyst) as a viscous yellow oil. The crude product was used without further purification. ¹H NMR δ 0.5 (t 2H), 1.1 (t, 9H), 1.4 (m, 4H), 1.6 (q, 2H), 3.2 (q, 2H), 3.8 (q, 6H). ¹⁹F NMR (282.2 MHz, $C_6D_6\delta$) -72.4.

Modification of A200 fumed silica, A200-C5NHTf (3). Diethyl amine (44 μ L, 0.43 mol) and A200 fumed silica were stirred in 50 mL of toluene for 30 minutes under nitrogen. Compound 2 was then added to the mixture and stirring was continued at room temperature overnight. The solution was filtered and the residue was washed alternately with toluene (3 × 100 mL) and diethyl ether (3 × 100 mL) then finally rinsed with diethyl ether (6 × 100 mL). The residue (4.05 g) was further dried under vacuum at 50-60 °C overnight. IR 3263, 2989, 2932, 2893, 1989, 1880, 1688, 1447, 1376 cm⁻¹.

Lithiation of A200-C5NHTf, A200-C5NTfLi (4). Butyllithium (2 mL, 1.6 M in hexanes) was added dropwise to a dispersion of 3 (1.0 g) in 50 mL of freshly distilled tolu-

ene. After stirring overnight at ambient temperature, the solution was filtered under an inert atmosphere and the residue was washed alternately with toluene (3×50 mL) and diethyl ether (3×50 mL). The residue (0.74 g) was further dried under vacuum at 50-60 °C overnight. IR 3681, 2967, 2927, 2876 cm⁻¹.

Preparation of PEO/A200-C5NTfLi composites – general procedure. All electrolytes were prepared in a helium filled dry box. A specific example, the preparation of a 30 wt% composite, is described below. The modified silica nanoparticles (0.0162 g) were combined with a 1 mL solution of PEG-dm-500 (0.0385 g) in acetonitrile. After mixing, the sample was concentrated under reduced pressure to afford a dry powder that was further dried under vacuum at 56 °C. Upon shearing the electrolyte samples became viscous pastes that were then loaded into the sample cell.

Appendices

5 Appendix A

AC impedance spectroscopy LabView VI

Introduction

LabView is a program from National Instruments that allows a user to design a custom program to interface with a device to send and collect information as well as automate procedures. Examples of such programs can be found in pilot plants.

These programs are referred to as virtual instruments (VI), of which there are two components. The first is the user interface, referred to as the front panel, and the second is the programming, referred to as the wire diagram. Functions for communications, loops, boolean statements and the like are placed in this diagram and connections that symbolize data flow are drawn in as wires between these components. LabView offers a myriad of functions from the basic while loop statements to advanced functions capable of image analysis.

In the case of AC impedance spectroscopy the device used to collect the data is an HP 4192A LF analyzer capable of measuring the complex impedance and the phase angle between the applied bias and the measured current through the sample. To ease data collection and automate the process, a program was designed to interface with the HP 4192A and collect data at frequencies specified by the user.

Description

This is program is designed to interface with the HP 4192A LF Analyzer for impedance spectroscopy. It will initiate communications, setup the instrument to read the complex impedance and the phase angle. Data from the instrument is collected and stored in a user specified file after each measurement point and displayed at the same time.

Algorithm

- Start a while loop to keep the application going.
 - o End when the boolean to exit is switched to true.
 - o Continue while the *boolean* to exit is *false*.
- As long as the *while loop* is running, the program is in a ready state to acquire data.
 - o If boolean is false, stay in ready state
 - o If boolean is true continue.
- Initiate communications with the HP 4192A through the GPIB interface.
- Send experiment parameters to the device. These are the applied bias and the data to collect. In this case the data are the complex impedance and the phase angle between the applied bias and the current.
- Collect the data from the instrument at each frequency, record the data to a file and display the data in a bode plot.
- The data collection ends after the impedance at the last frequency is collected.
- Return to ready state.

Implementation

The algorithm is implemented by starting with three control structures, a while loop and two boolean statements. The while loop runs continuously as long as the boolean statement is set to false, if it becomes true then the program will end and close the application. Embedded in the boolean statement is another boolean to control data acquisition. When it is true, the embedded functions initiate communications with the instrument, sets up the instrument and begin the data acquisition. Upon completion the boolean is reset to false, in which the application is in ready mode.

Front panel

The applied bias, starting frequency, ending frequency and acquisition interval are all set by the user. The default settings are 0.01 V, 5.00E-3 KHz, 1.30E+3 KHz, and 1.00 s respectively. Two graphs on the right will display the data as it is collected from the HP 4192A LF Analyzer. Acquisition is commenced by pressing on the START button. Should the impedance of the material be greater than or smaller than the detection limits of the instrument, the INSTRUMENT FLOW light will turn red. The application is closed by pressing on the STOP button.

After pressing the acquisition button, a dialogue will popup and ask the user for the filename and its location, after which, it will commence with data collection. The data is saved in a comma separated format in which the first entry is the complex impedance, the second the phase angle and the third, the frequency all separated by a comma. Each line in the file is a different measurement at that frequency as shown in **Table 10**.

Line #	Data:
1	180000.000000,-15.000000,0.005000
2	170000.000000,-13.000000,0.005903
3	170000.000000,-11.000000,0.007379
4	170000.000000,-10.000000,0.009223
5	170000.000000,-8.000000,0.011529

Table 10. An example of the saved data. The format is the complex impedance, phase angle, frequency.

Data manipulation

The user is encouraged to save the file as *.csv file in order to facilitate opening the file in Excel. The real and imaginary components of the complex impedance can then be calculated as follows:

$$Z_{real} = Z' = |Z| + cos(\theta \frac{\pi}{180})$$

$$Z_{img} = Z'' = |Z| - sin(\theta \frac{\pi}{180})$$

Due to the fact that Excel and SigmaPlot calculate cosine, sine and tangents in radians, $\pi/180$ is inserted to convert the phase angle from degrees to radians. A Nyquist plot can be created using Z' as the x-axis and Z" as the y-axis. A macro was written for SigmaPlot to automate the process. It may be accessed through the Toolbox menu and then impedance analysis. New dialogues will popup asking the user to input the files to analyze. After pressing the OK button, the macro will proceed to analyze each file, create a new worksheet with the original and calculated data and a nyquist plot for each data set. The text of the macro is included in Appendix B.

6 Appendix B

Impedance Analysis Macro for SigmaPlot

Option Explicit

Dim SelectedFiles\$(),SaveFile\$

Dim i, Index, ReportIndex As Integer Function FlagOn(flag As Long) FlagOn = flag Or FLAG SET BIT ' Use to set option flag bits on, leaving others unchanged End Function Function FlagOff(flag As Long) FlagOff = flag Or FLAG CLEAR BIT ' Use to set option flag bits off, leaving others unchanged End Function Sub Main 'Macro edited 08/19/01 Fadi Asfour 'For the purpose of batch analysis of impedance data collected from HP 4192A LF Impedance Analyzer 'the format of the data is assumed to be in comma delimited form and the extension of the files 'are .csv 'Macro created 01/19/2000 John Kuo 'This macro is an example of automating a batch process. You can create a 'list of any number of Excel files, then import a specified block of data from 'each file. The data from each Excel file is imported into a separate 'worksheet. You can then either plot and/or curve fit the first two columns 'of imported data, and save the results to a specified notebook. 'Note that only the data for the first sheet is currently imported, and there 'is no way to specify a different sheet. This import property will be forthcoming

```
'* Set default save file; edit this to *
'* change the default save path
**********
SaveFile = path + "\" + "BatchFile.jnb"
'Create Graph Type list
Dim GraphTypes$()
ReDim GraphTypes(1)
GraphTypes(0) = "Simple Scatter Plot"
GraphTypes(1) = "Simple Bar Chart"
'Initialize file list
ReDim SelectedFiles$(0)
    SelectedFiles(0) = Empty
'Initialize file name list
'Dim FileNames$(0)
   FileNames(0)=Empty
'Dim DataDir As String
    DataDir = path + "\"
'Dim Equations$()
'Dim FitLibrary$
'Defines the equation source. Edit to use a different fit
library
'FitLibrary = "Standard.jfl"
'Open the fit library
'Notebooks.Open(path + "\" + FitLibrary, ".jfl")
'Dim FitFile As Object
'Set FitFile = Notebooks(path + "\" + FitLibrary)
'FitFile.Visible=False
'Populate equation list with all equation items in fit li-
brary
'i=0
'Index = 0
'For i = 0 To FitFile.NotebookItems.Count - 1
    If FitFile.NotebookItems(i).ItemType = 6 Then
         ReDim Preserve Equations$(Index)
        Equations(Index) = FitFile.NotebookItems(i).Name
         Index = Index + 1
     'End If
'Next i
i=-1
MacroDialog:
```

```
Begin Dialog UserDialog 470,546, "Batch Process Excel
Files", .DialogFunc '%GRID:10,7,1,1
          'browsebutton for data path
          'PushButton
10,21,90,21, "Browse...", .BrowseButton1
          'TextBox 120,21,330,21,.DataPath
          CheckBox
                                   50,63,140,14, "Single-step
mode", .stepmode
          PushButton 240,63,90,21,"Add
                                          &File...",.AddFile
'Click Add File to add excel files to the list
          PushButton 350,63,90,21,"Delete File",.DeleteFile
          Text 10,84,90,14,"&Data files:",.Text1
          ListBox 10,105,450,126,SelectedFiles(),.Files
          OKButton 270,518,90,21
          CancelButton 370,518,90,21
          PushButton 10,518,90,21, "Help", .Help
          GroupBox 10,245,450,70,"Import Range", .Range
          Text 20,259,80,21, "&Start column", .Text2
          TextBox 110,259,60,21,.startcol
          Text 200,259,80,14,"&End column",.Text4
          TextBox 290,259,60,21,.endcol
          Text 20,287,90,14, "Start &row", .Text3
          TextBox 110,287,60,21,.startrow
          Text 200,287,60,14,"End ro&w",.Text5
          TextBox 290,287,60,21,.endrow
          GroupBox 10,329,450,105, "Process", .GroupBox1
          CheckBox 20,350,80,14, "&Plot data", .PlotData
          Text 110,350,20,14,"&as:",.Text6
          DropListBox
180,350,260,63,GraphTypes(),.GraphList
          'CheckBox
                           20,287,110,14,"&Curve
                                                          fit
data", .FitData
          'Text 136,287,90,14,"&using:",.Text7
          'DropListBox 180,284,260,154, Equations(), .FitList
          Text 20,399,420,28,"Note: columns 4 & 5 will be
created from imported data and will be plotted", .Text8
          Text 10,462,120,14, "Sa&ve notebook to:", .Text9
          TextBox 10,483,450,21,.SavePath
          PushButton
370,455,90,21, "Browse...", .BrowseButton
     End Dialog
     Dim dlq As UserDialog
'Default settings
'SaveFile
dlq.SavePath = SaveFile
```

```
'* Change this setting to change the default *
'* location of the source data block
dlq.startcol = "1"
dlg.startrow = "1"
dlg.endcol = "3"
dlq.endrow = "512"
'* You can also change whether the data are *
'* plotted or fitted by default
************
dlg.PlotData = 0
'dlq.FitData = 1
'* Sets the default Graph Type
'* 0=Simple Scatter Plot, 1=Simple Bar Chart *
***********
dlg.GraphList = 0
*************
'* Sets the default Fit Equation
*************
'dlg.FitList = 22 '4 parameter Logistic
'See the end of the file for a list of all built-in equa-
tions by number
'These numbers only apply to the factory default Stan-
dard.jfl library
Select Case Dialog(dlg)
    Case 0 'Handles Cancel button
        GoTo Finish
    End Select
'Error if no Excel files picked
If SelectedFiles(0) = Empty Then
    MsqBox
            "You
                  have not
                               selected any
                                               Excel
Files", vbExclamation, "No Files Selected"
    GoTo MacroDialog
End If
Dim CurrentNotebook
Set CurrentNotebook = Notebooks.Add
'Iterate through each selected Excel file
'You can change the extension to import files of different
types
Index = 0
ReportIndex = 0
```

```
For Index = 0 To UBound(SelectedFiles)
    CurrentNotebook.CurrentDataItem.Open
    CurrentNote-
book.CurrentItem.Import(SelectedFiles(Index),
                                               0,
                                     CLng(dlg.startrow)-1,
CLng(dlg.startcol)-1,
CLng(dlg.endcol) -1, CLng(dlg.endrow) -1, ".CSV")
     'Name the data sheet according to its file name
    CurrentNotebook.CurrentItem.Name
                                            GetFile-
Name (SelectedFiles(Index))
    If dlg.stepmode = 1 Then MsgBox("The data is imported
from the Excel Worksheet...", vbInformation, "SigmaPlot")
'Calculate Re|Z| and Img|Z|
Dim SPTransform As Object
Set SPTransform = ActiveDocument.NotebookItems.Add(9)
SPTransform.Open
'note must specify use trig functions in units of radians;
data is in units of degrees
'0 = Radians, 1= Degrees, 2 = Grads
SPTransform.TrigUnit = 0
SPTransform.Text = "pi=3.1415926" + vbCrLf +
"z=col(1)" + vbCrLf + _
"w=col(2)" + vbCrLf +
"col(4)=z*COS(w*pi/180)" + vbCrLf +
"col(5) = -z*SIN(w*pi/180)" + vbCrLf
'use + vbCrLf + to create a line break
'* Debug transform code; this opens the transform in *
'* the transforms dialog for viewing and editing
'SPTransform.RunEditor
SPTransform. Execute
SPTransform.Close(False)
'Plot the graph
If dlg.PlotData = 1 Then
    Dim SPPage
    Set
          SPPage
                  = CurrentNotebook.NotebookItems.Add(2)
'Creates graph page
    Dim PlottedColumns(1) As Variant
         PlottedColumns(0) = 3
         PlottedColumns(1) = 4
```

```
SPPage.CreateWizardGraph("Scatter Plot", "Simple Scat-
ter","XY Pair",PlottedColumns)
     'select current graph as CurrentPageItem
     Dim GPage
     Set GPage = ActiveDocument.CurrentPageItem
     GPage.GraphPages(0).Graphs(0).SelectObject
     'Sets the X-Axis title To "Re |Z|" And the Y-Axis ti-
tle To "Img |Z|".
     GPage.SetCurrentObjectAttribute(GPM SETPLOTATTR,
SLA SELECTDIM, 1)
     GPage.GraphPages (0).CurrentPageObject (GPT AXIS).NameOb
ject.SetObjectCurrent
     GPage.SetCurrentObjectAttribute(GPM SETAXISATTR,
SAA RTFNAME,
"{\rtf1\ansi0{\colortbl\red0\green0\blue0;}\deff0{\fonttbl\
f0\fi Arial;}{\s1240\s1mult0\f0\cf0\up0\fs16\i0\b0\u10\q1
Re |Z|}")
     GPage.SetCurrentObjectAttribute(GPM SETPLOTATTR,
SLA SELECTDIM, 2)
     GPage.GraphPages(0).CurrentPageObject(GPT AXIS).NameOb
ject.SetObjectCurrent
     GPage.SetCurrentObjectAttribute(GPM SETAXISATTR,
SAA RTFNAME,
"{\rtf1\ansi0{\colortbl\red0\green0\blue0;}\deff0{\fonttbl\
f0\fnil Arial; } `}")
     'Set the tick orientation inward on all sides
     GPage.SetCurrentObjectAttribute(GPM SETAXISATTR,
SAA SELECTLINE, 2)
     GPage.SetCurrentObjectAttribute(GPM SETAXISATTR,
SAA TICSIZE, 50)
     GPage.SetCurrentObjectAttribute(GPM SETAXISATTR,
SEA THICKNESS, 10)
     GPage.SetCurrentObjectAttribute(GPM SETAXISATTR,
SAA SUB1OPTIONS, &H0001515c&)
     GPage.SetCurrentObjectAttribute(GPM SETAXISATTR,
SAA SUB2OPTIONS, &H0000011c&)
     GPage.SetCurrentObjectAttribute(GPM SETAXISATTR,
SAA SELECTLINE, 2)
     GPage.SetCurrentObjectAttribute(GPM SETPLOTATTR,
SLA SELECTDIM, 1)
     GPage.SetCurrentObjectAttribute(GPM SETPLOTATTR,
SLA SELECTDIM, 1)
     GPage.SetCurrentObjectAttribute(GPM SETAXISATTR,
SAA SELECTTIC, 1)
```

```
GPage.SetCurrentObjectAttribute(GPM SETAXISATTR,
SAA SELECTLINE, 2)
     GPage.SetCurrentObjectAttribute(GPM SETAXISATTR,
SAA TICSIZE, 50)
    GPage.SetCurrentObjectAttribute(GPM SETAXISATTR,
SEA THICKNESS, 10)
    GPage.SetCurrentObjectAttribute(GPM SETAXISATTR,
SAA SUB1OPTIONS, &H0001515c&)
    GPage.SetCurrentObjectAttribute(GPM SETAXISATTR,
SAA SUB2OPTIONS, &H0000011c&)
     GPage.SetCurrentObjectAttribute(GPM SETAXISATTR,
SAA SELECTLINE, 2)
     'Set the symbols in the graph to small size 0.060in
circles
     GPage.SetCurrentObjectAttribute(GPM SETPLOTATTR,
SSA OPTIONS, &H00000201&)
    GPage.SetCurrentObjectAttribute(GPM SETPLOTATTR,
SSA EDGETHICKNESS, 10)
    GPage.SetCurrentObjectAttribute(GPM SETPLOTATTR,
SSA SIZE, 60)
    GPage.SetCurrentObjectAttribute(GPM SETPLOTATTR,
SSA SIZEREPEAT, 2)
    'Dim ColumnsPerPlot()
     'ReDim ColumnsPerPlot(2, 1)
     'ColumnsPerPlot(0, 0) = 0
     'ColumnsPerPlot(1, 0) = 0
     'ColumnsPerPlot(2, 0) = 31999999
     'ColumnsPerPlot(0, 1) = 1
     'ColumnsPerPlot(1, 1) = 0
     'ColumnsPerPlot(2, 1) = 31999999
     'Dim PlotColumnCountArray()
     'ReDim PlotColumnCountArray(0)
     'PlotColumnCountArray(0) = 2
     'Select Case dlg.GraphList
         Case 0 'Simple Scatter Plot
              SPPage.CreateWizardGraph("Scatter Plot",
"Simple Scatter", "XY Pair", ColumnsPerPlot, PlotCol-
umnCountArray)
         Case 1 'Simple Bar Chart
              SPPage.CreateWizardGraph("Vertical
Chart", "Simple Bar", "XY Pair", ColumnsPerPlot, PlotCol-
umnCountArray)
     'End Select
     'SPPage.GraphPages(0).Graphs(0).Plots(0).SelectObject
```

'Curve needs to be selected in order to plot curve fit

```
SPPage.Open
     If dlg.stepmode = 1 Then MsgBox("The data is plot-
ted...", vbInformation, "SigmaPlot")
End If
'Fit the data; modify the fit options to suit your needs
'On Error GoTo FitFailed
'If dlg.FitData = 1 Then
     'Dim FitEquation$
     'FitEquation = Equations(dlg.FitList)
     'Dim FitObject As Object
     'Set FitObject = FitFile.NotebookItems(FitEquation)
     'FitObject.Open
     'FitObject.DatasetType = CF XYPAIR
     'FitObject.Variable("x") = \overline{\text{"col}(1)}"
     'FitObject.Variable("y") = "col(2)"
     'FitObject.Run
     'FitObject.OutputReport = True
     'FitObject.OutputEquation = False
     'FitObject.ResidualsColumn = -1
     'FitObject.PredictedColumn = -1
     'FitObject.ParametersColumn = -1
     'FitObject.OutputGraph = False
     'FitObject.OutputAddPlot = True
     'FitObject.ExtendFitToAxes = True
     'FitObject.AddPlotGraphIndex = 0
     'FitObject.XColumn = -1
     'FitObject.YColumn = -1
     'FitObject.ZColumn = -2
     'FitObject.Finish
     'If dlq.stepmode = 1 Then MsqBox("The data is curve
             and
                                report
                                            is
ated...", vbInformation, "SigmaPlot")
'End If
Wait 1
'Close the document windows
CurrentNotebook.CurrentDataItem.Close(True)
        dlg.FitData
                                       Then
                             1
                                                 CurrentNote-
book.NotebookItems("Report " + CStr(ReportIndex
1)).Close(True)
'GoTo Skip
'GoTo Finish
'FitFailed:
                    have
'MsqBox("Error(s)
                            occurred
                                        in fitting
                                                         your
data.", vbExclamation, "SigmaPlot")
```

```
'ReportIndex = ReportIndex - 1
'Skip:
'If
        dlg.PlotData = 1
                                    Then
                                            CurrentNote-
book.NotebookItems("Graph Page " + CStr(Index
1)).Close(True)
'If dlg.stepmode = 1 Then MsgBox("The results windows are
closed...", vbInformation, "SigmaPlot")
'Create a new worksheet for the next file
If Index <> UBound(SelectedFiles) Then
     CurrentNotebook.NotebookItems.Add(1)
     If dlg.stepmode = 1 Then MsgBox("A worksheet is cre-
           for
                               next
                                         Excel
ated
                     the
sheet...", vbInformation, "SigmaPlot")
End If
ReportIndex = ReportIndex + 1
Next Index
'FitFile.Close(False) 'Close standard.jfl
'Save the file
If dlg.stepmode = 1 Then MsqBox("You are prompted to save
the file...", vbInformation, "SigmaPlot")
CurrentNotebook.SaveAs(SaveFile)
Finish:
End Sub
Rem See DialogFunc help topic for more information.
Private Function DialogFunc(DlgItem$, Action%, SuppValue&)
As Boolean
     Select Case Action%
    Case 1 ' Dialog box initialization
         DlgEnable ("DeleteFile", False)
    Case 2 ' Value changing or button pressed
        Select Case DlgItem$
       Case "CancelButton"
         DlgEnd 1000 'Handles Cancel button from file dia-
log
         Case "Help"
              Dim ObjectHelp, HelpID As Variant
              ObjectHelp = Path + "\SPW.CHM"
              HelpID = 70200
                                          Help ID number
for this topic in SPW.CHM
              Help(ObjectHelp, HelpID)
              DialogFunc = True 'do not exit the dialog
         Case "AddFile" 'Adds file to list
              Dim SelectedFile$
```

```
comma delimited File")'You can change the extension to im-
port files of different types
               If SelectedFile <> "" Then
                    i = i + 1
                    ReDim Preserve SelectedFiles$(i)
                    SelectedFiles(i) = SelectedFile
                    DlgListBoxArray "Files", SelectedFiles
               End If
               DialogFunc = True 'do not exit the dialog
          Case "DeleteFile" 'Removes files from list
               SelectedFiles(DlgValue("Files")) = Empty
               If DlgValue("Files") < UBound(SelectedFiles)</pre>
Then 'Re-indexes array if index removed from middle of ar-
ray
                    For Index = DlqValue("Files") To UB-
ound(SelectedFiles)-1
                         If SelectedFiles(Index) = Empty Then
                              Selected-
Files (Index) = SelectedFiles (Index+1)
                              SelectedFiles(Index+1) = Empty
                         End If
                    Next Index
               End If
               If i \ge 1 Then i=i-1
               If i \le 0 Then i=0
               DlgListBoxArray "Files", SelectedFiles
               ReDim Preserve SelectedFiles$(i)
               If i = 0 Then i = -1
               DlgEnable("DeleteFile", False)
               DialogFunc = True 'do not exit the dialog
          Case "BrowseButton" 'Set save path
               SaveFile = GetFilePath(,"JNB",, "Select Note-
book File",1)
                                                ** **
               Ιf
                        SaveFile
                                       <>
                                                         Then
DlgText("SavePath", SaveFile)
               DialogFunc = True 'do not exit the dialog
     Case "Files" 'Enables Delete button if a file is se-
lected
                      DlgValue("Files") <> -1
               Ιf
                                                         Then
DlgEnable("DeleteFile", True)
          End Select
     Case 4
        Select Case DlgItem$
```

SelectedFile = GetFilePath (,"csv",,"Select

```
Case "Files" 'Enables Delete button if a file is
selected
                     DlgValue("Files") <> -1 Then
               Ιf
DlgEnable("DeleteFile", True)
         End Select
    Case 5
        DialogFunc = True
    End Select
End Function
'Author: Maria Rapini
'Source: http://www.freevbcode.com/ShowCode.Asp?ID=1638
'Modified 8/19/01 Fadi Asfour
Public Function GetFileName(flname As String) As String
    'Get the filename without the path or extension.
    'Input Values:
       flname - path and filename of file.
    'Return Value:
       GetFileName - name of file with extension.
    Dim posn As Integer, i As Integer
   Dim fName As String
   posn = 0
   'find the position of the last "\" character in file-
name
   For i = 1 To Len(flname)
       If (Mid(flname, i, 1) = "\") Then posn = i
   Next i
    'get filename without path
    fName = Right(flname, Len(flname) - posn)
    'get filename without extension
    'posn = InStr(fName, ".")
        If posn <> 0 Then
             fName = Left(fName, posn - 1)
        End If
    GetFileName = fName
End Function
'Standard.jfl equation list
'Use the following values to set the default equation num-
ber:
'Polynomial
' 0' Linear
```

```
1'
         Ouadratic
    21
         Cubic
    3'
         Inverse First Order
    4 '
         Inverse Second Order
    5 '
         Inverse Second Order
'Peak
    6'
         Gaussian, 3 Parameter
    7'
         Gaussian, 4 Parameter
    8 '
         Modified Gaussian, 4 Parameter
    9'
         Modified Gaussian, 5 Parameter
    10'
         Lorentzian, 3 Parameter
         Lorentzian, 4 Parameter
    11'
    12'
         Pseudo-Voigt, 4 Parameter
    13' Pseudo-Voigt, 5 Parameter
    14'
         Log Normal, 3 Parameter
    15'
         Log Normal, 4 Parameter
    16'
         Weibull, 4 Parameter
    17'
         Weibull, 5 Parameter
'Sigmoidal
    18'
         Sigmoid, 3 Parameter
    19'
         Sigmoid, 4 Parameter
         Sigmoid, 5 Parameter
    20'
    21'
         Logistic, 3 Parameter
    22'
         Logistic, 4 Parameter
    23'
         Weibull, 4 Parameter
         Weibull, 5 Parameter
    24'
    25'
         Gompertz, 3 Parameter
    26'
         Gompertz, 4 Parameter
    27'
         Hill, 3 Parameter
    28'
         Hill, 4 Parameter
    29'
         Chapman, 3 Parameter
    30'
         Chapman, 4 Parameter
'Exponential Decay
    31'
         Single, 2 Parameter
    32'
         Single, 3 Parameter
    33'
         Double, 4 Parameter
    34'
         Double, 5 Parameter
    35'
         Triple, 6 Parameter
    36'
         Triple, 7 Parameter
    37'
         Modified Single, 3 Parameter
    38'
         Exponential Linear Combination
'Exponential Rise To Maximum
    39'
         Single, 2 Parameter
    40'
         Single, 3 Parameter
    41' Double, 4 Parameter
    42'
         Double, 5 Parameter
    43'
         Simple Exponent, 2 Parameter
```

```
44'
         Simple Exponent, 3 Parameter
'Exponential Growth
    45'
         Single, 1 Parameter
    46'
         Single, 2 Parameter
    47'
         Single, 3 Parameter
    48' Double, 4 Parameter
    49'
         Double, 5 Parameter
    50'
         Modified Single, 1 Parameter
    51' Modified Single, 2 Parameter
    52' Stirling Model
    53'
         Simple Exponent, 2 Parameter
    54'
         Simple Exponent, 3 Parameter
    55'
         Modified Simple Exponent, 2 Parameter
'Hyperbola
    56'
         Single Rectangular, 2 Parameter
    57'
         Single Rectangular i, 3 Parameter
    58'
         Single Rectangular II, 3 Parameter
    59' Double Rectangular, 4 Parameter
    60'
         Double Rectangular, 5 Parameter
         Hyperbolic Decay, 2 Parameter
    61'
    62'
         Hyperbolic Decay, 3 Parameter
    63' Modified Hyperbola i
    64'
         Modified Hyperbola II
    65'
         Modified Hyperbola III
'Waveform
    66'
         Sine, 3 Parameter
    67' Sine, 4 Parameter
    68' Sine Squared, 3 Parameter
    69' Sine Squared, 4 Parameter
    70' Damped Sine, 4 Parameter
    71' Damped Sine, 5 Parameter
    72'
         Modified Sine
    73' Modified Sine Squared
    74' Modified Damped Sine
'Power
    75'
         2 Parameter
    76' 3 Parameter
    77' Pareto Function
    78' Symmetric, 3 Parameter
    79'
         Symmetric, 4 Parameter
    80' 2 Parameter Modified i
    81'
         2 Parameter Modified II
    82' Modified Pareto Function
'Rational
    83' 1 Parameter i
    84' 1 Parameter II
    85' 2 Parameter i
```

```
86' 2 Parameter II
    87' 3 Parameter i
    88' 3 Parameter II
    89' 3 Parameter III
    90' 3 Parameter IV
    91' 4 Parameter
    92' 5 Parameter
    93' 6 Parameter
    94' 7 Parameter
    95' 8 Parameter
    96' 9 Parameter
    97' 10 Parameter
    98' 11 Parameter
'Logarithm
    99' 2 Parameter i
    100' 2 Parameter II
    101' 2 Parameter III
    102' 3 Parameter
    103' 2nd Order
    104' 3rd Order
'3D
    105' Plane
    106' Paraboloid
    107' Gaussian
    108' Lorentzian
'User-Defined
    109' Untitled
'Standard Curves
  110' Linear Curve
    111' Four Parameter Logistic Curve
```

7 Appendix C

Transference number measurements based on Bruce and Vincent papers

(J. Electroanal. Chem., 1987, 225, 1-17)

(Solid State Ionics, 1992, 53-56, 1087-1094)

A transference number is the fraction of current carried by a charged species relative to all mobile species in an electrolyte. To quantify transference numbers, it is necessary to measure the amount of current for each charged species. Bruce and Vincent provide a relatively simple technique to conduct such measurements.

First, recall that Onsager's equations relates the current flow of each species to the appropriate electrochemical potential gradient

$$i_{+} = -\frac{\sigma_{++}}{F} \frac{d\overline{\mu}_{+}}{dx} - \frac{\sigma_{+-}}{F} \frac{d\overline{\mu}_{-}}{dx}$$

$$i_{-} = -\frac{\sigma_{--}}{F} \frac{d\overline{\mu}_{-}}{dx} - \frac{\sigma_{+-}}{F} \frac{d\overline{\mu}_{+}}{dx}$$
(7.1)

where

 σ_{++}, σ_{--} = free cation & anion conductivities

 σ_{+-} = cation - anion interaction

F = Faraday's constant

 $\overline{\mu}_{+}, \overline{\mu}_{-} = \text{chemical potential}$

This means that the current carried by a charged species is dependent on the chemical gradient across the sample and its interactions with other ions.

Second, it must be understood that an ideal electrolyte is one where 1) ion-ion interactions may be neglected, 2) charge transfer processes are effectively infinitely fast, 3) convection does not contribute to ion transport within the electrolyte and 4) the concentration of the electrolyte remains sufficiently high such that the double layers at the electrodes can be neglected.

There are three states that need to be considered. The first is the initial state in which a bias has just been applied across the electrolyte. The second is at some intermediate state after t = 0 in which a concentration gradient begins to form. The third is when a steady state condition has been reached.

Initial State

When a DC potential of ΔV is applied across the electrolyte the potential drop $(\Delta \phi)$ is

$$\Delta \phi = \Delta V \tag{7.2}$$

and the initial current is given as

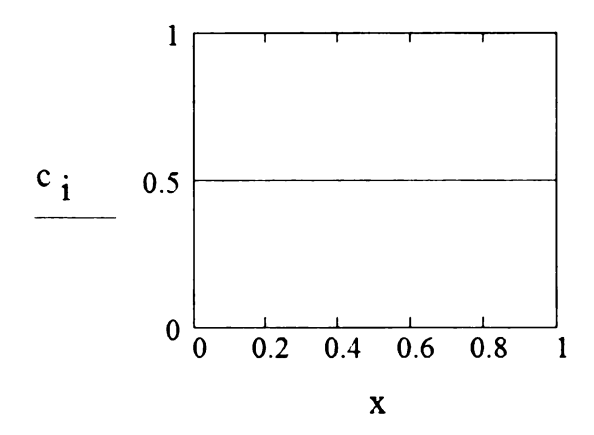
$$I_0 = F(u_+^\circ + u_-^\circ)c_0\Delta V = \sigma\Delta V \tag{7.3}$$

where u_{+}° and u_{-}° are the cationic and anionic mobilities respectively in an ideal electrolyte. Since mobilities are a function of diffusion one can use the Nernst-Einstein relationship to redefine the initial current as

$$I_0 = \frac{F^2(D_+^{\circ} + D_-^{\circ})c_{\circ}}{RT} \Delta V$$
 (7.4)

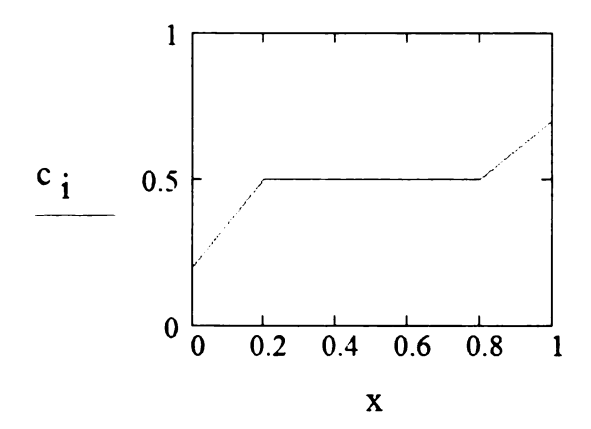
where D_{+}° and D_{-}° are the cationic and anionic diffusions in an ideal electrolyte respectively. The concentration of ions at this initial state is homogenously distributed and can

be represented by a plot of the concentration of an ion where c_i is the concentration of species i and x is the distance between the electrodes.



Intermediate state

At t > 0 cations arriving at the cathode are consumed while an equivalent number are produced at the anode. This creates a salt concentration gradient in the vicinity of each electrode



The change in concentration at the electrode surfaces causes each electrode to develop a potential difference, where

Cathode
$$\Rightarrow$$
 negative (low M⁺, high e⁻)

Anode
$$\Rightarrow$$
 positive (high M⁺, low e⁻)

The sum of the potential developed is

$$\Delta E = \frac{RT}{F} \ln \left(\frac{c_a}{c_c} \right) \tag{7.5}$$

which is the Nernst equation. This means that the potential drop across the electrolyte is

$$\Delta \phi = \Delta V - \Delta E \tag{7.6}$$

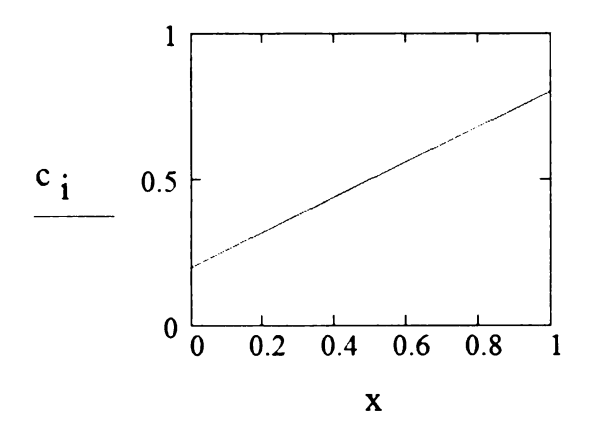
Note that ion diffusion opposes the migration current and the migration currents of the anions and cations decreases with time as ΔE increases. Ion transport is now influenced by diffusion due to the presence of the salt concentration gradients. In polymer electrolytes the diffusion layers will continue to grow until they merge and a steady state condition is established.

Steady state

In the steady state condition the electrolyte has reached an equilibrium where

- Electro-neutrality requires that $c_+ = c_- = c$
- Ion migration and diffusion must be equal and opposite $\left|I_{-}^{d}\right| = \left|I_{-}^{m}\right|$ and $\left|I_{+}^{d}\right| = \left|I_{+}^{m}\right|$

In this condition a chemical gradient has been established between the electrodes



This implies no further mobility of ions, which means that the electrochemical potential for the anions throughout the electrolyte is

$$d\overline{\mu}_{-} = RTd\ln c + Fd\phi = 0 \tag{7.7}$$

where the electrical and chemical potential gradients are related as

$$\frac{d\phi}{dx} = \frac{RT}{F} \frac{d\ln c}{dx} = \frac{RT}{Fc} \frac{dc}{dx} \tag{7.8}$$

Recall that in the steady state the current due to the cations (I_+) is

$$I_{+} = I_{+}^{d} + I_{+}^{m} \tag{7.9}$$

Consider the linear mass transfer or flux (J) of species i

$$-J_{i} = D_{i} \frac{dc_{i}}{dx} + \frac{z_{i}F}{RT} D_{i}c_{i} \frac{d\phi}{dx}$$
(7.10)

where z_i is the charge of the species, which in most cases is 1. D_i is the diffusion and c_i is the concentration of species i. Since the mass transfer of species i is based on diffusion and migration then the flux equation can be written as

$$-J_{i} = \frac{I_{i}}{FA} = \frac{I_{i}^{d}}{FA} + \frac{I_{i}^{m}}{FA}$$
 (7.11)

where A is the area through which the ions flow through. For simplification set A = 1.

The following equations are obtained by setting equation (7.10) equal to (7.11)

$$I_i^d = FD_i \frac{dc_i}{dx} \tag{7.12}$$

$$I_i^m = \frac{F^2 D_i}{RT} c_i \frac{d\phi}{dx} \tag{7.13}$$

Equation 7.8 can now be written as

$$I_{+} = FD_{+}^{\circ} \frac{dc}{dx} + \left(\frac{F^{2}D_{+}^{\circ}}{RT}\right)c\frac{d\phi}{dx}$$
 (7.14)

Substituting $\frac{d\phi}{dx}$ from equation (7.8) into equation (7.14) redefines I_+ in terms of a con-

centration gradient and equation (7.14) becomes

$$I_{+} = FD_{+}^{\circ} \frac{dc}{dx} + \left(\frac{F^{2}D_{+}^{\circ}}{RT}\right)c \left[\frac{RT}{Fc}\frac{dc}{dx}\right]$$
 (7.15)

$$I_{+} = 2FD_{+}^{\circ} \frac{dc}{dx} \tag{7.16}$$

This implies that under steady state conditions

$$I_{+} = 2I_{+}^{d} = 2I_{+}^{m} \tag{7.17}$$

so

$$I_{\perp}^d = I_{\perp}^m \tag{7.18}$$

The current due to the mass transfer of cations can also be written in terms of the anions as

$$I_{+}^{d} = \left(\frac{D_{+}^{\circ}}{D_{-}^{\circ}}\right) I_{-}^{d} \tag{7.19}$$

$$I_{+}^{m} = \left(\frac{D_{+}^{\circ}}{D_{-}^{\circ}}\right) I_{-}^{m} \tag{7.20}$$

Since the current flow is constant throughout the electrolyte, then, $D_{+}^{\circ}/D_{-}^{\circ}$ is constant.

This would mean that the concentration gradient is constant across the electrolyte, so

$$\frac{dc}{dx} = \frac{\Delta c}{\Delta x} = c_a - c_c \tag{7.21}$$

where c_a and c_c are the concentrations of ions at the anode and cathode respectively. Since $\Delta x = 1$ then $\Delta c = c_a - c_c$ so the concentration at any given point is

$$c = \Delta c x + c_c = (c_a - c_c) x + c_c \tag{7.22}$$

so

$$c_a + c_c = 2c_{\circ} \tag{7.23}$$

The potential drop across the electrolyte in the steady state becomes

$$\frac{d\phi}{dx} = I_{+}^{m} \left[\frac{RT}{F^{2}D_{+}^{\circ}} \right] \frac{1}{c} \tag{7.24}$$

$$\frac{d\phi}{dx} = I_{+}^{m} \left[\frac{RT}{F^{2}D_{+}^{\circ}} \right] \frac{1}{\left(c_{a} - c_{c}\right)x + c_{c}}$$

$$(7.25)$$

$$\phi_{a} - \phi_{c} = \Delta \phi = I_{+}^{m} \left[\frac{RT}{F^{2} D_{+}^{\circ}} \right]_{0}^{1} \frac{dx}{(c_{a} - c_{c})x + c_{c}}$$
(7.26)

$$\Delta \phi = I_{+}^{m} \left[\frac{RT}{F^{2}D_{+}^{\circ}} \right] \frac{1}{c_{a} - c_{c}} \ln \frac{c_{a}}{c_{c}}$$

$$(7.27)$$

Since

$$I_{+}^{m} = I_{+}^{d} = FD_{+}^{\circ} \frac{dc}{dx} = FD_{+}^{\circ} (c_{a} - c_{c})$$
 (7.28)

then

$$\Delta \phi = \left[F D_{+}^{\circ} \left(c_a - c_c \right) \right] \left[\frac{RT}{F^2 D_{+}^{\circ}} \right] \frac{1}{c_a - c_c} \ln \frac{c_a}{c_c}$$
 (7.29)

$$\Delta \phi = \frac{RT}{F} \ln \frac{c_a}{c_c} = \Delta E \tag{7.30}$$

so

$$\Delta \phi = \Delta V - \Delta E = \Delta V - \Delta \phi \tag{7.31}$$

$$\Delta V = 2\Delta \phi = 2\frac{RT}{F} \ln \frac{c_a}{c_c} \tag{7.32}$$

For any small value of ΔV , the equation 7.15 can be written as

$$I_{+} = 2FD_{+}^{\circ} \frac{dc}{dx} = 2FD_{+}^{\circ} (c_{a} - c_{c})$$
 (7.33)

Since current and voltage are the only variables that can be measured experimentally a relationship between the concentration gradient $(c_a - c_c)$ in equation (7.33) and $\ln \frac{c_a}{c_c}$

from equation 7.31 must be established. To do this let

$$\zeta = \frac{\left(c_a - c_c\right)}{c_c} \tag{7.34}$$

then

$$c_0 \ln \frac{c_a}{c_c} = \frac{c_a + c_c}{2} \ln \frac{c_a}{c_c} = c_c \left(1 + \frac{\zeta}{2} \right) \ln \left(1 + \zeta \right)$$
 (7.35)

in which $\ln(1+\zeta)$ can be expanded as $\left(\zeta - \frac{\zeta^2}{2} + \frac{\zeta^3}{3} - \frac{\zeta^4}{4} + \dots\right)$ when $\zeta < 1$. Equation

7.34 can be written as

$$\frac{c_a + c_c}{2} \ln \frac{c_a}{c_c} = \zeta \left(1 + \frac{\zeta^2}{12} - \frac{\zeta^3}{12} + 3\frac{\zeta^4}{40} - \dots \right)$$
 (7.36)

For small values of ζ then equation (7.36) simplifies to

$$\frac{c_a + c_c}{2} \ln \frac{c_a}{c_c} \simeq c_c \zeta = c_a - c_c \tag{7.37}$$

This implies that the current is

$$I_{+} = 2FD_{+}^{\circ} \left(c_{a} - c_{c}\right) \tag{7.38}$$

$$I_{+} = 2FD_{+}^{\circ}c_{0} \ln \frac{c_{a}}{c_{c}}$$
 (7.39)

Remember that $\Delta \phi = \frac{RT}{F} \ln \frac{c_a}{c_c}$ which means that

$$\ln \frac{c_a}{c_c} = \Delta \phi \frac{F}{RT} \tag{7.40}$$

current is then

$$I_{+} = \left(\frac{F^2 D_{+}^{\circ} c_0}{RT}\right) 2\Delta \phi \tag{7.41}$$

$$I_{+} = \frac{F^{2} D_{+}^{*} c_{0}}{RT} \Delta V \tag{7.42}$$

which simplifies to

$$I_{\perp} = F u_{\perp}^{\circ} c_0 \Delta V \tag{7.43}$$

This is important since equation (7.3) is

$$I_0 = F\left(u_+^{\circ} + u_-^{\circ}\right)c_0\Delta V = \sigma\Delta V$$

Recall that the transference number is defined as

$$t_i = \frac{|z_i|u_ic_i}{\sum_i |z_i|u_ic_i} \tag{7.44}$$

Remembering that $z_i = 1$ and the concentrations are equal then equation 7.38 simplifies to

$$t_i = \frac{u_i}{\sum_i u_i} \tag{7.45}$$

Rewriting equations (7.3) and (7.43) the following equation are obtained

$$\Delta V = \frac{I_0}{F(u_+^0 + u_-^0)c_0} \tag{7.46}$$

$$\Delta V = \frac{I_{+}}{Fu_{-}^{0}c_{0}} \tag{7.47}$$

Since ΔV is constant, then the ratio of the cationic steady state current to the initial current can be written as

$$\frac{I_{+}}{I_{0}} = \frac{Fu_{+}^{\circ}c_{\circ}\Delta V}{Fu_{+}^{\circ}c_{\circ}\Delta V + Fu_{-}^{\circ}c_{\circ}\Delta V}$$
(7.48)

which simplifies to

$$\frac{I_{+}}{I_{0}} = \frac{u_{+}^{\circ}}{u_{+}^{\circ} + u_{-}^{\circ}} = t_{+} \tag{7.49}$$

This means that a chronoamperometry experiment with an applied volatage of $\leq 10 \text{ mV}$ is needed to determine t_+ .

Conditions of use

The following conditions must be met in order to use the above equation

- a) The applied potential must be $\leq 10 \text{ mV}$
- b) The ratio of $c_0 \ln \frac{c_a}{c_c} / (c_a c_c)$ must be = 1 ± 1%
- c) The concentration of salt must be very small. In terms of lithium ion polymer electrolytes the O:Li ratio <<<<< 20!!

Otherwise for O:Li = 20 then the calculation of lithium ion transference numbers is determined through the following equation

$$t_{Li} = \frac{I_{ss}}{I_0} \left(\frac{\Delta V - I_0 R_0}{\Delta V - I_{ss} R_{ss}} \right)$$
 (7.50)

where the subscript ss denotes steady state conditions of the cation. This determination still involves a chronoamperometry step with an applied bias of ≤ 10 mV. However, it is conducted after the measurement of the initial interface resistance (R_0) and prior to measurement of the final interfacial resistance (R_{ss}) . Both resistances are determined through AC impedance spectroscopy.

Bibliography

8 Bibliography

- (1) Linden, D. Handbook of Batteries; 2nd ed.; McGraw-Hill Inc.: New York, 1995
- (2) Schalkwijk, W. A. V.; Scrosati, B., Eds. Advances in Lithium-Ion Batteries; Kluwer Academic / Plenum Publishers: New York, 2002.
- (3) Carvalho, L. M.; Guegan, P.; Cheradame, H.; Gomes, A. S. Eur. Polym. J., 2000, 36, 401-409.
- (4) Aabloo, A.; Thomas, J. Solid State Ionics., 2001, 143, 83-87.
- (5) Borodin, O.; Smith, G. D. *Macromolecules*, **1998**, *31*, 8396-8406.
- (6) Lemaitre-Auger, F.; Prud'homme, J. *Electrochim. Acta*, **2001**, *46*, 1359-1367.
- (7) Song, L.; Evans, J. W. J. Electrochem. Soc., **2000**, 147, 2086-2095.
- (8) Armand, M. B. Fast Ion Transport in Solids; Gool, W. V., Ed.; North-Holland: Amsterdam, 1973, pp 665-673.
- (9) Aihara, Y.; Appetecchi, G. B.; Scrosati, B.; Hayamizuc, K. *Phys. Chem. Chem. Phys.*, **2002**, *4*, 3443-3447.
- (10) Bayoudh, S.; Parizel, N.; Reibel, L. *Polym. Int.*, **2000**, *49*, 703-711.
- (11) Kataoka, H.; Saito, Y.; Sakai, T.; Deki, S.; Ikeda, T. J. Phys. Chem. B, 2001, 105, 2546-2550.
- (12) Mello, N. C.; Bonagamba, T. J.; Panepucci, H.; Dahmouche, K.; Judeinstein, P.; Aegerter, M. A. *Macromolecules*, **2000**, *33*, 1280-1288.
- (13) Brissot, C.; Rosso, M.; Chazalviel, J. N.; Lascaud, S. J. Power Sources, 2001, 94, 212-218.

- (14) Capiglia, C.; Imanishi, N.; Takeda, Y.; Henderson, W. A.; Passerinib, S. J. Electrochem. Soc., 2003, 150, A525-A531.
- (15) Song, M.-K.; Kim, Y.-T.; Kim, Y. T.; Cho, B. W.; Popov, B. N.; Rhee, H.-W. J. *Electrochem. Soc.*, **2003**, *150*, A439-A444.
- (16) Kato, Y.; Suwa, K.; Ikuta, H.; Uchimoto, Y.; Wakihara, M.; Yokoyama, S.; Yabe, T.; Yamamoto, M. J. Mater. Chem., 2003, 13, 280-285.
- (17) Gnanaraj, J. S.; Levi, M. D.; Gofer, Y.; Aurbach, D.; Schmidt, M. J. Electrochem. Soc., 2003, 150, A445-A454.
- (18) Yamaguchi, H.; Takahashi, H.; Kato, M.; Arai, J. J. Electrochem. Soc., 2003, 150, A312-A315.
- (19) Gray, F. M. Solid Polymer Electrolytes--Fundamentals and Technological Applications; VCH publishers, Inc.: New York, 1991; pp 45-53.
- (20) Christie, L.; Christie, A. M.; Vincent, C. A. Electrochem. Solid State Lett., 1999, 2, 187-188.
- (21) Gauthier, M.; Belanger, A.; Kapfer, K.; Vassort, G.; Armand, M. *Polymer Electrolyte Reviews*; MacCallum, J. R., Vincent, C. A., Eds.; Elsevier: London, 1989; Vol. 2, pp 285-332.
- (22) Vincent, C. A. Prog. Solid State Chem., 1987, 17, 145-261.
- (23) Bruce, P. G.; Vincent, C. A. J. Electroanal. Chem., 1987, 225, 1-17.
- (24) Chandrasekhar, V. Adv. Poly. Sci., 1998, 135, 139-205.
- (25) Scrosati, B. *Electrochim. Acta*, **2000**, *45*, 2461-2466.
- (26) Chen, H. P.; Fergus, J. W.; Jang, B. Z. J. Electrochem. Soc., 2000, 147, 399-406.
- (27) Klassen, B.; Aroca, R.; Nazri, M.; Nazri, G. A. J. Chem. Phys. B., 1998, 102, 4795-4801.

- (28) Ding, M. S.; Xu, K.; Jow, T. R. J. Electrochem. Soc., 2000, 147, 1688-1694.
- (29) Peled, E.; Golodnitsky, D.; Menachem, C.; Bar-Tow, D. J. Electrochem. Soc., 1998, 145, 3482-3486.
- (30) Aurbach, D.; Ein-Eli, Y. J. Electrochem. Soc., 1995, 142, 1746-1752.
- (31) Chu, A.; Josefowicz, J.; Farrington, G. J. Electrochem. Soc., 1997, 144, 4161.
- (32) Ogumi, Z.; Inaba, M. Bull. Chem. Soc. Jpn., 1998, 71, 721.
- (33) Blomgren, G. E. J. Power Sources, 1999, 81-82, 112-118.
- (34) Aurbach, D.; Ein-Ely, Y.; Zaban, A. J. Electrochem. Soc., 1994, 141, L1-L3.
- (35) Wright, P. V. J. Polym. Sci. Part B: Polym. Phys., 1976, 14, 955-957.
- (36) Fenton, D. E.; Parker, J. M.; Wright, P. V. *Polymer*, **1973**, *14*, 589-589.
- (37) Wright, P. V. Brit. Polym. J., 1975, 7, 319-327.
- (38) MacCallum, J. R.; Vincent, C. A. *Polymer Electrolyte Reviews 2*; Elsevier Science Publishers Ltd.: New York, 1989
- (39) Wagner, A.; Kliem, H. J. Appl. Phys, **2002**, 91, 6638-6649.
- (40) MacCallum, J. R.; Vincent, C. A. *Polymer Electrolyte Reviews-1*; Elsevier Applied Science: New York, 1987
- (41) Staudinger, H.; Lohmann, H. Ann. Chim., 1933, 505, 41.
- (42) Hill, F. N.; Bailey, F. E.; Fitzpatrick, J. T. Ind. Eng. Chem., 1958, 50, 5.
- (43) Tashiro, K.; Tadokoro, H. Reports Prog. Poly. Phys. Jpn., 1978, 21, 417-420.

- (44) Takahashi, Y.; Sumita, I.; Tadokoro, H. J. Polym. Sci. Part B: Polym. Phys., 1973, 11, 2113-2122.
- (45) Tadokoro, H.; Chatani, Y.; Yoshihara, T.; Tahara, S.; Murahashi, S. *Makromol. Chem.*, **1964**, *73*, 109-127.
- (46) Bailey, F. E., Jr.; Koleske, J. V. *Poly(ethylene oxide)*; Academic: New York, N.Y., 1976; p 174.
- (47) Yoshihara, T.; Tadokoro, H.; Murahashi, S. J. Chem. Phys., 1964, 11, 2902-2904.
- (48) Koenig, J. L.; Angood, A. C. J. Polym. Sci., Part A: Polym. Chem., 1970, 3, 1787-1796.
- (49) Liu, K.-J.; Parsons, J. L. *Macromolecules*, **1969**, *2*, 529-533.
- (50) Machida, K.; Miyazawa, T. Spectr. Acta, 1964, 20, 1865-1873.
- (51) Matsuura, H.; Fukuhara, K. J. Mol. Struct., 1985, 126, 251-260.
- (52) Matsuura, H.; Miyazawa, T. Spectr. Acta, 1967, 23A, 2433-2447.
- (53) Matsuura, H.; Fukuhara, K. J. Polym. Sci. Part B: Polym. Phys., 1986, 24, 1383-1400.
- (54) Mullerplathe, F.; Vangunsteren, W. F. J. Chem. Phys., 1995, 103, 4745-4756.
- (55) Meyer, W. H. Adv. Mater., **1998**, 10, 439-448.
- (56) Scrosati, B. Chem. Rec., 2001, 1, 173-181.
- (57) Souquet, J. L.; Duclot, M. Solid State Ionics., 2002, 148, 375-379.
- (58) Wright, P. V. MRS Bull., 2002, 27, 597-602.

- (59) Chandrasekhar, V.; Krishnan, V.; Athimoolam, A.; Nagendran, S. Curr. Sci., 2000, 78, 464-472.
- (60) Nagaoka, K.; Naruse, H.; Shinohara, I.; Watanabe, M. J. Polym. Sci. Part A: Polym. Chem., 1984, 22, 659-663.
- (61) Blonsky, P. M.; Shriver, D. F.; Austin, P.; Allcock, H. R. J. Amer. Chem. Soc., 1984, 106, 6854-6855.
- (62) Shriver, D. F. J. Electrochem. Soc., 1987, 134, 270.
- (63) Abraham, K. M.; Alamgir, M. Chem. Mater., 1991, 3, 339-348.
- (64) Spindler, R.; Shriver, D. F. J. Amer. Chem. Soc., 1988, 110, 3036-3043.
- (65) Qiao, J.; Chen, Y. Y.; Baker, G. L. Chem. Mater., 1999, 11, 2542-2547.
- (66) Hall, P. G.; Davies, G. R.; Ward, I. M.; McIntyre, J. E. *Polym. Commun.*, **1986**, 27, 100-102.
- (67) Inoue, K.; Nishikawa, Y.; Tanigaki, T. *Macromolecules*, **1991**, *24*, 3464-3465.
- (68) Feuillade, G.; Perche, P. J. Appl. Electrochem., 1975, 5, 63-69.
- (69) Tarascon, J. M.; Gozdz, A. S.; Schmutz, C.; Shokoohi, F.; Warren, P. C. Solid State Ionics., 1996, 86-8, 49-54.
- (70) Dias, F. B.; Plomp, L.; Veldhuis, J. B. J. J. Power Sources, 2000, 88, 169-191.
- (71) Lee, K. H.; Park, J. K.; Kim, W. J. J. Polym. Sci. Part B: Polym. Phys., 1999, 37, 247-252.
- (72) Choe, H. S.; Carroll, B. G.; Pasquariello, D. M.; Abraham, K. M. Chem. Mater., 1997, 9, 369-379.

- (73) Forsyth, M.; MacFarlane, D. R.; Hill, A. J. *Electrochim. Acta*, **2000**, *45*, 1243-1247.
- (74) Abbrent, S.; Plestil, J.; Hlavata, D.; Lindgren, J.; Tegenfeldt, J.; Wendsjo, A. *Polymer*, **2001**, *42*, 1407-1416.
- (75) Hou, X. P.; Siow, K. S. *Polymer*, **2000**, *41*, 8689-8696.
- (76) Rajendran, S.; Uma, T. Bull. Mat. Sci., 2000, 23, 27-29.
- (77) Rajendran, S.; Mahendran, O.; Kannan, R. J. Phys. Chem. Solids, 2002, 63, 303-307.
- (78) Yue, Z.; McEwen, I. J.; Cowie, J. M. G. J. Mater. Chem., 2002, 12, 2281-2285.
- (79) Aihara, Y.; Kuratomi, J.; Bando, T.; Iguchi, T.; Yoshida, H.; Ono, T.; Kuwana, K. *J. Power Sources*, **2003**, *114*, 96-104.
- (80) Gray, F.; Armand, M. *Handbook of Battery Materials*; Wiley-VCH: New York, 1999, pp 499-523.
- (81) Weston, J. E.; Steele, B. C. H. Solid State Ionics., 1982, 7, 75.
- (82) Capuano, F.; Croce, F.; Scrosati, B. J. Electrochem. Soc., 1991, 138, 1918-1922.
- (83) Raghavan, S. R.; Riley, M. W.; Fedkiw, P. S.; Khan, S. A. Chem. Mater., 1998, 10, 244-251.
- (84) Krawiec, W.; Scanlon, L. G.; Fellner, J. P.; Vaia, R. A.; Giannelis, E. P. J. Power Sources, 1995, 54, 310-315.
- (85) Cho, J. P.; Liu, M. L. Electrochim. Acta, 1997, 42, 1481-1488.
- (86) Hou, J.; Baker, G. L. Chem. Mater., 1998, 10, 3311-3318.
- (87) Ballauff, M. Angew. Chem. Int. Ed. Engl., 1989, 28, 253-267.

- (88) Lenz, R. W. Faraday Discuss., 1985, 79, 21-32.
- (89) Ballauff, M. Macromolecules, 1986, 19, 1366-1374.
- (90) McHattie, G. S.; Imrie, C. T.; Ingram, M. D. *Electrochim. Acta*, **1998**, *43*, 1151-1154.
- (91) Baum, P.; Meyer, W. H.; Wegner, G. *Polymer*, **2000**, *41*, 965-973.
- (92) Lauter, U.; Meyer, W. H.; Wegner, G. Macromolecules, 1997, 30, 2092-2101.
- (93) Arnautov, S. A.; Gavrilenko, V. V. Synth. Met., 1997, 84, 283-284.
- (94) Shimura, T.; Funaki, H.; Nishihara, H.; Aramaki, K.; Ohsawa, T.; Yoshino, K. *Chem. Lett.*, **1992**, 457-460.
- (95) Bringmann, G.; Walter, R.; Weirich, R. Angew. Chem. Int. Ed. Engl., 1990, 29, 977-991.
- (96) Fanta, P. E. Synthesis, 1974, 9-21.
- (97) Wirth, H. O.; Herrmann, F. U.; Hern, W. Makromol. Chem., 1964, 80, 120-140.
- (98) Percec, V.; Hill, D. H. Step-Growth Polymers For High-Performance Materials; American Chemical Society: Washington, D.C., 1996; Vol. 624, pp 2-56.
- (99) Percec, V.; Pugh, C.; Cramer, E.; Okita, S.; Weiss, R. *Makromol. Chem.*, **1992**, 54-5, 113-150.
- (100) Durairaj, K. Curr. Sci., 1994, 66, 833-838.
- (101) Goodson, F. E.; Wallow, T. I.; Novak, B. M. J. Amer. Chem. Soc., 1997, 119, 12441-12453.
- (102) Saa, J. M.; Martorell, G. J. Org. Chem., 1993, 58, 1963-1966.

- (103) Rehahn, M.; Schluter, A. D.; Wegner, G.; Feast, W. J. *Polymer*, **1989**, *30*, 1060-1062.
- (104) Kwiatkowski, G. T.; Colon, I.; Elhibri, M. J.; Matzner, M. *Macromol. Symp.*, 1992, 54-5, 199-224.
- (105) Maccallum, J. R.; Tomlin, A. S.; Vincent, C. A. Eur. Polym. J., 1986, 22, 787-791.
- (106) Doyle, M.; Newman, J. Electrochim. Acta, 1995, 40, 2191-2196.
- (107) Doyle, M.; Fuller, T. F.; Newman, J. Electrochim. Acta, 1994, 39, 2073-2081.
- (108) Riley, M.; Fedkiw, P. S.; Khan, S. A. J. Electrochem. Soc., 2002, 149, A667-A674.
- (109) Bannister, D. J.; Davies, G. R.; Ward, I. M.; McIntyre, J. E. *Polymer*, **1984**, *25*, 1291-1296.
- (110) Tsuchida, E.; Kobayashi, N.; Ohno, H. Macromolecules, 1988, 21, 96-100.
- (111) Hardy, L. C.; Shriver, D. F. J. Amer. Chem. Soc., 1985, 107, 3823-3828.
- (112) Jacob, M. M. E.; Hackett, E.; Giannelis, E. P. J. Mater. Chem., 2003, 13, 1-5.
- (113) Ratner, M. A.; Johansson, P.; Shriver, D. F. MRS Bull., 2000, 25, 31-37.
- (114) Scrosati, B.; Vincent, C. A. MRS Bull., 2000, 25, 28-30.
- (115) Wieczorek, W.; Florjanczyk, Z.; Stevens, J. R. *Electrochim. Acta*, **1995**, *40*, 2251-2258.
- (116) Croce, F.; Curini, R.; Martinelli, A.; Persi, L.; Ronci, F.; Scrosati, B.; Caminiti, R. *J. Phys. Chem. B*, **1999**, *103*, 10632-10638.

- (117) Fujinami, T.; Tokimun, A.; Mehta, M. A.; Shriver, D. F.; Rawsky, G. C. Chem. *Mater.*, 1997, 9, 2236-2239.
- (118) Doan, K. E.; Ratner, M. A.; Shriver, D. F. Chem. Mater., 1991, 3, 418-423.
- (119) Onishi, K.; Matsumoto, M.; Nakacho, Y.; Shigehara, K. Chem. Mater., 1996, 8, 469-472.
- (120) Rawsky, G. C.; Fujinami, T.; Shriver, D. F. Chem. Mater., 1994, 6, 2208-2209.
- (121) Fujinami, T.; Tokimune, A.; Mehta, M. A.; Shriver, D. F.; Rawsky, G. C. Chem. *Mater.*, 1997, 9, 2236-2239.
- (122) Walls, H. J.; Zhou, J.; Yerian, J. A.; Fedkiw, P. S.; Khan, S. A.; Stowe, M. K.; Baker, G. L. J. Power Sources, 2000, 89, 156-162.
- (123) Levesque, I.; Leclerc, M. J. Chem. Soc., Chem. Commun., 1995, 2293-2294.
- (124) Chang, S.; Han, C. D. Macromolecules, 1997, 30, 1670-1684.
- (125) Steuer, M.; Ballauff, M. J. Polym. Sci. Pol. Chem., 1993, 31, 1609-1619.
- (126) Majnusz, J.; Catala, J. M.; Lenz, R. W. Eur. Polym. J., 1983, 19, 1043-1046.
- (127) Stern, R.; Ballauff, M.; Lieser, G.; Wegner, G. Polymer, 1991, 32, 2096-2105.
- (128) Majnusz, J.; Lenz, R. W. Eur. Polym. J., 1989, 25, 847-855.
- (129) Steiner, U. B.; Caseri, W. R.; Suter, U. W.; Rehahn, M.; Rau, I. U. Langmuir, 1994, 10, 1164-1170.
- (130) Delnoye, D. A. P.; Sijbesma, R. P.; Vekemans, J. A. J. M.; Meijer, E. W. J. Amer. Chem. Soc., 1996, 118, 8717-8718.
- (131) Kato, T.; Kihara, H.; Uryu, T.; Fujishima, A.; Frechet, J. M. J. *Macromolecules*, 1992, 25, 6836-6841.

- (132) Moriya, K.; Mizusaki, H.; Kato, M.; Suzuki, T.; Yano, S.; Kajiwara, M.; Tashiro, K. Chem. Mater., 1997, 9, 255-263.
- (133) Song, H. H.; Dotrong, M.; Price, G. E.; Dotrong, M. H.; Vakil, U. M.; Santhosh, U.; Evers, R. C. *Polymer*, **1994**, *35*, 675-680.
- (134) Ciferri, A. Polym. Eng. Sci., 1994, 34, 377-378.
- (135) Krause, S. J.; Haddock, T. B.; Price, G. E.; Adams, W. W. *Polymer*, **1988**, *29*, 195-206.
- (136) Meyer, W. H. Adv. Mater., 1998, 10, 439-448.
- (137) Eisenbach, C. D.; Hofmann, J.; Goeldel, A.; Noolandi, J.; Shi, A. C. *Macromole-cules*, **1999**, *32*, 1463-1470.
- (138) Bouachrine, M.; Lere-Porte, J.-P.; Moreau, J. J. E.; Spirau, F. S.; Augusta da Silva, R.; Lmimouni, K.; Ouchani, L.; Dufour, C. Synth. Met., 2002, 126, 241-244.
- (139) Johansson, T.; Mammo, W.; Andersson, M. R.; Inganas, O. Chem. Mater., 1999, 11, 3133-3139.
- (140) Lauter, U.; Meyer, W. H.; Enkelmann, V.; Wegner, G. *Macromol. Chem. Phys.*, 1998, 199, 2129-2140.
- (141) Colon, I.; Kelsey, D. R. J. Org. Chem., 1986, 51, 2627.
- (142) Colon, I.; Kwiatkowski, G. T. J. Polym. Sci., Part A: Polym. Chem., 1990, 28, 367-383.
- (143) Ueda, M.; Ichikawa, F. *Macromolecules*, **1990**, *23*, 926-930.
- (144) Ueda, M.; Miyaji, Y.; Ito, T.; Oba, Y.; Sone, T. *Macromolecules*, **1991**, *24*, 2694-2697.

- (145) Pasquale, A. J.; Sheares, V. V. J. Polym. Sci., Part A: Polym. Chem., 1998, 36, 2611-2618.
- (146) Luzinov, I.; Julthongpiput, D.; Bloom, P. D.; Sheares, V. V.; Tsukruk, V. V. *Macromol. Symp.*, **2001**, *167*, 227-242.
- (147) Percec, V.; Zhao, M.; Bae, J.-Y.; Hill, D. H. *Macromolecules*, **1996**, *29*, 3727-3735.
- (148) Percec, V.; Asandei, A. D.; Hill, D. H.; Crawford, D. *Macromolecules*, 1999, 32, 2597-2604.
- (149) Chen, Y.; Baker, G. L. J. Org. Chem., 1999, 64, 6870-6873.
- (150) Kwiatkowski, G. T.; Matzner, M.; Colon, I. J. Macromol. Sci., Pure Appl. Chem., 1997, A34, 1945-1975.
- (151) Kwiatkowski, G. T.; Colon, I. Contemporary Topics in Polymer Science; Pearce, E. M., Schaefgen, J. R., Eds.; Plenum Press: New York, 1992; Vol. 7, pp 57-74.
- (152) Flory, P. J. Principles of Polymer Chemistry; Cornell University Press: Ithaca, 1953
- (153) Petekidis, G.; Vlassopoulos, D.; Fytas, G.; Kountourakis, N.; Kumar, S. *Macro-molecules*, 1997, 30, 919-931.
- (154) Goodson, F. E.; Wallow, T. I.; Novak, B. M. Macromolecules, 1998, 31, 2047-2056.
- (155) Bouachrine, M.; Lere-Porte, J.-P.; Moreau, J. J. E.; Spirau, F. S.; Augusta da Silva, R.; Lmimouni, K.; Ouchani, L.; Dufour, C. Synthetic Metals, 2002, 126, 241-244.
- (156) Dubois, M.; Naji, A.; Buisson, J. P.; Humbert, B.; Grivei, E.; Billaud, D. Carbon, **2000**, 38, 1411-1417.
- (157) Hernandez, V.; Soto, J.; Navarrete, J. T. L. Synth. Met., 1993, 57, 4461-4466.

- (158) Louarn, G.; Athouel, L.; Froyer, G.; Buisson, J. P.; Lefrant, S. Synth. Met., 1993, 57, 4762-4767.
- (159) Marucci, A.; Pimenta, M. A.; Brown, S. D. M.; Matthews, M. J.; Dresselhaus, M. S.; Endo, M. J. Mater. Res., 1999, 14, 3447-3454.
- (160) Asfour, F. H.; Ruud, C. J.; Baker, G. L., submitted for publication in *Chem. Mater*.
- (161) Janssen, R. G.; Utley, J. H. P.; Carre, E.; Simon, E.; Schirmer, H. J. Chem. Soc., Perkin Trans. 2, 2001, 1573-1584.
- (162) Asakawa, M.; Ashton, P. R.; Balzani, V.; Boyd, S. E.; Credi, A.; Mattersteig, G.; Menzer, S.; Montalti, M.; Raymo, F. M.; Ruffilli, C.; Stoddart, J. F.; Venturi, M.; Williams, D. J. Eur. J. Org. Chem., 1999, 985-994.
- (163) Delamarche, E.; Donzel, C.; Kamounah, F. S.; Wolf, H.; Geissler, M.; Stutz, R.; Schmidt-Winkel, P.; Michel, B.; Mathieu, H. J.; Schaumburg, K. *Langmuir*, **2003**, 19, 8749-8758.
- (164) Leaper, J. M. F.; Raman, H. P. J. US Patent 3 703 546, 1972.
- (165) Cowie, J. M. G. *Polym. Int.*, **1998**, 47, 20-27.
- (166) Scrosati, B. *Polym Int*, **1998**, 47, 50-55.
- (167) Murata, K.; Izuchi, S.; Yoshihisa, Y. Electrochim. Acta, 2000, 45, 1501-1508.
- (168) Burke, L. M., Jr.; Khan, I. M. Macromol. Chem. Phys., 2000, 201, 2228-2233.
- (169) Wang, Y. C.; Quirk, R. P. *Macromolecules*, **1995**, 28, 3495-3501.
- (170) Philips, R. W.; Sheares, V. V.; Samulski, E. T.; Desimone, J. M. *Macromolecules*, **1994**, *27*, 2354-2356.
- (171) Baker, K. N.; Fratini, A. V.; Resch, T.; Knachel, H. C.; Adams, W. W.; Socci, E. P.; Farmer, B. L. *Polymer*, **1993**, *34*, 1571-1587.

- (172) Pasco, S. T.; Baker, G. L. Synth. Met., 1997, 84, 275-276.
- (173) Kim, Y. W.; Lee, W.; Choi, B. K. *Electrochim. Acta*, **2000**, *45*, 1473-1477.
- (174) Nafshun, R. L.; Lerner, M. M.; Hamel, N. N.; Nixon, P. G.; Gard, G. L. J. Electrochem. Soc., 1995, 142, L153-L155.
- (175) Dygas, J. R.; Misztal-Faraj, B.; Florjanczyk, Z.; Krok, F.; Marzantowicz, M.; Zygadlo-Monikowska, E. Solid State Ionics, 2003, 157, 249-256.
- (176) Wendsjoe, A.; Yang, H. Int. Symp. Polym. Electrolytes, 2nd, 1990, 225-237.
- (177) Wright, P. V. J. Mater. Chem., 1995, 5, 1275-1283.
- (178) del Rio, C.; Wright, P. V. J. Mater. Chem., 1996, 6, 947-952.
- (179) Gray, F. M. Solid Polymer Electrolytes--Fundamentals and Technological Applications; VCH publishers, Inc.: New York, 1991; p 245.
- (180) Kim, J.; Park, M. K.; Bae, J. Y.; Ahn, J. H. Electrochem. Commun., 2001, 3, 643-648.
- (181) Hou, W. H.; Chen, C. Y.; Wang, C. C.; Huang, Y. H. *Electrochim. Acta*, **2003**, 48, 679-690.
- (182) Nishimoto, A.; Agehara, K.; Furuya, N.; Watanabe, T.; Watanabe, M. *Macromolecules*, **1999**, *32*, 1541-1548.
- (183) Gnanaraj, J. S.; Karekar, R. N.; Skaria, S.; Rajan, C. R.; Ponrathnam, S. *Polymer*, **1997**, *38*, 3709-3712.
- (184) Kerr, J. B.; Liu, G.; Curtiss, L. A.; Redfern, P. C. *Electrochim. Acta*, **2003**, *48*, 2305-2309.
- (185) Watanabe, M.; Endo, T.; Nishimoto, A.; Miura, K.; Yanagida, M. *J. Power Sources*, **1999**, *81-82*, 786-789.

- (186) Kerr, J. B.; Sloop, S. E.; Liu, G.; Han, Y. B.; Hou, J.; Wang, S. J. Power Sources, **2002**, 110, 389-400.
- (187) Asfour, F. H.; Ruud, C. J.; Baker, G. L., submitted for publication in *Macromole-cules*.
- (188) Bruce, P. G.; Hardgrave, M. T.; Vincent, C. A. Solid State Ionics, 1992, 53-56, 1087-1094.
- (189) Egashira, M.; Scrosati, B.; Armand, M.; Beranger, S.; Michot, C. *Electrochem. Solid State Lett.*, **2003**, *6*, A71-A73.
- (190) Wieczorek, W.; Such, K.; Przyluski, J.; Florianczyk, Z. Synth. Met., 1991, 45, 373-383.
- (191) Croce, F.; Scrosati, B. Advanced Membrane Technology; New York Academy of Sciences: New York, 2003; Vol. 984, pp 194-207.
- (192) Croce, F.; Appetecchi, G. B.; Persi, L.; Scrosati, B. Nature, 1998, 394, 456-458.
- (193) Matsushita, K.; Shimazaki, Y.; Mehta, M. A.; Fujinami, T. Solid State Ionics, 2000, 133, 295-301.
- (194) Chen, H.-W.; Chang, F.-C. *Polymer*, **2001**, *42*, 9763-9769.
- (195) Li, Y.; Fedkiw, P. S.; Khan, S. A. *Electrochim. Acta*, **2002**, *47*, 3853-3861.
- (196) Zhou, J.; Fedkiw, P. S.; Khan, S. A. J. Electrochem. Soc., 2002, 149, A1121-A1126.
- (197) Lascaud, S.; Perrier, M.; Vallee, A.; Besner, S.; Prudhomme, J.; Armand, M. *Macromolecules*, 1994, 27, 7469-7477.
- (198) Krause, L. J.; Lamanna, W.; Summerfield, J.; Engle, M.; Korba, G.; Loch, R.; Atanasoski, R. J. Power Sources, 1997, 68, 320-325.

- (199) Fulcher, C.; Crowell, M. A.; Bayliss, R.; Holland, K. B.; Jezorek, J. R. Anal. Chim. Acta, 1981, 129, 29-47.
- (200) Roesky, H. W. Angew. Chem. Int. Ed., 1967, 6, 711.
- (201) Glemser, O.; Roesky, H. W.; Heinze, P. R. Angew. Chem. Int. Ed., 1967, 6, 710-711.
- (202) Leonardelli, S.; Facchini, L.; Fretigny, C.; Tougne, P.; Legrand, A. P. J. Amer. Chem. Soc., 1992, 114, 6412-6418.
- (203) Siska, D. P.; Shriver, D. F. Chem. Mater., 2001, 13, 4698-4700.
- (204) Edman, L.; Doeff, M. M.; Ferry, A.; Kerr, J.; De Jonghe, L. C. J. Phys. Chem. B, **2000**, 104, 3476-3480.
- (205) Gagne, M. R.; Stern, C. L.; Marks, T. J. J. Amer. Chem. Soc., 1992, 114, 275-294.
- (206) Larock, R. C.; Yang, H.; Weinreb, S. M.; Herr, R. J. J. Org. Chem., 1994, 59, 4172-4178.